POLITECNICO

MILANO 1863

Investigation of polyynes in polymeric electrospun nanofibers

TESI DI LAUREA MAGISTRALE IN

MATERIALS ENGINEERING AND NANOTECHNOLOGY - INGEGNERIA DEI MATERIALI E DELLE NANOTECNOLOGIE

Author: **Andrea Taini**

Student ID: 968544
Advisor: Carlo S. Casari
Co-advisor: Simone Melesi
Academic Year: 2021-22

Abstract

Carbon Atomic Wires (CAWs) are linear chains composed by only sp-hybridized carbon atoms, representing a true unidimensional material among carbon allotropes. Depending on their structures, they can be divided into polyynes and cumulenes: the firsts present an alternation of single and triple C-C bonds, while the seconds are made only by equal double bonds. CAWs can be terminated by different heteroatoms or chemical groups, which affect their structure and opto-electronical properties (i.e., bond length alternation, energy gap, π-electron conjugation). Despite having very appealing theoretically predicted mechanical, optical, and electronic properties, CAWs are not widely diffused due to the easiness of their degradation; in literature, stabilization and detection of polyynes has been successfully achieved embedding these molecules inside polymeric films. Carbon wires have been synthesized exploiting chemical routes or physical ablation methods; the latter are versatile and scalable processes, but only low concentrated polyynes are obtainable. In these cases, due to low concentration, the detection and characterization can be performed with the aid of metallic nanoparticles, exploiting Surface Enhanced Raman Scattering (SERS) effect.

The purpose of this thesis is in continuity with the investigation of low concentrated polyynes in polymeric matrices. In this work, polyynes were integrated in polymeric nanofibers obtained from electrospinning. The detection of polyynes inside electrospun nanofibers was conducted for two different terminated chains, halogenated and hydrogenated polyynes. Both systems were characterized at low polyynes concentration, therefore the use of silver nanoparticles (AgNP) was necessary to exploit SERS effect. Measurements in liquid and in PVA films were done to study the interaction of polyynes with AgNP, showing a good response for both carbon chains. The investigation of polyynes inside polymeric fibers was conducted with several SERS configurations, in order to verify which one was the most effective: AgNP at various concentrations were placed above, under and inside nanofibers of PVA or PMMA. It was found that nanofibers electrospun from a PVA solution containing concentrated AgNP were effective to detect characteristic signals of hydrogenated polyynes; both a mixture of chains with various length and a solution of size-selected chains (HC_8H) were successfully embedded and detected inside these nanofibers. Their stability in time was verified up to one month. These

are the first examples of detection of low concentrated polyynes produced by physical ablation methods and embedded in electrospun nanofibers. On the contrary, halogenated polyynes were not detected in this or any other configuration, thus confirming how different chemical end-groups can affect the interaction of polyynes with AgNP, influencing the SERS detection of these molecules.

Keywords: Carbon Atomic Wires, polyynes, electrospinning, silver nanoparticles, SERS.

Abstract in italiano

I Carbon Atomic Wires (CAWs) sono catene lineari composte da soli atomi di carbonio con ibridazione sp, e rappresentano un vero materiale unidimensionale tra gli allotropi del carbonio. A seconda della loro struttura si possono suddividere in poliine e cumuleni: le prime presentano un'alternanza di legami C-C singoli e tripli, mentre i secondi sono costituiti solo da doppi legami equivalenti. I CAWs possono essere terminati da diversi eteroatomi o gruppi chimici, che ne influenzano la struttura e le proprietà optoelettroniche (ad esempio, la differenza di lunghezza del legame, il gap energetico, la coniugazione elettronica). Nonostante le teoriche proprietà meccaniche, ottiche ed elettroniche siano molto incoraggianti, i CAWs non sono ampiamente diffusi a causa della facilità con cui degradano; in letteratura, la stabilizzazione e la rilevazione di poliine è stata ottenuta con successo incorporando queste molecole all'interno di film polimerici. I Carbon atomic wires sono sintetizzati sfruttando metodi chimici o di ablazione fisica; questi ultimi sono processi versatili e scalabili, ma permettono di ottenere solo poliine a bassa concentrazione. In questi casi, a causa della bassa concentrazione, il rilevamento e la caratterizzazione possono essere eseguiti con l'ausilio di nanoparticelle metalliche, sfruttando l'effetto SERS (Surface Enhanced Raman Scattering).

Lo scopo di questa tesi è in continuità con lo studio di poliine a bassa concentrazione in matrici polimeriche. In questo lavoro, le poliine sono state integrate in nanofibre polimeriche ottenute tramite elettrofilatura. Il rilevamento delle poliine all'interno di nanofibre elettrofilate è stato condotto per due gruppi di catene con diverse terminazioni, cioè poliine alogenate e idrogenate. Entrambi i sistemi sono stati caratterizzati a bassa concentrazione di poliine; pertanto, è stato necessario l'uso di nanoparticelle d'argento (AgNP) per sfruttare l'effetto SERS. Sono state effettuate misurazioni in liquido e in film di PVA, al fine di studiare l'interazione delle poliine con le AgNP; una buona risposta di entrambe le catene di carbonio è stata verificata. L'indagine riguardo le poliine all'interno delle fibre polimeriche è stata condotta con diverse configurazioni SERS, al fine di verificare quale fosse la più efficace: nanoparticelle a varie concentrazioni sono state poste sopra, sotto e all'interno di nanofibre di PVA o PMMA. È stato riscontrato che nanofibre elettrofilate da una soluzione di PVA contenente AgNP concentrate erano efficaci nel rilevare i segnali caratteristici delle poliine idrogenate; all'interno di queste nanofibre sono state incorporate e rilevate con successo sia una miscela di catene di varia lunghezza che una soluzione di catene con dimensione selezionata (HC_8H). La loro stabilità nel tempo è stata verificata fino ad un mese. Questi sono i primi esempi di rilevamento di poliine

a bassa concentrazione prodotte con metodi di ablazione fisica e integrate in nanofibre elettrofilate. Al contrario, le poliine alogenate non sono state rilevate con questa o qualsiasi altra configurazione, confermando così come i diversi gruppi chimici terminali possano influenzare l'interazione delle poliine con le AgNP, influenzando il rilevamento SERS di queste molecole.

Parole chiave: Carbon Atomic Wires, poliine, elettrofilatura, nanoparticelle di argento, SERS.

Contents

Introduction

Carbon allotropes are a broad family of structures with peculiar properties, which have made them promising materials for the next technological revolution; graphene, fullerenes and carbon nanotubes have been studied for electronic, optoelectronic, photovoltaic, and biomedical applications. Among this group of interesting materials, Carbon Atomic Wires (CAWs) have obtained a relevant spot in many research fields. CAWs are linear chains made of sp-hybridized carbon atoms; they have gained increasing attention due to their superlative mechanical, thermal, and electrical properties. CAWs theoretical model consists in an infinite wire (carbyne), which can possess two structures: an alternating sequence of single and triple C-C bonds (polyyne) or a repetition of double bonds (cumulene). Real CAWs are polyynic or cumulenic finite chains terminated by various heteroatoms or chemical groups, from the simplest hydrogen capping termination to several bulky groups. Endgroup effects are crucial in determining real CAWs' structural, electronic, and vibrational properties; moreover, they influence carbon wires stability. Polyynes are unstable systems which tend to crosslink into a more stable sp^2-hybridized carbon structure; their stabilization has been achieved by exploiting bulky capping groups or embedding them into polymeric matrices. CAWs production can be achieved by different chemical routes or by exploiting physical ablation methods. Among the latter, Pulsed Laser Ablation in Liquid (PLAL) is one of the most used techniques, due to its versatility and scalability; the main drawback is the low polyyne concentration obtainable (10^{-6} mol/L).

Polymeric nanocomposites can be produced with different dimensionalities; a fascinating technique to produce fibres with submicrometric dimension is electrospinning. It possesses huge versality and a rather simple working principle: a liquid polymeric solution is electrified by the application of a high potential difference between the needle of a syringe (containing the solutions) and a conductive collector. This process allows to create very thin fibers with high surface density; electrospun nanofibers have been exploited for biomedical, textile, energy, and filtration applications.

The aim of this work is to investigate low concentrated polyynes embedded in electrospun polymeric nanofibers. Carbon chains with different terminations, namely halogenated and hydrogenated polyynes, were investigated. Since the low concentration of polyynes makes them non-detectable by Raman spectroscopy, characterization was performed with the help of silver nanoparticles (AgNP),

exploiting Surface Enhanced Raman Spectroscopy (SERS) effect. Several SERS configurations were implemented, with the purpose of finding the most suitable one for polyynes detection. The possibility to investigate different polyynes with various configurations allows us to observe the variability in their SERS behaviour; moreover, it makes possible to optimize an extremely effective SERS process for the detection of these molecules.

The thesis work is organized in four chapters:

Chapter 1: Overview of the main carbon allotropes, followed by a description of CAWs structure, properties, synthesis methods and characterization techniques; a brief introduction to CAWs nanocomposites concludes the chapter.

Chapter 2: Description of electrospinning theoretical principles and instrumental apparatus, a focus on parameters effects and an overview on application fields.

Chapter 3: Description of the materials and the experimental methods exploited for samples preparation and investigation.

Chapter 4: Experimental results, organized in two parts: investigation of halogenated polyynes and of hydrogenated polyynes. Results are compared and discussed.

1 Carbon atomic wires (CAWs)

Carbon is far from being simply the sixth element of the periodic table; it is one of the most abundant elements in the universe, and it has been defined "the element of life" since carbon compounds are at the basis of each living creature on Earth [1, 2]. This statement should be enough to confer a particular position of importance for carbon and its derivatives. Moreover, there is a reason if an entire field of chemistry (the organic chemistry) has been focusing on the study of carbon containing substances; their impact is tangible in numerous technological applications, from optoelectronics to drug delivery [2]. This unique versatility is mainly due to the ability of carbon to bond with several elements and to exploit different architectures thanks to its hybridization states (sp^3, sp^2, sp): carbon can build single, double, or triple bonds, opening the possibility to have tri-, bi- or mono-dimensional structures from the same element [3]. Carbon allotropes have gained an increasing attention starting from the study of the first "non-natural" forms of carbon, the fullerenes, discovered in 1985 [4]. The growing interest was accentuated by the synthesis of carbon nanotubes and graphene around the beginning of the XXI century [5, 6]. Among carbon allotropes, carbon atomic wires (CAWs) can be seen as a promising addition to the carbon family. CAWs are linear chains composed by a sequence of sp-hybridized carbon atoms; their theoretical model is an infinite chain, but in reality, CAWs are finite linear arrangements of carbon atoms terminated by different capping elements. Their structure makes them the unidimensional materials filling a void in the group of achievable carbon allotropes. Even if CAWs are not a stable form of carbon in nature (like graphite or diamond), they have been found inside interstellar gasses and trapped in some meteorite's samples [7-9]. The quest for the synthetization of sp-carbon chains can be brought back to XIX century, with the works of Glaser and Baeyer [9, 10], but only in the last three decades a strong acceleration in the ability to produce and stabilize CAWs was observed [9, 11]. Nowadays, linear carbon chains can be synthesized in many ways and integrated in more complex structures, even with other carbon allotropes [11, 12]. The principal focus of this chapter is the description of CAWs properties, production, and characterisation. Before that, the next section is dedicated to the discussion of other carbon allotropes main properties, (and the role that they have gained in their technological fields) to offer a more extensive overview on the world to which CAWs belong.

1.1. Overview on carbon allotropes

The existence of many different carbon allotropes is due to carbon particular ability to bond with other atoms; a single carbon atom can form up to four chemical bonds. This possibility seems to be impossible by just looking at its electronic structure, which is [He] $2s^2$ $2p^1_x$ $2p^1_y$; here, only two unpaired electrons are presents, which allow to presume that carbon possesses a valence of two and therefore could not be able to coordinate four bonds. However, the existence of a simple molecule like methane, which molecular formula is CH_4 (with tetrahedral geometrical structure) suggest that a more accurate description is needed. The Valence Bond (VB) and the Linear Combination of Atomic Orbitals (LCAO) theories have helped to describe properly the formation of molecular bonds and explaining carbon behaviour [13]. The idea behind these theories is that a chemical bond is formed when two atomic orbitals interact with each other creating a single molecular orbital. In the framework of quantum mechanics, this interaction can be described by a linear combination of the electronic wavefunctions; a simpler description for depicting this bond formation is the visualization of electron clouds superposition. A bond formed by orbitals oriented along the molecule axis is called σ bond, while, if the orbitals are oriented perpendicularly, the result is a π bond. The key feature of the molecular orbitals' theory is that even the different atomic orbitals of a specific atom can combine themselves to form new bonds; this process is called hybridization and that is exactly what allows carbon atoms to make more than two bonds. The electronic structure of carbon valence shell ($2s^2$ $2p^1_x$ $2p^1_y$) can be changed if the bond formation brings an overall decrease of potential energy. The phenomenon can be simply described by a promotion of one electron from the 2s orbital to the empty $2p_z$ orbital; the four valence orbitals of carbon (2s, $2p_x$, $2p_y$, $2p_z$) can interact between themselves and linearly combine to form hybrid orbitals. A LCAO of all the orbitals will result in four sp^3 hybrid orbitals oriented in a tetrahedral shape; by bonding with four hydrogen atoms, methane can form. If the linear combination does not involve all the 2p orbitals, different hybrid orbitals are created: three planar sp^2 orbitals or two linear sp orbitals. The remaining 2p orbitals are the responsible for the formation of higher order chemical bonds: in a carbon-carbon double bond, a σ bond is formed between two sp^2 orbitals (one from each carbon) and the two $2p_z$ orbitals form a π bond. Triple bond formation follows a similar path: one σ bond between two sp orbitals two π bonds between the $2p_x$ and $2p_y$ orbitals [13].

This brief explanation highlights the versatility of carbon atoms in the bond formation and clarify the presence of many carbon allotropes with different hybridization states. Some of them present outstanding properties and their discovery has opened a new era in which carbon will be the material of the future, as silicon has been from the XX century up to present days [14]. The main carbon allotropes are now described, with some outlooks on their applications.

Diamond

It is one of the most known allotrope of carbon since it has been used for centuries in decorations: however, diamond is not only a very precious gem but it is also widespread in many fields of materials sciences. Its structure is made by only sp^3 carbon atoms arranged in a face-centred cubic crystal with a basis of two atoms. Its synthetization is not effortless since pressure around 5-6 GPa and temperatures of 1000-1400 °C are needed [15]. These extreme conditions create a meta-stable allotrope, but the conversion to graphite (which thermodynamically is the only stable form of carbon in a standard environment) requires a high activation energy; therefore, the rate is negligible, and diamonds is considered a stable form as well [16].

What makes diamond very interesting from a technological point of view is its huge thermal conductivity. Due to its strong covalent structure, almost defectless, thermal conductivity of diamond reaches approximately 2200 W/(mK) (five times higher than copper). This property is exploited in semiconductor industry to prevent the overheating of silicon and other materials. From an electronic point of view, it is considered as an insulator (bandgap of 5.5 eV), while it exhibits some interesting nonlinear optical properties [17]. Other relevant properties of diamond are high chemical and physical resistance (it is the hardest material in Mohs scale) and biocompatibility: some common applications are in the cutting and polishing tools field [2].

Graphite

It is the stable form of carbon at standard conditions. It is composed by multiple layers of sp^2 carbon atoms covalently bonded in a hexagonal structure; layers are piled on top of each other and held together by weak van der Waals forces. Graphite is a good electrical conductor since its unpaired electrons in the p_z orbitals form a delocalized π electron band which allows carrier movement; it possesses also a good thermal conductivity. From a mechanical point of view, graphite is flexible but not elastic, and it is a very soft material. Moreover, it is often used as a lubricant, because of the weak intermolecular forces holding the layers, which are not able to hinder the horizontal slip motion when an external force is applied [2].

Graphene

It is probably the most investigated carbon allotrope in the last decade [2]. Graphene is essentially a monolayer of graphite, therefore possesses the same planar honeycomb structure (however, the crystallographic structure is different, since graphite is a 3D crystal and graphene a 2D hexagonal lattice with a basis of two atoms). It can be obtained by simple mechanical exfoliation of graphite, but over the years more refined techniques have been implemented: chemical vapour deposition (CVD), molecular beam epitaxy (MBE), epitaxial growth on silicon-carbides (SiC) substrates and several others[18]. The huge number of studies around graphene are due to its incredible

electronic, thermal, and optical properties; graphene is a metallic material with a very high ambipolar conductivity (electron mobility can theoretically reach $2.5x10^5 cm^2/Vs$), a thermal conductivity of 3000 W/mK (larger than diamond) and a considerably low optical absorption of 2.3% per layer [19, 20]. Moreover, by exploiting confinement effects, a bandgap can be opened, thus becoming a semiconductor. Graphene shows also a particular non-linear optical behaviour [21]. All these qualities have made graphene the ideal candidate in various field of electronics and optoelectronics. There are several examples of works in which graphene has been implemented, covering several research topics, like field effect transistors, photodetectors, light emitting devices, photovoltaics, optical modulators, and transparent electrodes [19-21]. Moreover, from a mechanical perspective, graphene is one of the strongest materials existing (1 TPa of Young modulus), due to its solid covalent planar structure, but still remarkably elastic (can be stretched up to 20%).

The crucial role of graphene is evident considering also that its structure can be seen as the building block of many other carbon allotropes, like fullerenes, carbon nanotubes, and even graphite (Figure 1.1); therefore, understanding its properties is fundamental for the exploitation of other carbon materials [2].
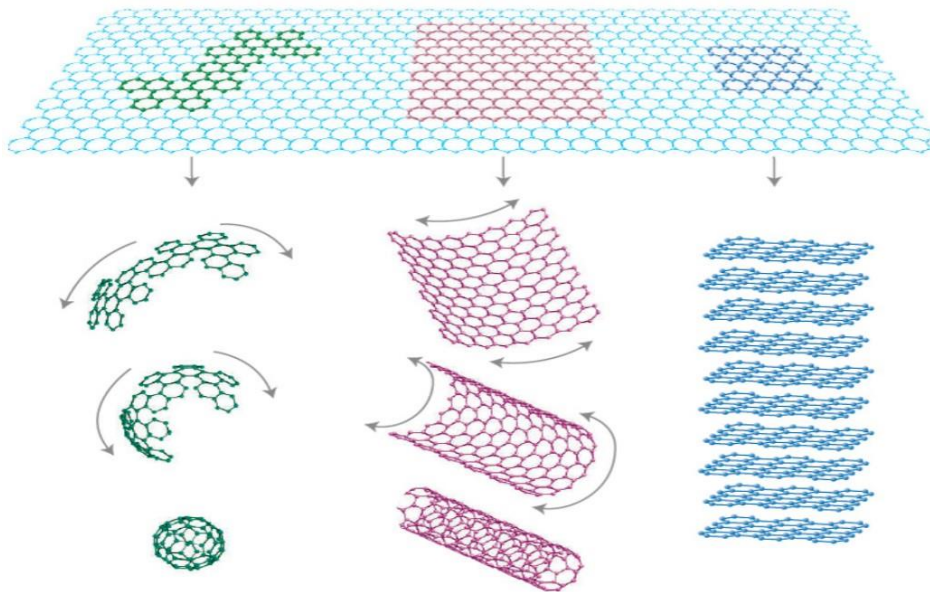

Figure 1.1 Fullerenes, carbon nanotubes and graphite structures in relation to graphene lattice [2]

Fullerenes

Fullerenes family includes many compounds with a hollow cage structure made of sp^2 carbon atoms; to be precise, since their arrangement is not planar, they can be seen as allotropes with hybridization between sp^2 and sp^3 [22]. They represent the oldest zero-

dimensional carbon allotropes. The first discovered fullerene was the C_{60} in 1985 [4]; it consists of 12 pentagons (which allow the curvature) and 20 hexagons, arranged in truncated icosahedron shape (the same of a football) [1]. Over the decades, many different forms of fullerenes have been synthesized, like C_{70}, C_{76}, C_{82}, and C_{84}, but also with lower carbon atoms (C_{20} is the smallest one) [15, 22]. The simplest production process for fullerenes involves the vaporization of a carbon source (generally graphite) by a laser irradiation or a plasma/arc discharge; other routes involve combustion processes. After vapour recondensation, multiple forms are usually produced, with C_{60} being the most abundant; the separation of single fullerenes can be done by liquid chromatography. However, the entire process still brings multiple challenges, and it is characterized by low yields [15, 22].

Fullerenes have been intensively studied due to their potential functionalization properties; Figure 1.2 offers a visive example of many functionalization achievable with those molecules. The advantages are manifold: for example, a better solubility in solvents or the modification of the electronic properties. Functionalized fullerenes have been exploited in photovoltaic and photochemical applications, but also in biomedical and non-linear optics fields [1].
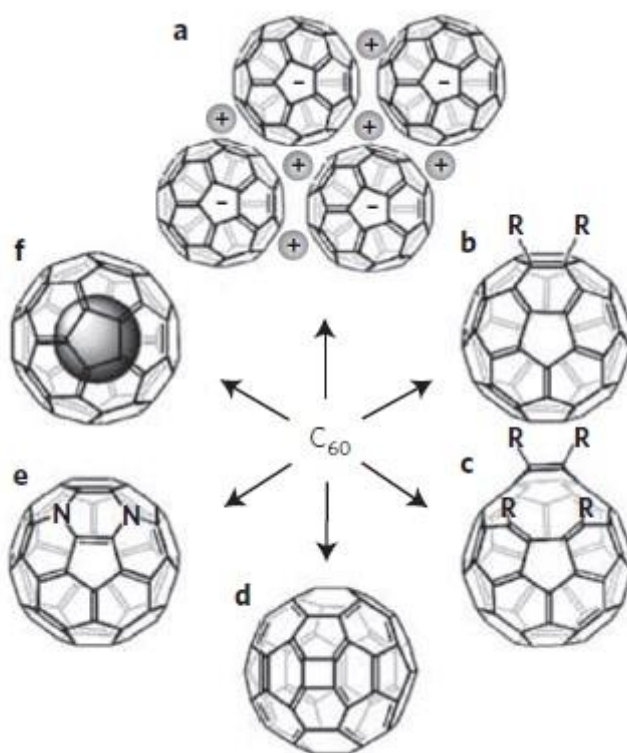

Figure 1.2 Possible functionalizations of C_{60}: a) fullerene salts; b) exohedral adducts: c) open cage fullerenes; d) quasi-fullerenes; e) heterofullerenes; f) endohedral fullerenes [1].

Carbon nanotubes (CNTs)

CNTs are ideally made by "wrapping up" a graphene layer in a tubular form, therefore their structure can be depicted as a slightly distorted sp^2 hexagonal lattice; as fullerenes, they have been synthesized before graphene itself [5]. They are usually classified based on the number of graphene layers concentrically rolled up: the main distinctions are between single-walled carbon nanotubes (SWNTs), double-walled (DWNTs) and all the other configurations, generically referred as multiwalled (MWNTs). The cylindrical shape highlights their fundamental one-dimensional structure: the aspect ratio of CNTs (length/diameter) can reach values of hundreds of thousands [15, 22]. The axial shape introduces a more confined direction with respect to graphene, and it is the cause of their unique electronic properties. Carbon nanotubes can be, in fact, metallic or semiconducting depending on the chirality of the tube; chirality is determined by the angle between the nanotube axis and the hexagonal lattice of graphene. Figure 1.3 helps to visualize the differences. The chiral vector (C_h) can be written as the sum of the two lattice vectors of graphene: $\mathbf{C_h} = n\mathbf{a} + m\mathbf{b}$. Armchair nanotubes are always metallic, while for zigzag or generic chiral nanotubes the electronic behaviour depends on specific values of chiral angle and chiral vector (for example, zigzag CNTs are metallic if n is an integer of 3) [15, 22]. The unidimensional covalent structure is also responsible for their high Young modulus (around 1 TPa) and a tensile strength up to 100 GPa: moreover, nanotubes are low density materials [2].

CNTs can be produced by different methods, for example: arc discharge between two carbon electrodes in an inert environment or with addition of specific gases (like He, CH_4) to influence the properties of the resulting nanotubes; laser ablation of a graphite target containing catalytic nanoparticles; chemical vapour deposition (CVD) on a
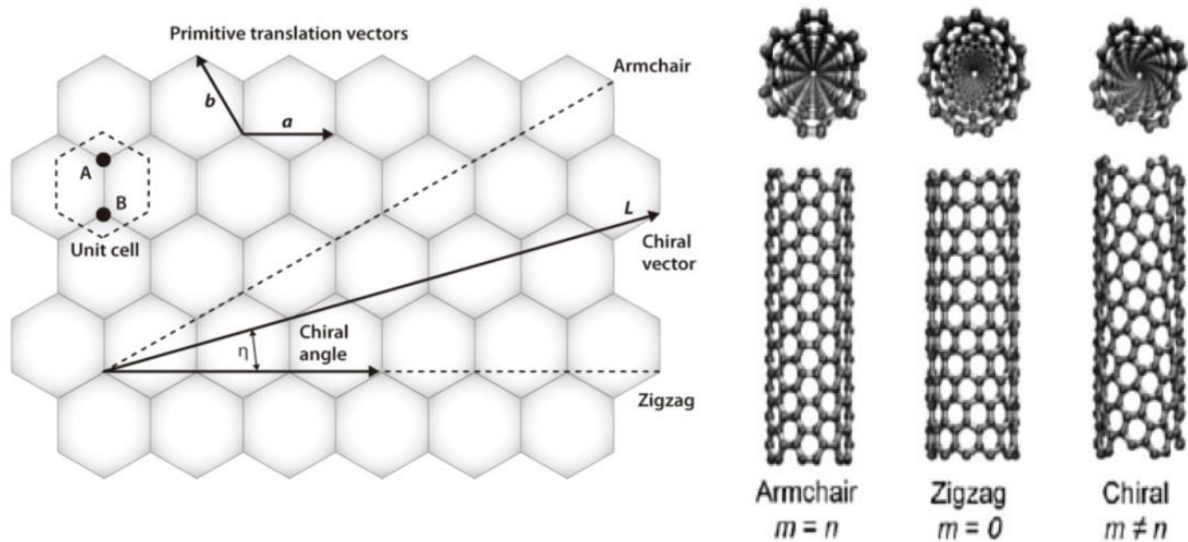

Figure 1.3 Graphene sheet with indication of chiral vector, chiral angle and orientation of specific chiral CNTs (left); types of single-walled carbon nanotubes (right) [15].

metal catalyst, usually performed exploiting methane, ethane and other hydrocarbons on Fe, Co, or Ni nanoparticles. The main aim regarding the production processes is to find a suitable way to precisely control the chirality, which is still very hard to achieve [22].

Carbon nanotubes have been exploited in numerous research field, from biomedical applications (drug delivery, biosensors) to optoelectronics (FETs); moreover, their superb mechanical properties have been exploited in composite reinforcement [2, 15].

Figure 1.4 offers an overview on the carbon allotropes broad family. As can be clearly seen, this brief section has only explored a little part of the possible carbon architectures.
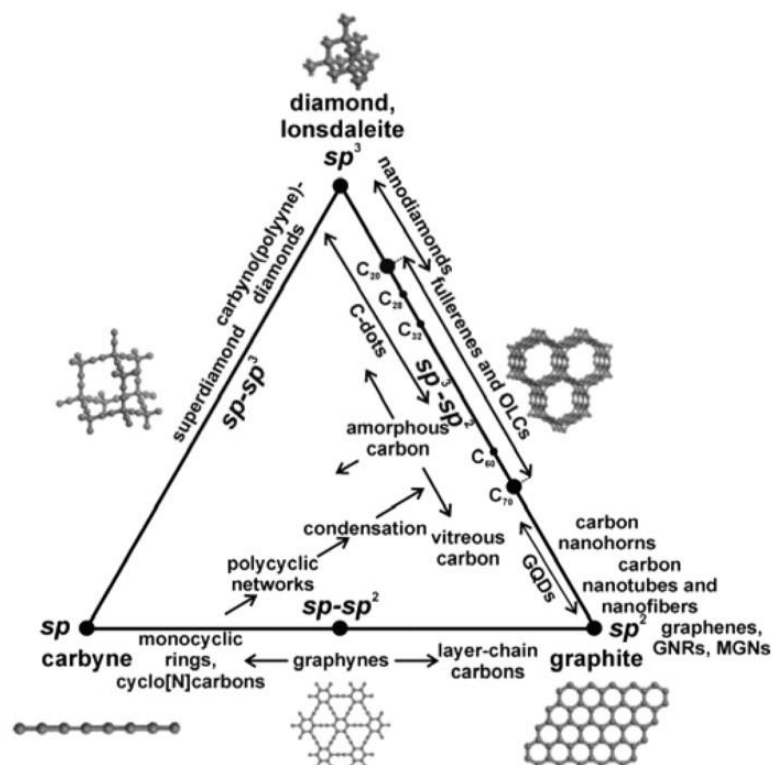
Figure 1.4 Carbon allotropes family, organized in relation to carbon hybridization [22]

1.2. Carbon atomic wires

The carbon allotropes described in the previous section were zero-, one-, two- and three-dimensional (or quasi-dimensional) structures made of carbon atoms with sp^2 or sp^3 hybridization (or a hybrid between them, as for fullerenes and CNTs). The remaining part of this chapter is focused on the description of structures made from the third existing hybridization of carbon, the sp structure. The presence of diamond and graphite, which are respectively the solid forms of only sp^3 and sp^2 carbon atoms,

has led to the pursuit of a solid entirely made of sp carbon atoms. The existence of this material is still debated [11]. However, the discovery of linear sp carbon structures in interstellar gases and meteorites [7-9], and the huge advancement in their synthesis techniques have kept high the interest on CAWs. As happened for the other carbon allotropes, the possibilities to exploit architectures with different dimensionalities and to integrate them in other systems, are the driving force in carbon atomic wires research. Here, an overview on the properties and on the synthesis methods of linear chains made only of sp-hybridized carbon atoms is presented. We will start with the infinite ideal model (also referred as *carbyne*) and we will end with the realistic finite sp-carbon chains.

1.2.1. Structural, physical, and vibrational properties

The simplest model that allows to describe electronic and vibrational properties of carbon atomic wires is an infinite carbon chain (*carbyne*) [23]. All the specific properties of finite CAWs can be then related to the carbyne description. The first important point to be considered is that a unidimensional sequence of carbon atoms can in principle possess two structures: one in which atoms are all connected by double bonds (*cumulene*), and the other one in which there is an alternating sequence of single and triple bonds (*polyyne*), as represented in Figure 1.5. However, due to delocalization of π-electrons, the real length of CC bonds in polyynes does not exactly correspond to carbon triple or single bonds, with the firsts being a little longer and the seconds being shorter [11].
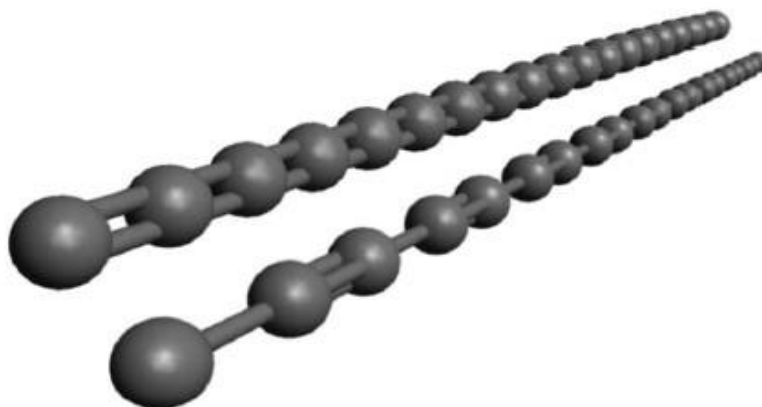

Figure 1.5 Cumulene and polyyne molecular structures [23].

The structural differences between cumulenes and polyynes are also reflected in the theoretical description (with a solid-state physics approach) of these two systems. Cumulene can be treated as a unidimensional crystal with one atom in the unit cell, while polyyne possesses two atoms per unit cell. Therefore, the first ones are metallic materials with a half-filled conduction band; on the contrary, polyynes are semiconductors, since they possess a valence band completely filled by electrons (Figure 1.6).
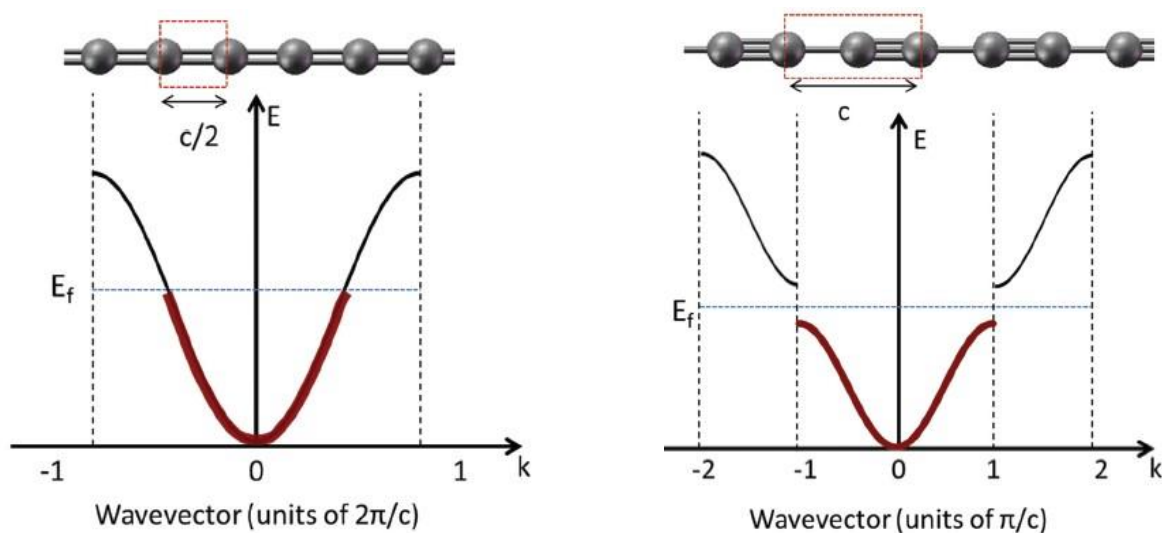

Figure 1.6 Molecular arrangement and corresponding electronic band structure for an infinite cumulene (left) and polyyne (right), according to a solid-state physics approach [11].

Vibrational properties are also different for the same reasons: a cumulene is simply a monoatomic infinite chain, and that implies the existence of only acoustic phonons. Polyynes, instead, possess two bonds with different strength, and this brings to the rise of optical branches in the phonon dispersion plot (Figure 1.7) [11, 24]. Those considerations are also important from an experimental point of view, since some characterization techniques (i.e., Raman and IR) are based on the material vibrational response (a more detailed discussion is present in chapter 1.3) [11].
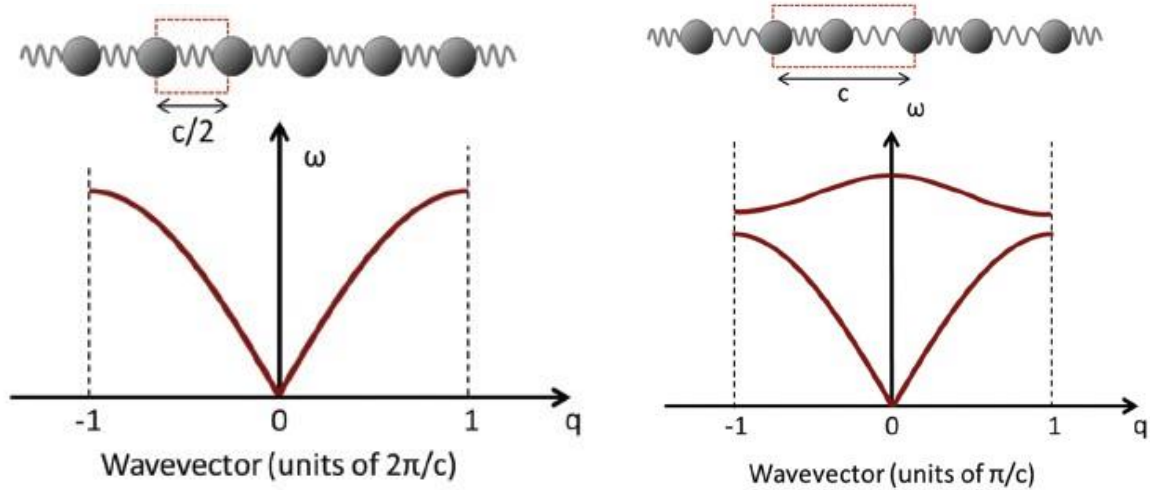
Figure 1.7 Molecular arrangement and corresponding phonon dispersion for an infinite cumulene (left) and polyyne (right), according to a solid-state physics approach [10].

Other differences are present between cumulenes and polyynes. The cumulene configuration has a higher potential energy, and due to Peierls distortion effects, an infinite cumulenic systems tends spontaneously to transform into a polyynic structure [11, 23]. This behaviour is true only if infinite chains are considered; in reality, CAWs are finite carbon chains, since it is impossible to synthesize infinite systems. Finite linear chains are terminated by various elements or chemical groups; the simplest endgroup is the hydrogen atom, but various terminated CAWs have been produced over the years, even with large bulky groups [25]. Thanks to endgroup effects, which will be better explained later, also a cumulene structure can be stabilized. A useful parameter for carbon atomic chains description is the bond length alternation (BLA), defined as the modulus of the difference between two adjacent bonds. For a perfect cumulene this value is 0, while, for polyynes, it is higher than 0. Higher BLA also means a less conjugated chain [11, 23, 24]. Moreover, BLA offers an important connection between the theoretical model of carbyne and size-terminated linear carbon chains. For a generic polyyne, BLA value depends on several factors, like the termination or the interaction with other elements in the environment; nevertheless, its properties can be deducted by considering an infinite ideal chain with the same BLA value. Figure 1.8 shows the effect of BLA on CAWs bandgap; of course, this parameter also affects the vibrational behaviour [11].
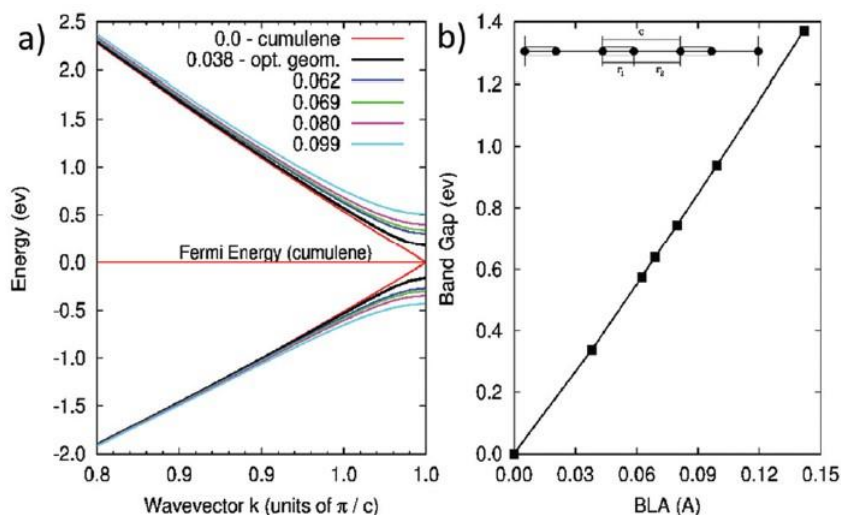
Figure 1.8 (a) Band structure of an infinite carbon atomic wire for different values of BLA (Å) (b) Band gap as a function of BLA [11].

Endgroup effects deserve a more detailed description, since they are fundamental in determining the properties of finite polyynes; in fact, the passage from the infinite model to real CAWs brings some issues. First, it has been demonstrated that Peierls distortion is relevant only for molecules longer than 52 carbon atoms; therefore, for shorter structures a cumulenic configuration can be possible [11]. The presence of a polyynic or cumulenic structure is mainly due to the chemical nature of endgroups; they influence the carbon hybridization, which then is reflected along the chain. For example, a hydrogen termination requires that a single C-H bond is formed at one end; consequently, the adjacent CC bond will be a triple bond and, in this way, a polyynic structure is formed (Figure 1.9, top). On the contrary, a vinylidene endgroup (>CH2) induces the formation of a cumulenic structure with subsequent double bonds (Figure 1.9, down). However, it should be said that for a finite cumulenic carbon chain the BLA value is still different from 0, even if it is very low compared to a polyyne with equal length. Moreover, a general trend for the BLA of short CAWs (both cumulenes and polyynes) is that for longer chains there is a reduction in the BLA, due to the increasing π conjugation; this behaviour is maintained up to the onset of Peierls distortion, which determines an asymptotic limit [11, 23]. Those simple examples are sufficient to describe the importance of the endgroups choice, since it deeply affects CAWs structure and, consequently, their electronic and vibrational properties. By properly tuning the length and the bond alternation, the bandgap can be controlled, influencing optical absorption and electrical behaviour [26]; moreover, it affects phonon dispersion and therefore the response to vibrational spectroscopic methods.
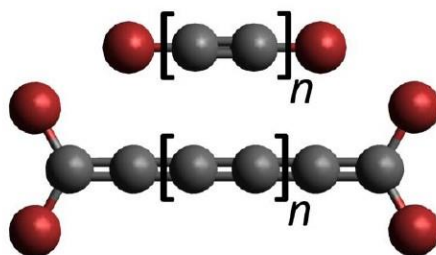
Figure 1.9 Endgroup effect in determining carbon wire structure:
hydrogen termination (top), vinylidene termination (bottom) [23].

Another important issue related to sp-carbon wires is their stability. They show a tendency towards crosslinking and formation of a sp^2 network, which is a more stable configuration [11, 23, 27]. Endgroups can play a role also in this field: for example, exploiting bulky groups, crosslinking interactions between adjacent chains can be prevented by steric hindrance. This effect allows to stabilize polyynes and synthesize longer chains [23]. The stabilization of polyynes terminated with smaller groups (like H-polyynes) can be performed in specific solvents (better if apolar [28]) or by embedding CAWs in polymeric matrices [11]. Moreover, it has been observed that silver nanoparticles solutions are functional in polyynes stabilization [23]. The huge interest in CAWs production and stabilization is due to their expected properties; theoretical predictions on carbynes have calculated an effective surface area of 13000 m^2/g (four times larger than graphene), and a Young modulus up to 32 TPa. Moreover, thermal conductivity has been estimated to be around 200 kW/mK for cumulenes and 80 kW/mK for polyynes; electrical transport is expected to be very high, showing a ballistic behaviour [23].

Other studies have focused on the integration of polyynes in other carbon systems (like nanotubes or complex graphene-like sp^2 structures) that are promising for stabilization and implementation of carbon wires in optoelectronic field [24, 27, 29].

1.2.2. Synthesis of CAWs

Production methods are fundamental for CAWs, because, as was explained in the previous section, both length and terminations of a carbon chain determine its properties. Several methods have been implemented over the years, and a common classification is between the so-called *chemical* and *physical* methods.

Chemical synthesis

This process exploits a series of chemical reactions to produce CAWs with accurate control. Generally, two different approaches are exploited. The first one consists in polymerization reactions, starting from precursors like acetylene or halides molecules

[11]. The main advantage of this strategy is in the possibility to obtain the synthetization with a single step; however, the polydispersity of obtained CAWs is usually high. Another approach consists in dimerization of ethynyl groups (the Glaser reaction); it provides a more accurate control over CAWs length and terminations, thus allowing a more consistent study on the effects of endgroups and chain length [11, 30]. The general stability is also increased. Over the years several end-capped polyynes have been synthesize, for example with alkyl, aryl, and metal terminations [12, 24, 31]; chain length has reached values higher than 40 carbon atoms [32]. However, the main drawback of chemical synthesis methods is related to the number and the complexity of the involved reactions, which often exploit dangerous solvents and require multiple purification steps [33].

Physical synthesis

Production of polyynes with physical methods consists in the generation of a carbon plasma, or vapour, which is then rapidly quenched; this procedure leads to the formation of a carbon atom clusters in an out-of-equilibrium condition [11]. Different techniques can be exploited for carbon vapour production and subsequent fast cooling (Figure 1.10); among them, laser ablation or arc discharge in liquid have proved to be very efficient in the polyynes production. They are cost effective procedures, offering a fast and relatively easy way to obtain carbon chains. Moreover, less armful solvents are used, and it has been experimental demonstrated that by changing the type of solvent different endcapped polyynes can be produced [11, 24]. The main drawbacks related to physical synthesis are the low concentration of synthesized chains and the presence of several unwanted by-products in the final solution; the first issue makes more difficult the characterization of polyynes (see chapter 1.3) while the second one is the main cause of their poor stability [28].Arc discharge technique consists in the
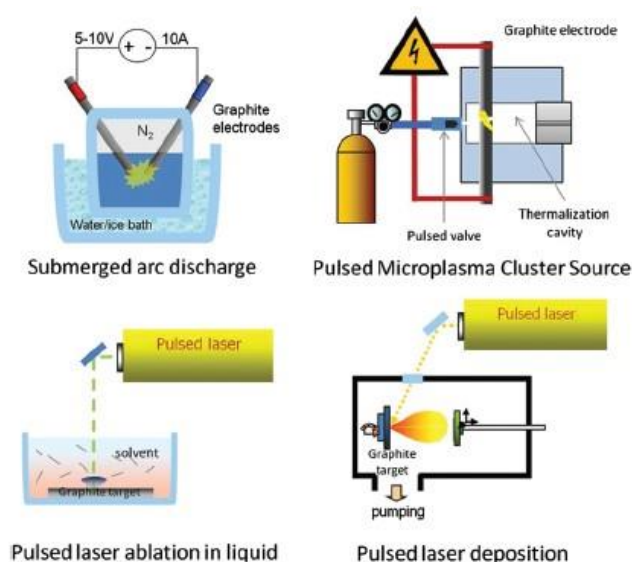

Figure 1.10 Examples of known physical methods adapted to synthesize CAWs [11].

application of a voltage difference between two electrodes and the subsequent generation of a direct current. It is a well-known procedure exploited also for production of other carbon allotropes, like fullerenes or CNTs [34]. The most adopted configuration for polyynes production is the Submerged Arc Discharge in Liquid (SADL); here, two graphite electrodes are placed in a solution (water or an organic solvent). A voltage in the order of 5-30 V is applied and the generated current is about 5-10 A. The Joule effect caused by the discharging process creates a plasma region in which the carbon vapour released from graphite is quenched by the surrounding solvent; endcapping atoms (usually hydrogens) are radical species coming from the dissociations of solvent molecules. In this way polyynes with different length can be produced [35]. The liquid environment also offers a better stabilization of the carbon chains with respect to procedures carried on in gas phase [36]. The most relevant contributions for polyyne production by SADL were made by Cataldo [33, 34, 36], who analysed the role of different organic solvents, and, by exploiting liquid chromatography, was able to determine the presence of specific size-selected polyynes.

Laser ablation technique involves a similar physical principle; in this case, the plasma region is generated by a laser beam on a target surface. Similarly to arc discharge, the adopted configuration for polyynes production involves the use of a liquid environment, defined as Pulsed Laser Ablation in Liquid (PLAL). The mechanism governing the formation of polyynes is not completely understood, but the work of Amendola *et al* [37] is helpful to describe the phenomena happening in the plasma region, highlighted in Figure 1.11. The first step is referred to the laser pulse penetration in the liquid; in this stage, liquid breakdown and scattering events must be avoided, and solvent should present a minimum absorption. The second step is related to laser pulse absorption at the target surface, which for polyynes production is generally made of graphite; when the laser hits the target, the onset of linear and nonlinear absorption processes is observed. Depending on the pulse duration, different effects are involved: mainly target photoionization and other thermal processes, like thermionic emission, vaporization, boiling, and melting. All these phenomena bring to detachment of ablated material, caused by multiple contributions: locally induced space-charge separation fields, electron-ion collisions, and thermal energy transfer. For a nanosecond (ns) laser pulse (the one exploited in this work) the thermal process is described as "explosive boiling": it consists in a homogeneous nucleation of vapor and liquid phase. The subsequent step is the confinement of the plasma plume above the target, thanks to the liquid phase. This causes the decreasing of the cooling rate and increasing the heating; the energy transfer towards target comes both from the laser and the surrounding plasma. The collapse of the plasma plume causes cavitation bubbles which contribute to more material detachment. Eventually, a chemical and physical steady state is reached. In these last two phases it should be

placed the formation of polyynes and of other nanomaterials, but it is still difficult to precisely define the subsequent growing steps [37].
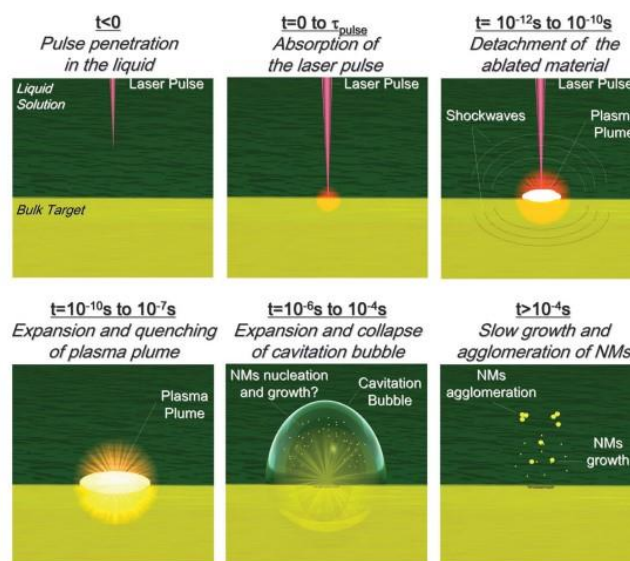

Figure 1.11 Sketch of the timeline of laser ablation, considering nanosecond pulses and with hypothesis on nucleation and growth of nanomaterials (NMs) [37].

For what concerns carbon atomic wires, their generation is due to the competition between two processes: polymerization by addition of carbon radicals and chain termination due to hydrogenation [38, 39]. An optimization of the ablation parameters is therefore crucial to obtain a high polyynes yield. Most of them are laser parameters: wavelength, fluency, spot dimension, pulse duration, and time of ablation. Moving towards the materials, graphite targets are the common choice for polyyne production, but there are some studies exploiting other carbon sources, like nanodiamonds [40]. Solvent plays a crucial role, because it can represent a further source of carbon atoms and it affects the lengths and terminations of produced CAWs; for example, some cyano (CN-) terminated polyynes have been found from ablation in acetonitrile [28, 39]. Solvent viscosity is also an important parameter: a higher value is related to longer polyynes production, due to the hindrance of crosslinking phenomena [41]. All these aspects highlight that PLAL (but in general all the physical methods) are very useful techniques for CAWs production, but their optimization is way far to be fully accomplished.

1.3. Characterization of carbon wires

This section describes the main characterization methods for CAWs. The investigation of carbon wires is often performed by exploiting light-matter interactions; characterization techniques can be divided in the ones dealing with light absorption phenomena (as the UV-vis technique) or in the ones related to scattering phenomena (Raman and SERS). Other methods are based on chemical processes, like High Performance Liquid Chromatography (HPLC), which is used for accurate collection of size-selected polyynes.

1.3.1. UV-vis absorption technique

UV-vis spectroscopy is a widespread technique for the investigation of several substances. The physical principle consists in the optical absorption of a light beam ranging from the visible to the ultraviolet range; the material interacts with the electromagnetic radiation and some of its electrons are promoted to higher energy levels. This phenomenon can only happen if the energy difference between the final and the initial electronic states (E_f - E_i) is equal to the energy of an incoming photon (E_{ph}); this simple rule is at the basis of any optical transition. Therefore, when the light beam interacts with the analyte substance, only photons possessing the same energy of permitted electronic transitions are absorbed, while the remaining ones pass through the material. For each wavelength, the ratio between the intensity of the transmitted light beam (I) and the incoming one (I_0) is called transmittance (T); transmittance is a number between 0 (complete absorption) and 1 (complete transmission). Absorbance (A) value is simply calculated from the transmittance by exploiting the equation (1.1):

$$A = -\log_{10} T$$

(1.1)

A UV-Vis spectrometer calculates absorbance (or transmittance) values for each incident wavelength, plotting the intensities of these transitions as a function of the photon wavelengths. The absorption values also give information on the concentration of analytes in solution. In fact, the Lambert-Beer law (equation (1.2) correlates the absorbance to the molar concentration (c) of the analyte:

$$A = \varepsilon c L$$

(1.2)

Where A is the absorbance, ε the molar extinction coefficient (cm^2/mol), L the optical path (cm) and c the molar concentration (mol/cm^3) to be determined.

Carbon atomic wires have been widely investigated by UV-Vis spectroscopy since they absorb light in the ultraviolet range (200-400 nm). The main absorbance peaks are related to the transitions between HOMO (Highest Occupied Molecular Orbital) and LUMO (Lowest Unoccupied Molecular Orbital) energy levels, corresponding to the

bandgap of a polyyne. The length of the carbon chain affects π conjugation, lowering the bandgap and therefore shifting the electronic transition at a lower energy (o higher wavelength) [35, 36]. Thus, longer polyynes absorbs at higher wavelengths. Moreover, also the endgroups play a role in absorption, due to their influence in the molecule vibronic properties and BLA [28]. As can be seen in Figure 1.12, for a fixed chain length, both methyl and cyano terminations cause a redshift of the absorbance peaks, if compared with H-terminated chains. In the end, by exploiting Lambert-Beer law, some hints on polyynes concentration in solution can be obtained.
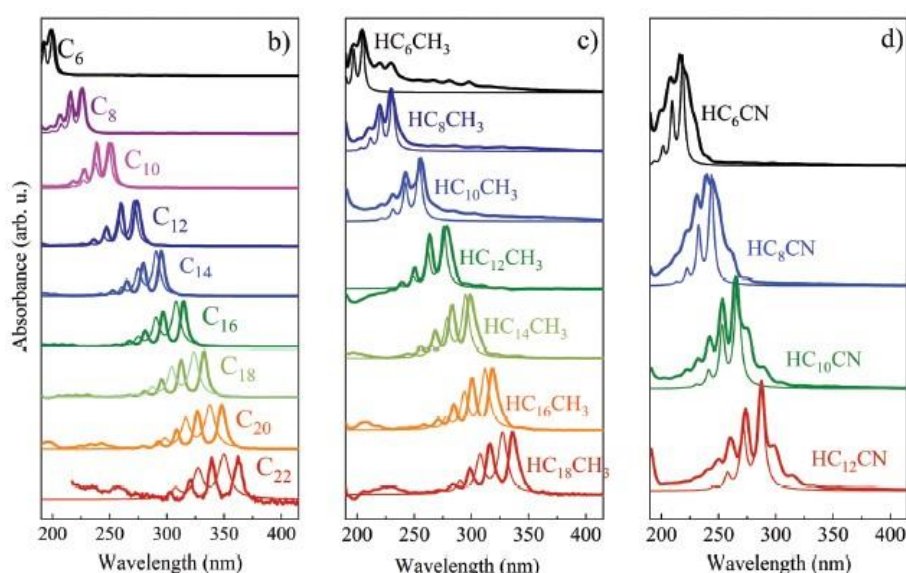
Figure 1.12 Normalized experimental (thick lines) and simulated (thin lines) UV-vis spectra of (b) H-polyynes, (c) CH3-polyynes and (d) CN-polyynes obtained after the ablation of a graphite target in acetonitrile [28]

1.3.2. Raman and Surface Enhanced Raman Spectroscopy

Raman spectroscopy is one of the most used techniques in carbon wires characterization. As the UV-Vis spectroscopy, also Raman is a technique that exploits light-matter interaction; however, in this case the vibrational response is indagated. The basic principle of Raman consists in the excitation of a sample by a monochromatic electromagnetic radiation (a laser beam); the beam causes the promotion of electrons to higher virtual states. After the excitation process, relaxation occurs in the sample through a radiative process; the instrument collects the scattered radiation, which is composed by a strong elastic contribution (a radiation with the same frequency of the incident one) and numerous inelastic signals. The origin of these signals can be easily visualized in the Figure 1.13. The elastic contribution, defined as Rayleigh scattering, is determined by the return of the electron to the original level occupied before

excitation. Therefore, the emitted energy is the same of the absorbed photon; this phenomenon is the most probable relaxation process, but it is not useful to obtain information about the analysed sample. However, there are some cases in which the electron returns to a vibrational level higher than the original one; the emitted radiation is at lower energy (or higher wavelength) and this contribution is called Stokes scattering. The last contribution, symmetric to the Stokes scattering, is the Anti-Stokes; in this case the electron was initially in a higher vibrational state before excitation, and then it returns to the ground level. The emitted radiation is at higher energy (lower wavelength). Quantum mechanical considerations, related to the distribution of electrons population in higher vibrational states, state that Stokes scattering is more probable than Anti-Stokes, therefore its signal is usually more intense; due to their symmetry, usually only the Stokes signal are analysed, while the elastic and the Anti-Stokes contributions are neglected. A Raman spectrum is a plot of the Stokes signals intensity versus the shift, in cm^{-1}, of the radiation with respect to the elastic contribution. Each shift value corresponds to the energy of a vibrational transition in the material; energies of the vibrational states depend on the molecular structure of the analytes, therefore the spectrum can be seen as a collection of peaks that represent the atoms arrangements and the chemical groups possessed by the analysed molecules.
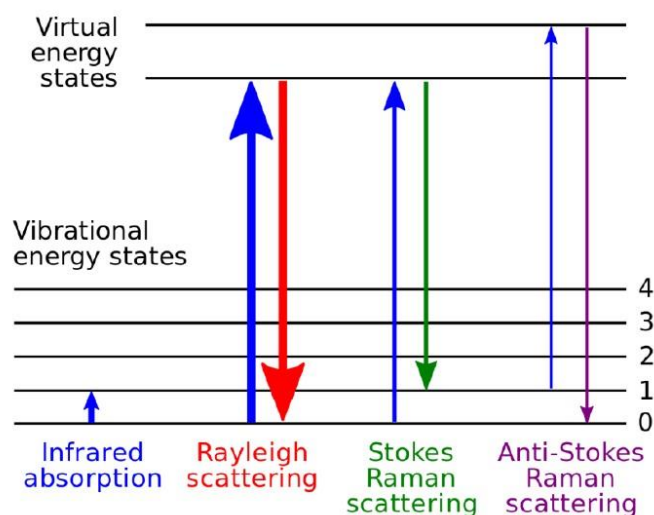
Figure 1.13 Sketch of the photons absorption and emission processes that generates Raman signals

Carbon allotropes have been widely investigated using Raman spectroscopy, which is helpful in distinguish the various hybridizations. Figure 1.14 summarizes the main peaks related to different structures. Among them, CAWs occupied a special position in the Raman spectrum, since they are the only allotropes presenting a sharp response in the 1800-2300 cm^{-1} region. Theoretical studies have characterized Raman response of polyynes and cumulenes starting from their respective theoretical infinite chains;

the most intense signal has been defined "effective conjugation coordinate" (ECC) mode and corresponds to the in-plane oscillation of BLA values [11, 42]. This is the characteristic peaks of CAWs observed in the 1800-2300 cm^{-1} region. In this region, for finite H-terminated polyynes, experimental observations have highlighted two main signals: the most intense, called α-line, related to the ECC mode, and a second minor band, called β-line, related to out-of-phase stretching. The first one is usually found at 2000-2200 cm^{-1}, while the second at 1800-2000 cm^{-1} [43, 44]. Both ECC mode wavenumber and intensity are found to decrease for higher chain lengths; this is because of π-conjugation, which grows with chain length, and it also explains why the ECC signal in finite cumulenes has a small intensity [45].
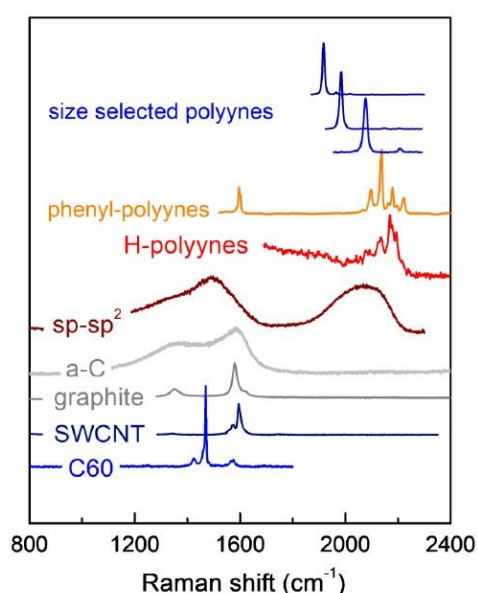
Figure 1.14 Raman spectra of various carbon allotropes

The main issue related to CAWs characterization by Raman spectroscopy is the detection limit of this technique. Low concentrated polyynes (under 10^{-3} mol/L) cannot be detected, and with physical synthetization methods the final concentration is in the order of 10^{-6} mol/L. Therefore, a more sensitive technique is needed for their analysis, and it is represented by Surface Enhanced Raman Spectroscopy (SERS).

With SERS there is an amplification of the sensitivity of Raman spectroscopy by several order of magnitude (up to 10^6) [11]. It exploits the interaction between analyte and plasmonic metallic nanoparticles (usually gold or silver). SERS response is the consequence of two complementary contributions; the first one is the local enhancement of electric field, due to the surface plasmon resonance effect at metallic nanoparticles. This local increment is higher if the laser excitation wavelength is closer to the characteristic plasmonic frequency of nanoparticles (which depends on the specific metal and particle dimension). The second contribution is defined as

"chemical enhancement" and can be exploited when the analyte creates a complex with the metal nanoparticles, favouring charge transfer; this brings an additional increase of the signal [46].

Polyynes have been widely analysed through SERS measurements [28, 39, 47-50], usually exploiting silver nanoparticles (but there are also examples with gold [51]); the choice of metallic enhancer is always done considering the employed laser frequency, to get closer to the resonance peak. Carbon wires have been mixed with nanoparticles colloids and huge enhancements in their response have been observed. Compared with Raman, SERS spectra possess broader and redshifted peaks in the characteristic ECC-region; moreover, there is the appearance of new signals at lower wavenumbers (below 2000 cm^{-1}). Several studies suggest that this behaviour is due to the interaction between polyynes and nanoparticles, which causes aggregation phenomena [49, 52]; BLA modification due to charge transfer [53] and formation of Ag-substituted polyynes [48, 50] are some of the proposed explanations. In any case, it is evident that both types of enhancement (electromagnetic and chemical) are present, which explains why SERS is so effective for polyynes detection; Figure 1.15 shows the huge difference between a SERS and a Raman spectrum for the same polyyne mixture.
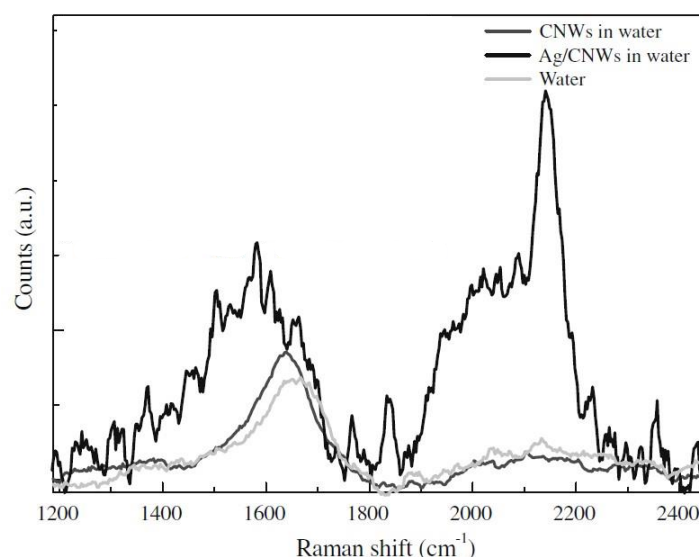
Figure 1.15 Spectra of carbon wires (CNWs) in water. Black line represents the SERS spectrum obtained with addition of silver nanoparticles colloid; dark grey line is the Raman spectrum of carbon wires. The light grey line is the Raman spectrum of water [50].

1.3.3. High-Performance Liquid Chromatography (HPLC)

High-Performance Liquid Chromatography (HPLC) is a technique employed for separation of chemical compounds. The procedure exploits two main elements: the *mobile* and the *stationary* phases. The first one is a liquid component which, after

solvent injection, dilutes the solution and helps the transport of analyte molecules through a porous column, inside which the stationary phase is present. The latter is solid substance, usually silica, (but also zirconia or alumina) which has been functionalized to promote selective interaction with the molecules injected; this functionalization usually consist in exploiting a polar or an apolar behaviour, in relation with the properties of the compounds to be separated. In this way, each molecule experiences a weaker or stronger interaction with the stationary phase, leading to a different elution time; separation is therefore achieved. A HPLC instrument can possess many chromatographic columns with various dimensions and stationary phases. Moreover, the mobile phase is usually a mixture of different solvents, which can be optimized in relation to the column and the analyte to be characterized; the volume ratio of the various solvents can be kept constants during all the analysis or can be modified following a programmed method. The HPLC apparatus is usually equipped with a UV-Vis spectrometer, which constantly analyses the liquid phase coming out from the column and can reveal the presence of a specific substance; knowing the elution time is fundamental to perform the collection of separated molecules.

Separation of CAWs with HPLC is crucial because with physical synthetizations methods only a mixture of polyynes with different lengths and terminations can be obtained. Size-separated polyynes are usually collected exploiting a reverse-phase configuration, consisting in a non-polar stationary phase and a polar mobile phase (common for apolar molecules like carbon chains). This procedure has been extensively applied in several works [28, 34, 35, 47, 48]. Generally, shorter polyynes are eluted first, but when different end-capped species are present, the interaction with the stationary phase could make difficult to stabilize *a priori* a reliable elution sequence of chains with different terminations. However, thanks to the characteristic UV-Vis footprint of each polyyne, molecules can be recognized and collected (Figure 1.16); of course, there could be issues related to the rapidity of the elution or the presence of unwanted by-products which disturb the absorption spectra.
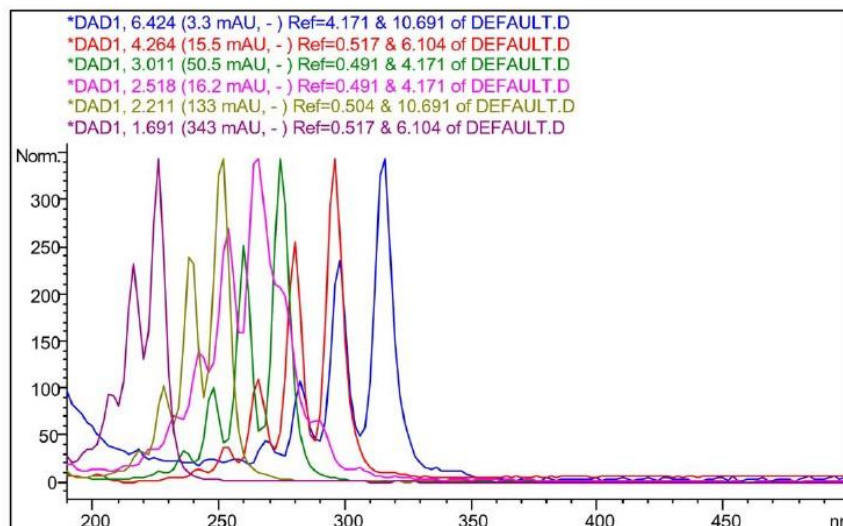
Figure 1.16 Normalized UV-Vis spectra of size-selected polyynes performed with a Diode-Array Detector (DAD1) equipped in HPLC apparatus. Retention times (in minutes) are reported (first value after DAD1): longer polyynes absorb at higher wavelengths and are eluted later than shorter ones. [34]

1.4. Carbon wires nanocomposites

Over the years, CAWs have been also exploited in the production of polymer nanocomposites. A composite material is usually made from a matrix and a reinforcement filler; the first one provides a stable and uniform environment that stabilizes the filler, which is added to improve specific properties, like mechanical strength, but also thermal and electrical conductivity. Nanocomposite are obtained when very small fillers are used; this ensures an extremely higher surface area between the reinforcing material and the matrix, thus increasing filler effects. Among the wide family of nanocomposites, polymer-carbon structures have gained attention, due to the incredible properties of carbon nanostructures and the versatility of polymer matrices in terms of production and shaping [54, 55]. Synthesis routes are essentially three: in situ polymerization, solution mixing, and melt blending. The first one consists in the dispersion of the filler inside a solution containing monomer or oligomer; polymerization is then subsequently activated by opportune methods (like heat treatment or UV irradiation). Solution mixing consists in the addition of the filler in a polymer solution, usually performed with mechanical stirring or ultrasonication to promote a homogeneous dispersion. Lastly, in melt mixing the filler is added to the melted polymer by exploiting high temperature and shear forces (an extruder is often used) [55]. The main properties of carbon nanocomposites depend on crucial parameters like filler dispersion and eventual alignment, along with the matrix morphology. A more detailed description of procedures exploited to have a good nanofiller dispersion, and the benefits that this could bring, can be found in the

literature, together with several examples concerning also other carbon allotropes (like CNTs, graphene, fullerenes) [54, 55].

For what concerns carbon atomic wires, their implementation in polymer matrices has been the focus of several studies. The reason to exploit CAWs-polymer integration is due to the possibility to stabilize polyynes inside the polymer matrix; this prevents the interaction between chains and therefore hinders the crosslinking effect, that causes degradation of sp carbon structures [56]. Moreover, CAWs possess remarkable mechanical, electrical, and thermal properties [23], and the perspective of using them as functional nanofillers for enhancing the properties of the polymeric matrices is an appealing topic.

The use of metallic nanoparticles during nanocomposite production offers a simple and efficient detection method for polyynes dispersed in a polymer matrix. In several works, polyynes have been produced *via* physical methods (PLAL or SADL) and integrated in polymeric solutions with the addition of silver or gold nanoparticles [51, 56]. The production of metallic nanoparticles is usually performed by chemical (reduction processes) or physical methods (ablation of a metallic target). When polyynes and nanoparticles are blended in a polymeric solution, the aggregation phenomena previously described take place and polyynes are stabilized in nanoparticles agglomerates by formation of complexes [48, 49, 52]. After deposition and evaporation of the solvent, the polymer nanocomposite is formed. Polyynes can be detected inside the matrix by exploiting SERS effect: polyynes mixtures or size-selected chains can be investigated, and their signals intensity has been evaluated even after several weeks, confirming the stability conferred by the polymer matrix [51, 56]. In a previous work [57], polyynes were synthesized directly by laser ablation in solutions with different polymeric concentrations (a procedure defined *in situ synthesis*); then a silver nanoparticles colloid was added. The main results of this work have been reported in Figure 1.17.

This chapter has highlighted the importance of carbon atomic wires, both from theoretical and a practical point of view. The possibility to exploit their interesting properties demonstrates why it is important to work on polyynes production, characterization and integration in more complex systems.
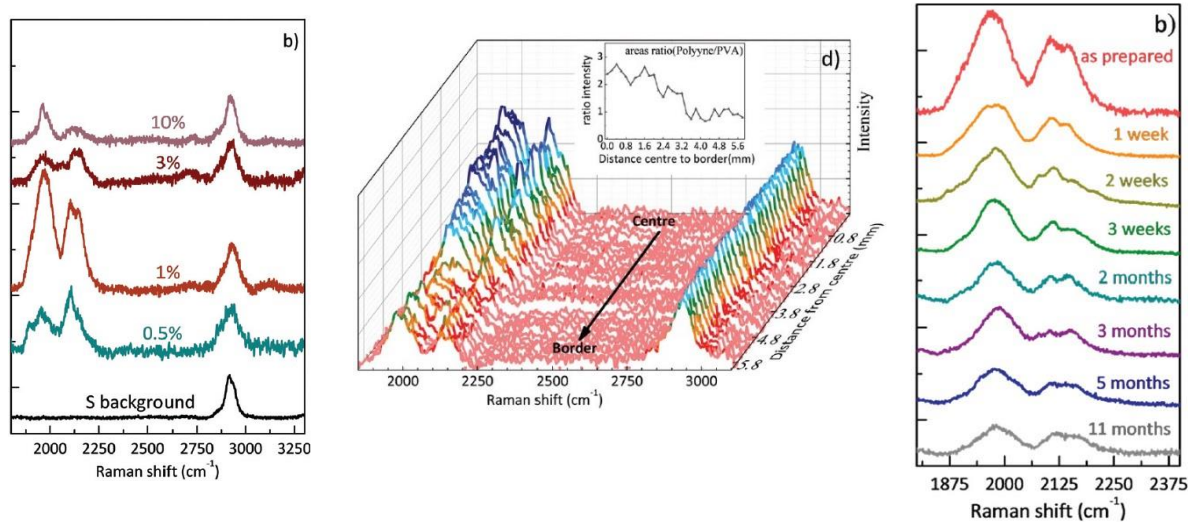
Figure 1.17 Analysis performed by Peggiani *et al* [57]: SERS spectra of Ag/PVA/polyynes nanocomposites with varying PVA concentration in solution (left); normalized SERS spectra of a nanocomposite, taken from the centre to the border of the sample (centre); evolution in time of a nanocomposite SERS spectra (right).

2   Electrospinning

One of the objectives of this work is to produce polymeric fibers with nanometric dimension. The most used method to achieve that is the electrospinning technique. In this chapter a brief overview of this process is provided. First, a description of electrospinning setup and its physical principles is provided, followed by a section in which the relevant parameters and their effect on fibers morphology are presented. Then, some techniques for nanofibers morphology observation are described and the last section is about an overview on potential applications for electrospun nanofibers.

2.1.   Introduction

Electrospinning (contraction of "electrostatic spinning" [58]) is a well-known technique which allows the production of very thin polymeric fibers, with diameters that can be lower than 100 nm. Due to its simple design, reduced cost, and huge versatility, it is a widespread process that enable the synthesis of numerous 1D architectures with high surface-to-volume ratio [59]. The history of electrospinning is peculiar: even if some of its main features were observed during the XVII and XVIII centuries, this phenomenon was firstly studied by Lord Rayleigh only at the end of XIX century and the first patent was deposited in 1934, in the US, by Formhals. Despite this, it was only during the '90 that the academic attention for this technique started to grow exponentially thanks to a mix of factors: the work of several research groups (in particular, the Reneker group), the increasing interest for nanotechnologies, and the availability of new and more powerful microscopes [59, 60]. Since that decade, the number of publications concerning electrospinning applications have been increasing at a fast pace (Figure 2.1) [61].
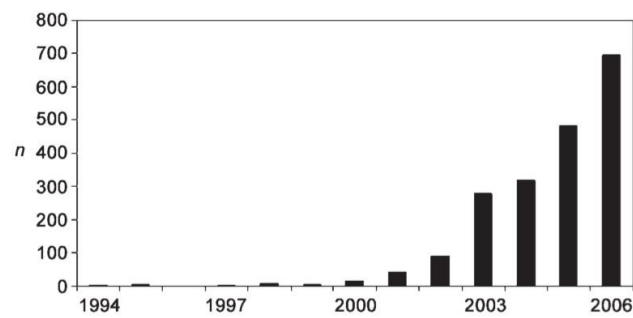
Figure 2.1 Number (n) of scientific publications and patents per year
(1994–2006) with the keyword "electrospinning" [61]

One of the main advantages of electrospinning is its simplicity: through the application of a high potential difference between a liquid solution and a conductive surface, a liquid droplet is electrified and elongated to form a thin fiber that is collected on a proper substrate. Electrospinning is usually performed starting from a dissolved polymer in a specific solvent, but also a melted polymer can be used as liquid precursor, if it is not too viscous. The instrumental apparatus can be divided into three main components [59-62]:

- A spinneret, which often consists in a metallic needle with a diameter in the order of hundreds of microns. It is usually placed at the end of a syringe containing the polymeric solution. To maintain a constant flow rate of the liquid solution, the syringe's piston is moved by a mechanical system.

- A high voltage power supply, which should be able to reach a potential in the order of tens of kV. The typical apparatus uses direct current, but also alternate current is feasible.

- A conductive collector (usually metallic), which act as a counter electrode and needs to be grounded. The collector itself can be the surface upon which fibers are deposited, but in general it is a support for the appropriate substrate, which can be either conductive or not. A practical example of a non-conductive substrate is glass, that is often used to observe spun fibers at the optical microscope.

The collector itself can be of different types and can be grouped into two major categories: static and dynamic. With static collectors, the deposition of the fibers on the surface is irregular and the result of the electrospinning process is a material made of random fibers. By using dynamic collectors, the orientation of the spun fibers can be better controlled, although a final irregularity is still present due to the intrinsic instability of the process. The typical setup can be placed in horizontal and vertical

direction (both in a top-to bottom alignment or in a bottom-to-top one, even if the choice is not insignificant due to gravity effect) (Figure 2.2) [59, 61].
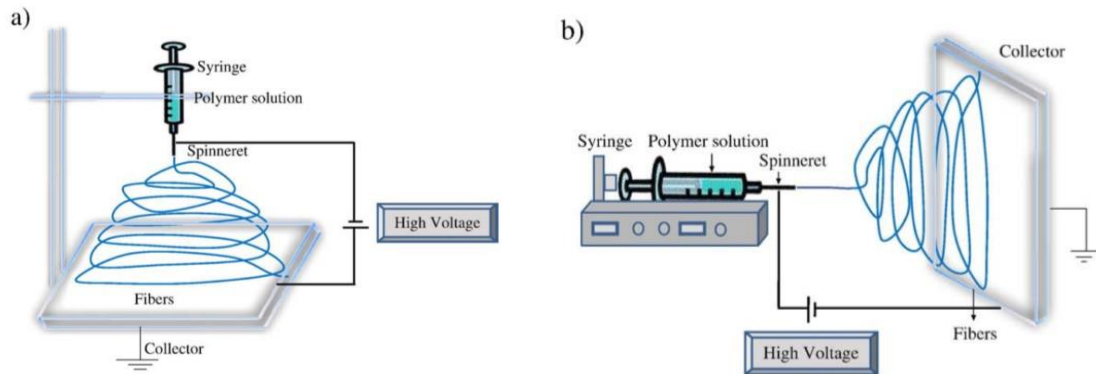
Figure 2.2. Schematic diagram of different electrospinning setups: (a) typical vertical setup and (b) horizontal setup [59]

The description of the physical principle behind electrospinning is not obvious because it involves electro-fluid-mechanical issues. The process itself can be divided into several subsequent steps (Figure 2.3). First, the polymeric solution is extruded from the spinneret and forms a little droplet at the tip that is charged, due to the applied potential difference. The drop is subjected to two major forces: the repulsion force between charges in the liquid and the external electric field present between the spinneret and the collector. As the electric field increases, the drop starts to elongate
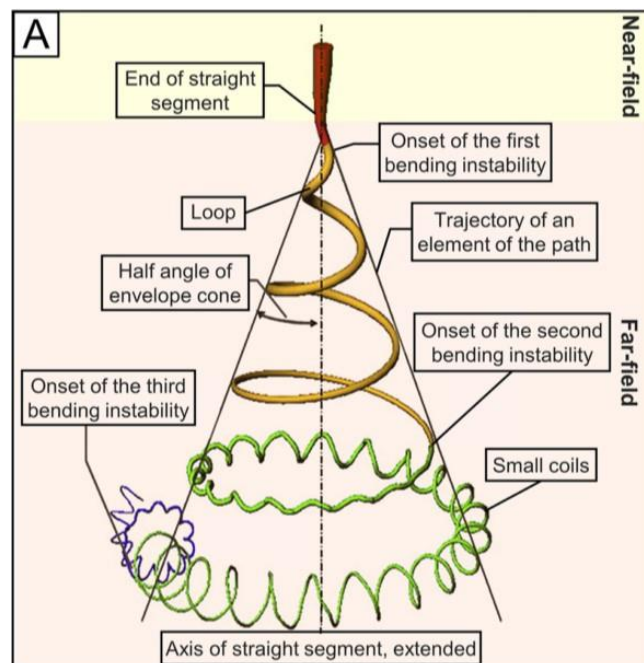
Figure 2.3. Diagram showing the path of an electrospun jet [60]

and form a characteristic conical shape known as Taylor cone. At a certain point, these two contributions overcome the surface tension and a jet is ejected from the cone: the polymeric solution is stretched by the strong electric filed and the jet becomes thin and straight. However, the charge repulsion effect is still present and it causes the rise of different instabilities. The most relevant one, the whipping instability, causes the bending of the jet at a very high frequency (it can be appreciated only with high-speed photography, as can be seen in Figure 2.4); this phenomenon, due to the stretching and acceleration of the fluid, enables the formation of very thin fibers. Meanwhile, the solvent present in the solution evaporates (or, with melted polymers, it starts to solidify) and at the end of the process a random disposition of nanometric fibers is achieved upon the collector [60, 62, 63].
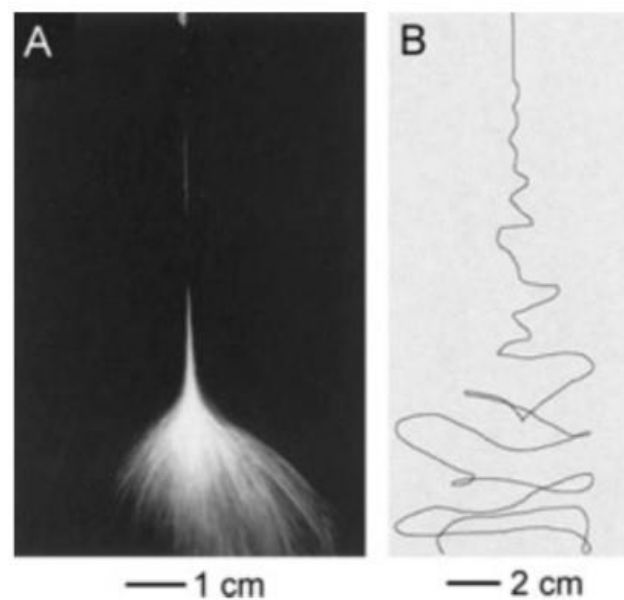
Figure 2.4. Photographs illustrating the instability region of a liquid jet electrospun from an aqueous solution of PEO. The capture time is on two different scales: A) 1/250 s, and B) 18 ns, respectively. The path of the jet shown in B has been traced to improve the visibility [62]

Other instabilities are present during the jet elongation. For example, the ones who cause splaying of the filament, which is another effect that could contribute to the formation of fibers with very small diameter [63]. Axisymmetrical instabilities are responsible for the formation of beads, regions with enlarged dimension which are the most common defects of a non-correct setting of electrospinning parameters; their formation is due to surface tension working in contrast with the jet elongation. Lastly, the Rayleigh instability leads to the breakup of the jet into droplets and the formation of characteristic pearl-necklace arrangements [61]. A more solid physical and mathematical approach to describe all the interactions presented can be found in the literature, but it is out the purpose of this brief introduction [58, 60, 64].

Several examples of polymers that can be electrospun are present in literature [58-60, 62]. A typical grouping is between natural and synthetic materials. Some natural polymers are collagen, fibrinogen, chitosan, silk, cellulose acetate, gelatin, which are often implemented for biomedical applications due to their biocompatibility and other properties that will be described in section 2.4 [59]. The group of synthetic polymers includes different categories: for example, water-soluble polymers (polyvinyl alcohol (PVA), polyethylene oxide (PEO), polyacrylic acid (PAA), etc. [61]); materials soluble in organic solvents (polymethyl methacrylate (PMMA), polystyrene (PS), polyvinyl chloride (PVC), etc.); biodegradable synthetic polymers (poly(lactic-co-glycolic acid) (PLGA), polycaprolactone (PCL), poly(lactic acid) (PLA)); and others [59].

For what concerns solvents used for electrospinning, the most common are: alcohols, dichloromethane, chloroform, dimethylformamide (DMF), tetrahydrofuran (THF), acetone, dimethyl sulfoxide (DMSO). Water is usually used only for polymers that cannot be dissolved in organic solvents (e.g., PVA), because its high dielectric constant doesn't make it a good solvent for electrospinning [60].

2.2. Influencing parameters

Considering that electrospinning process is strongly influenced by instabilities, it is important to have a control over several parameters to obtain nanofibers with required dimensions and morphologies. These parameters are usually divided in three main categories: solution, process, and environment [59].

2.2.1. Solution parameters

Viscosity: it is one of the crucial parameters for obtaining defectless fibers. If the viscosity is too low, surface tension becomes the dominant factor and it causes an agglomeration of the jet toward a more spheroidal shape: this leads to the formation of beads with various shapes (Figure 2.5). However, if the viscosity is too high, the liquid will not flow easily through the spinneret hindering the continuity of the process. Therefore, there is a range of optimum values of viscosity within which continuous fibers are formed. Inside this range, fibers diameter increases as the viscosity rises. The value of viscosity for a polymer solution depends on multiple factors, such as polymer concentration and molecular weight, but also on an environmental parameter like temperature [58, 59].
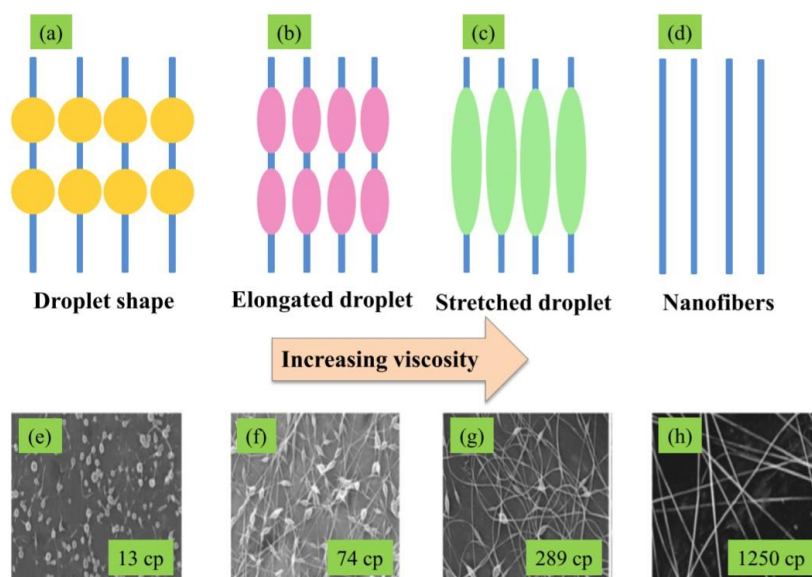
Figure 2.5. Morphology variations of PEO electrospun nanofibers at different
values of viscosity: (a–d) schematic and (e–h) SEM micrographs [65].

Polymer concentration: this parameter is strictly related to the former one since an increase of polymer mass in the solution leads to an increment of the viscosity. Thus, also in this case, a low amount of polymer in the solution causes the formation of beads. As the concentration increases, beads pass from spherical to spindle-like shapes until the generation of continuous and uniform fibers is achieved. The same considerations made for a highly viscous solution are valid for a elevate polymer concentration: when a critical value is reached, defective fibers are formed due to non-continuous feed of material and, eventually, due to the solidification of the liquid
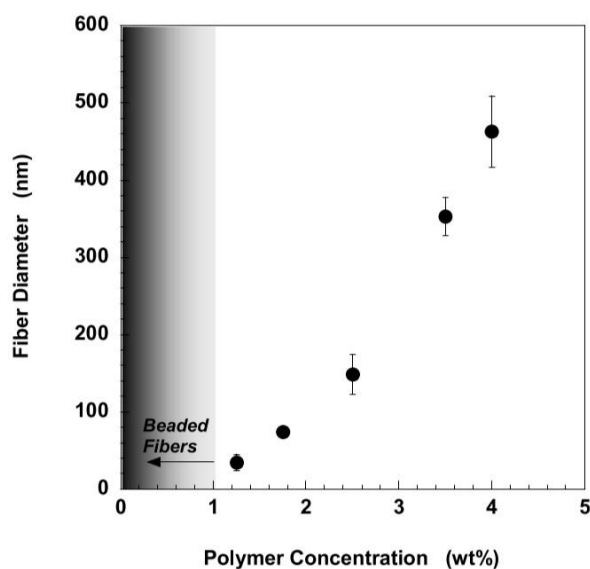
Figure 2.6. Polymer concentration effects on the diameter
of electrospun PLLA (MW: 300 K) fibers [66]

solution at the needle tip. Moreover, the diameter grows with the increment of concentration (Figure 2.6) [58, 59, 65, 66].

Molecular weight (MW): for electrospinning, polymers with high molecular weight are usually exploited since they are most likely to grant the desired viscosity. Also in this case, it is observed that, increasing the polymer's MW, the resulting electrospun fibers pass from defective to continuous and beadless; also, by increasing the MW there is an increase in the average diameter [59].

Molecular weight is linked to the number of entanglements between polymer chains. It is interesting to report that all the considerations made for these first three presented parameters can be integrated by looking at the behaviour of the entanglements in a polymer solution. Shenoy *et al.* [67] proposed a semi-empirical approach based on the calculation of the entanglement number in solution to obtain a model for an *a priori* prediction of fiber morphology. They applied this model to several polymers; Figure 2.7 shows the results obtained for polystyrene dissolved in THF.
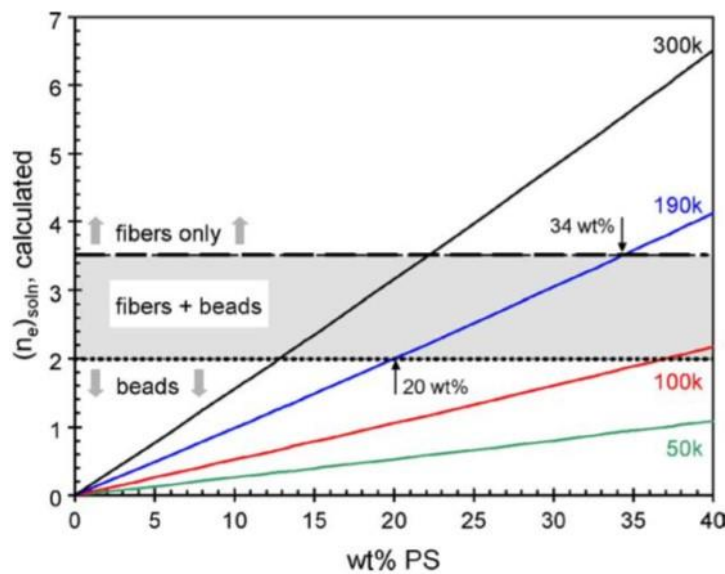
Figure 2.7. Plot of the calculated entanglement number $(n_e)_{soln}$ as a function of concentration for PS/THF system. Each line represents a different average molecular weight (MW): 50, 100, 190 and 300k. Arrows indicate the onset of fiber formation (20 wt%) and complete fiber formation (34 wt%) for 190k sample [67].

Solvent: it is important because it affects morphology, structure, and other fibers properties. Each polymer possesses adequate solvents for electrospinning. The first condition is, of course, that the polymer itself is completely soluble in each of them.

Some other properties usually required for solvents used for electrospinning are good volatility and a moderate boiling point [59]. Volatility is an important factor because it is necessary that all the liquid phases evaporate before reaching the collector. Low volatile solvents cause formation of beaded fibers in which the liquid is still visible at the microscope. However, highly volatile solvents could cause jet drying at the needle tip and so they are not feasible for electrospinning [59, 65]. Solvent affects also other relevant solution parameters, like surface tension and charge distribution; for this reason, the conductivity and the polarity of the solvent are important properties to be considered [65].

Surface tension: it is strongly dependant on the solvent composition rather than the polymer concentration [58]. This parameter works against the elongation force during the spinning; therefore, in general it is beneficial to have a low surface tension to prevent the formation of defects. Moreover, a low value permits to perform the electrospinning with a reduced electric field (thus, lower applied voltage) [59]. However, there can be some cases in which electrospun fibers are obtained without defects by exploiting a solvent with a higher surface tension [68]. Therefore, also in this case there is a window of optimal values, whose width is related to the other parameters [59].

Conductivity: depends both on the solvent and polymer used. An increase in this value causes the growth of the surface density of charges in the liquid drop at the needle tip. That brings to a higher electrical repulsion and the stretching effect, due to the applied electric field, is enhanced; this results in fibers with smaller diameter. On the contrary, formation of beads is observed if the conductivity is too low [59].

If the polymeric solution needs to be more conductive, a simple and often used strategy is to add few percent in weight of salts, like KH_2PO_4, NaH_2PO_4, and $NaCl$ [59]. This procedure brings more charges in liquid and therefore increases the electrostatic force from the electric filed, with all the benefits already explained (more uniformity and thinner diameters, Figure 2.8). However, highly conductive solutions show a wide instability due to the decreasing of the tangential electric field along fluid surface, which at a certain point doesn't allow anymore the proper formation of the Taylor cone. This phenomenon can lead to a broad diameter distribution [59, 65]. It is noteworthy to underline that the effects of bringing more charges in the solution are not equivalent to the ones of increasing the applied electric field [61], which will be discussed in the next section.
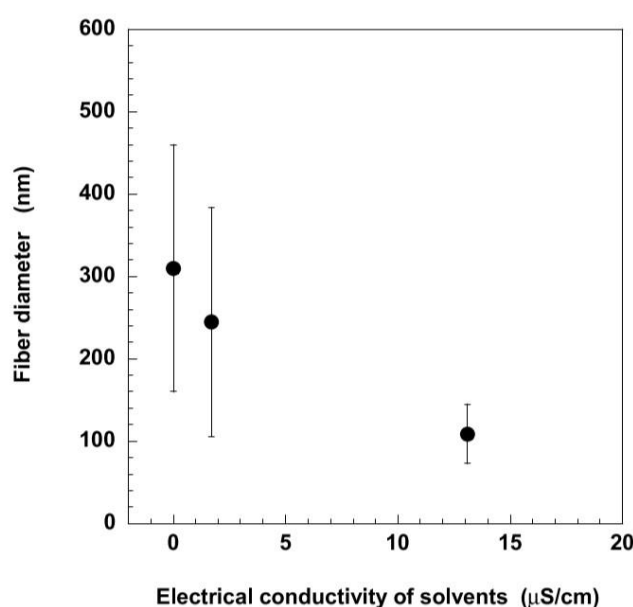
Figure 2.8. Solution conductivity effects on the diameter
of P(LLA-CL) (70/30 wt%) fibers [66].

2.2.2. Process parameters

Applied voltage: it is a crucial parameter for electrospinning since it is necessary to reach a threshold value of applied potential to allow the onset of the spinning process [59]. However, there is a debate around the effect of an increasing applied voltage on the nanofiber's morphology. Some studies show that with a growth of the potential, the stretching effect acting on the liquid jet is enhanced, obtaining thinner fibers. Other studies present the opposite result, with several explanations. First, a stronger electric field could cause a larger fluid ejection from the needle and an increase in the jet width, therefore larger diameters are obtained [58, 65]. Moreover, a higher voltage causes a change in the shape of the liquid droplet, with a decrease in Taylor cone's size, which is related to a higher instability of the jet (Figure 2.9): eventually that leads to the formation of beads and other irregularities in the fibers [62, 65]. Hence, the effects of applied voltage variations are not obvious, and the final fiber morphology is the result of the influence of the applied potential on other parameters, like jet shape, feed rate and elongation force. This effect is also dependent on distance between tip and collector and on polymer concentration. For example, Tan *et al* [66] have shown that for low polymer concentrations the voltage effect is negligible, while it becomes significant with higher values of polymer mass in the solution (Figure 2.10).
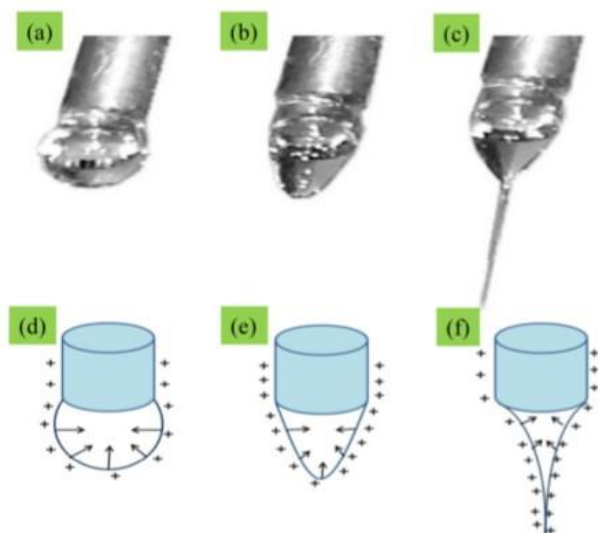
Figure 2.9. (a–c) Digital images showing deformation of the PVP droplet under the influence of increasing electric field. The cartoon (d–f) shows the mechanism of the effect of charges on the polymeric droplets [65]
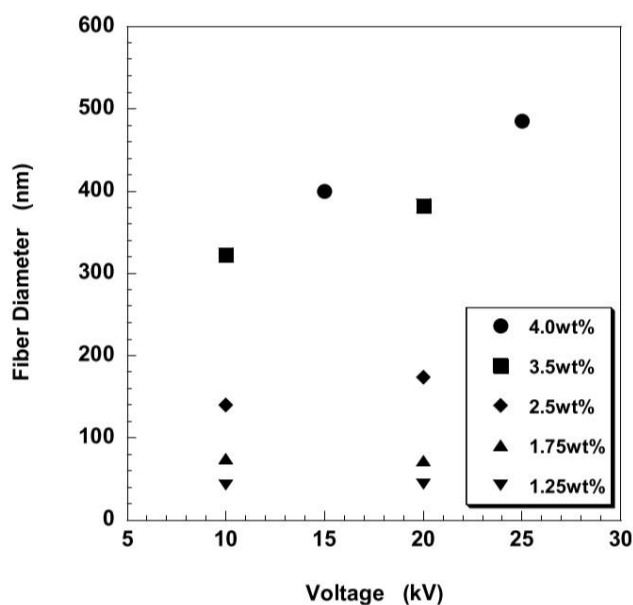
Figure 2.10. Applied voltage effects on the diameter of PLLA (MW: 300 K) fibers electrospun from solutions with different polymer concentration [66].

Flow rate: low feed rate is more advantageous for electrospinning because it allows solvent evaporation to be properly completed before the polymer reaches the collector [59]. An increase in the flow rate leads to an incomplete drying of the spun solution, resulting in larger diameters. With a rate higher than a critical value, beads, unspun droplets, pores, ribbon-like defects, and other irregularities are formed [65]. Similar as

before, Tan *et al*. [66] have shown that, also in this case, the flow rate effect is negligible for low polymer concentrations (Figure 2.11)
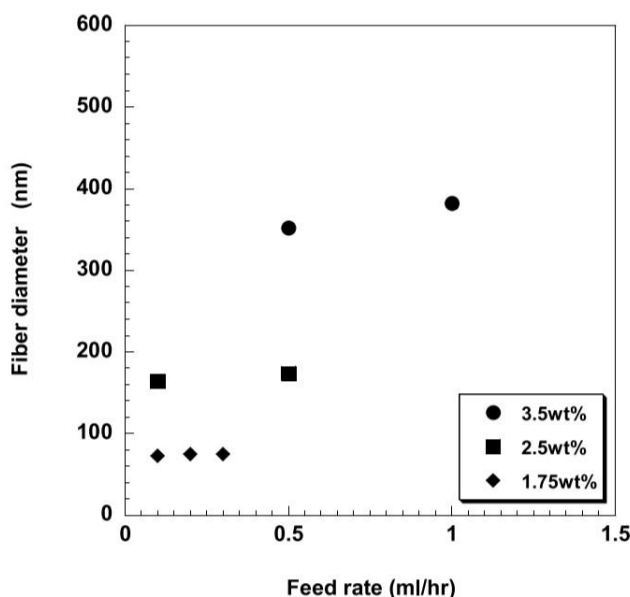
Figure 2.11. Volume feed rate effects on the diameter of PLLA (MW: 300 K) fibers electrospun from solutions with different polymer concentration [66].

Tip to collector distance: it is strictly associated with the previous point. A minimum distance is necessary to allow complete solvent evaporation, otherwise beads are easily formed. A higher distance implies also a more effective stretching of the fibers, therefore thinner diameters. Anyhow, this parameter is not as significant as the ones previously described [59, 65].

Types of collectors: in a standard electrospinning setup, as the one described in the previous section, the nanofibers are collected in a random mat because the liquid jet instability doesn't allow an ordinate motion during the stretching phase. The obtainment of aligned nanofibers can be important for several application, for example in the fabrication of electronic and photonic devices, in which the spatial control is crucial [62].

Several studies have implemented collection techniques to obtain aligned nanofibers, and some of these approaches are discussed here.

   1. High-speed rotating cylinder/drum (Figure 2.12)

Due to its simple configuration, it is one of the most used collectors to obtain almost parallel fibers. The rotating surface takes-up the incoming fibers and the rotation effect helps the alignment. One simple requirement is that the surface speed of the rotating

drum must be similar to the jet one, otherwise the fibers could be collected in a random way (if cylinder speed is too low) or the continuous jet could break (if it is too high) [58].
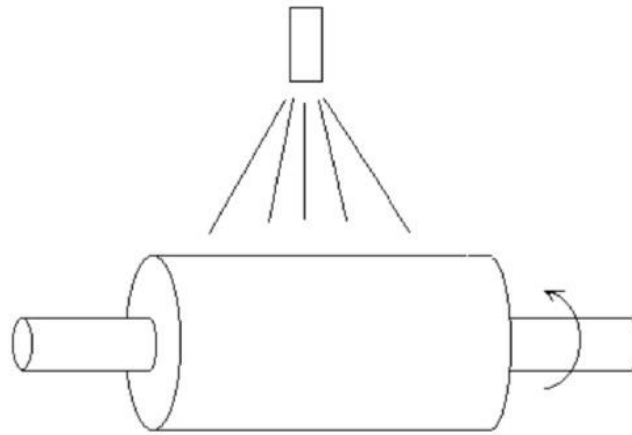
Figure 2.12. A schematic representation of a classical
rotating collector [58].

2. Wheel with a sharp edge (Figure 2.13)

It is similar to the rotating drum, but it exploits a different effect. In this configuration, the main driving force is the concentration of the electric field at the edge, which brings the stretched fluid at the wheel tip. The nanofibers are collected in a small area but the residual surface charges on the polymer create a relevant repulsion and help them to keep a distance between one another. The rotating movement promotes the alignment [58].
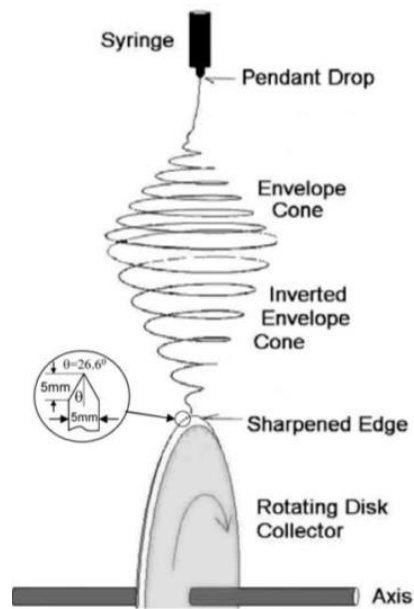
Figure 2.13. A schematic representation of the sharp-edged
wheel setup [58].

3. Split electrodes (Figure 2.14)

In this configuration, two conductive collectors are placed in parallel, with a void between them. This disposition alters the electric field in the region; there is a rise of field lines directed perpendicular to the collectors. Polymeric fibers, during the deposition, follow this new electric field orientation; eventually, an array of aligned nanofibers perpendicular to collectors' edges is generated. One of the advantages of this technique is the possibility to transfer the aligned fibers on other substrates and even to collect single fibers, useful for specific devices [62].

Figure 2.15 gives a summary of the most relevant solution and process parameters, highlighting their main effect. They are divided into two major groups, the first including factor affecting the jet elongation, and the second including parameters related to the mass of polymer available at the needle tip. This schematization is, of course, simplistic, since many elements influence the morphology in different ways, but it is useful to give a general overview.
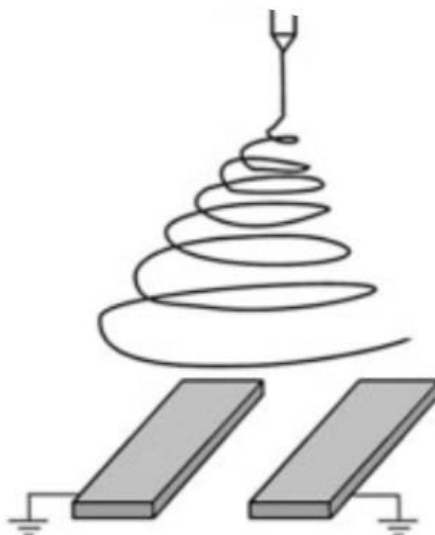
Figure 2.14. Schematic illustration of a setup for the alignment of electrospun nanofibers exploiting split electrodes [62].
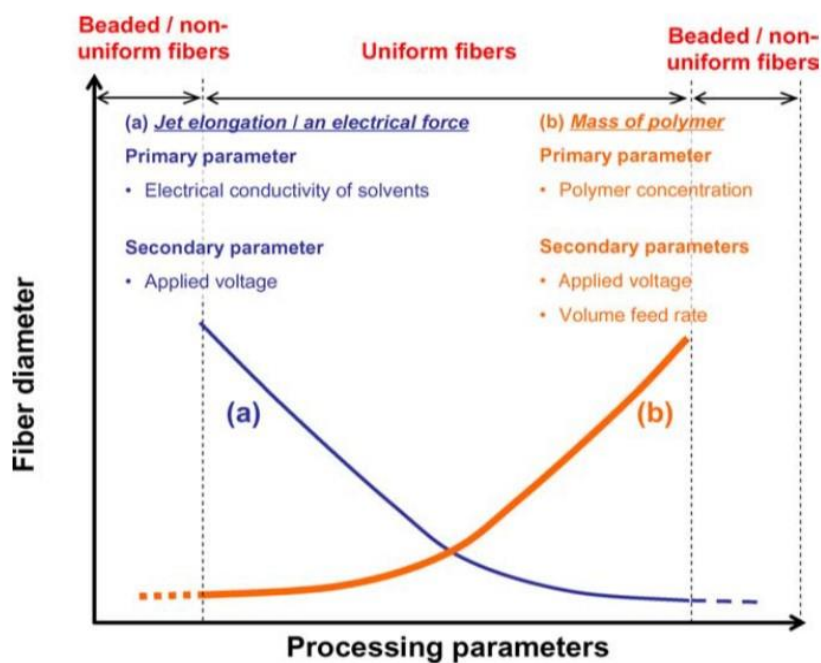
Figure 2.15. Graphic representation of the effects that different parameters have on nanofibers diameters and morphologies: (a) jet elongation/an electrical force (affected by electrical conductivity of solvents, applied voltage), (b) mass of polymer (affected by polymer concentration, applied voltage, volume feed rate) [66].

2.2.3. Environmental parameters

Temperature: it gives two principal contributions. First, a temperature growth leads to a viscosity decrease, since they are inversely proportional [59]. Second, temperature accelerates the rate of solvent evaporation. Both these effect causes a decrease in fiber diameter [58].

Relative Humidity (RH): it affects the evaporation of the solvent. For a low value of humidity, the drying process is faster and sometimes this can be a problem if the evaporation is too rapid that solidification happens at the needle tip. On the contrary, a too high value of relative humidity could lead to broader diameter distribution and formation of defects [59, 65]. Moreover, the type of polymer influences the behaviour when RH is high: for hydrophobic polymers the formation of pores was observed, because of the nonsolvent behaviour of water [69].

Pelipenko *et al* [69] studied the evolution of fibers diameter with the growth of relative humidity for PVA, PEO and their blend with other polymers. They found out that, at low RH, nanofibers were thicker with a homogeneous size distribution, while at high RH they were thinner and more disperse. For PVA nanofibers, starting from 4% to 70% of RH, the average diameter decreased from 667 ± 83 nm to 161 ± 42 nm, with beads present at 70% HR (Figure 2.16). For PEO, beads started to appear even at 50%HR, but still the average diameter followed a decreasing path.

	Relative humidity [%]	Average fiber diameter [nm]	RSD [%]
A	4 ± 1	667 ± 83	12
B	10 ± 1	550 ± 72	13
C	20 ± 1	445 ± 63	14
D	30 ± 1	349 ± 54	15
E	40 ± 1	258 ± 54	21
F	50 ± 1	174 ± 40	23
G	60 ± 1	161 ± 42	26
H	70 ± 1	$74 \pm 99*$	134*
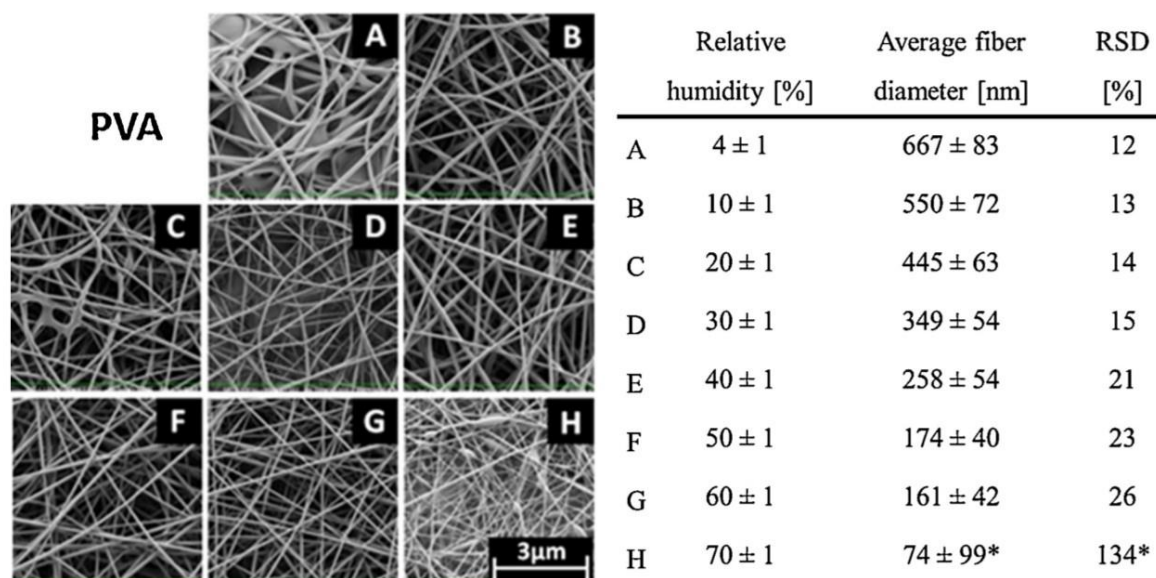
Figure 2.16. SEM images of PVA electrospun fibers (left) and data regarding average fiber diameter, fiber diameter relative standard deviation (RSD) and RH (right). Nanofibers with bead morphology are indicated with an asterisk [69]

2.3. Techniques for nanofibers observation

The previous sub-chapter contained several examples of critical parameters which influence the morphology of electrospun nanofibers. Since quality need to be verified, in this section the most relevant geometrical characterization techniques are presented [58, 59]. The main properties that are measured with these processes are: average diameter and its distribution, orientation and morphology.

The simplest instrument that can be implemented is the optical microscope. It is a rapid and simple technique and, therefore, usually it is performed right after the electrospinning process to have a rough evaluation of the fiber's quality. The type of microscope available determines which substrates can be placed on the collector. If the instrument works in transmission of light, the substrate needs of course to be transparent: a common choice is to use glass. On the contrary, for a microscope working in reflection, the choice should be made considering the reflectivity of the substrate and the obtainable contrast with the fibers sample. A magnification of 20x or 50x could be useful to appreciate nanofibers distribution density on the substrate surface, and to notice big defects (larger beads can be pointed with no difficulty). With a higher magnification, like 100x or 150x, smaller defects, especially in regions with multiple overlaying fibers, can be observed; at this level a qualitative impression of the diameter distribution can be made.

A more relevant technique is scanning electron microscopy (SEM). It is still a quite quick procedure to observe geometrical properties of fibers (Figure 2.17) and, moreover, it has the advantage of requiring samples with a small surface area [59]. The crucial requirement to be satisfied is the conductivity of the sample: since, in general, nanofibers made from polymeric solutions are poorly conductive (except specific cases of spun fibers from conductive polymers), the substrate needs to be conductive. Fibers can be collected, for example, on a small piece of silicon or aluminium. With SEM, it is possible to reach hundreds of thousands of magnifications, up to a nanometre scale of resolution; this is more than enough to observe single nanofibers clearly, and to measure their diameter with precision. Collecting several diameters from different fibers, it is possible to build a correct statistical distribution of diameters.
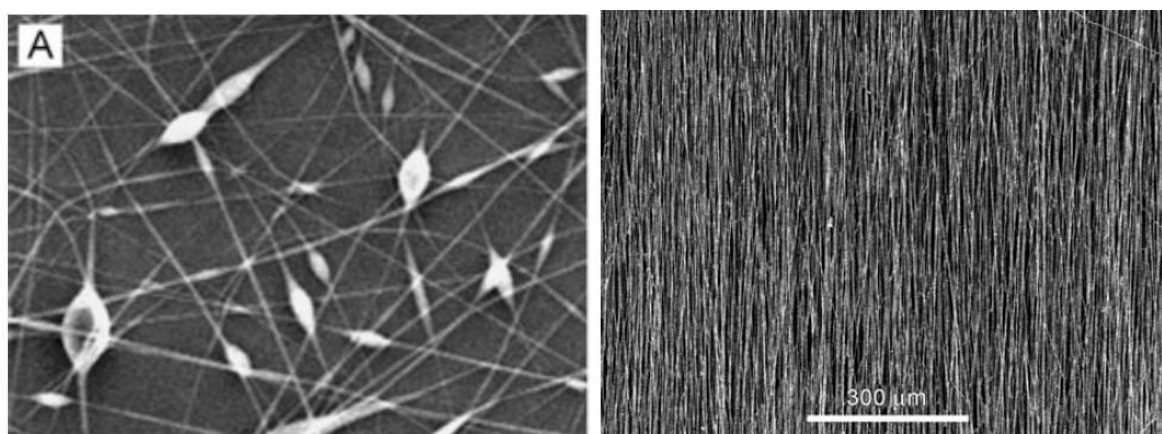
Figure 2.17. SEM images of PVP nanofibers with visible beads (left) [62] and of a planar nonwoven composed of parallel PLA nanofibers (right) [61]

One major drawback of SEM is the inability to see inside the analysed materials, therefore another powerful instrument often used to observe nanofibers morphology is transmission electron microscopy (TEM). This technique is implemented when there are some other materials dispersed inside the fibers and their distribution must be checked (Figure 2.18, on the left). Another advantage of TEM compared to SEM is the possibility to use also not-dried samples, in principle even defective nanofibers can be observed under TEM directly after spinning [58].

The last instrument briefly cited is atomic force microscope (AFM). It allows to measure fibers diameter with an extreme accuracy (Figure 2.18, on the right [70]), but its major drawback is related to the working condition which are slower than the other techniques presented. AFM can also measure surface roughness of single nanofibers [58, 70].
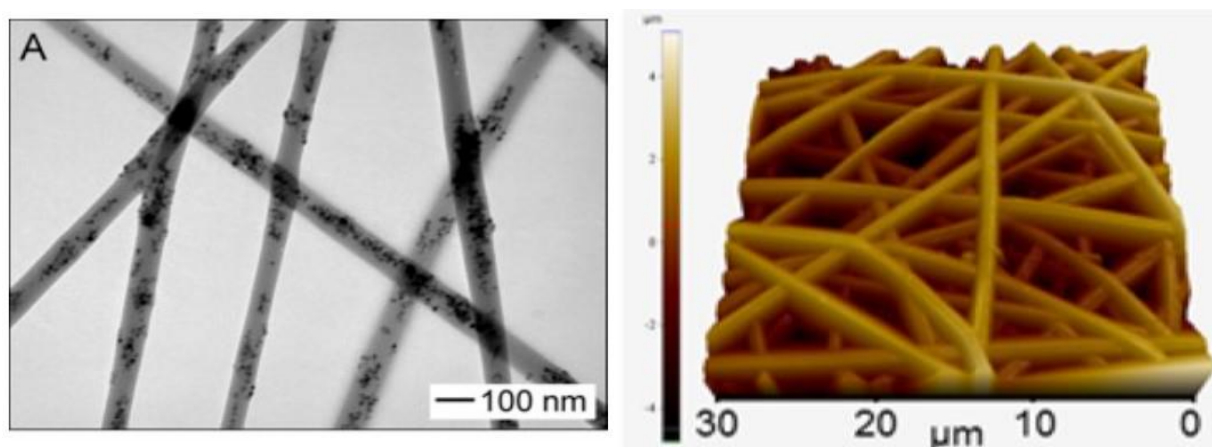
Figure 2.18. TEM image of PVP nanofibers whose interiors had been filled with iron oxide nanoparticles (left) [58] and AFM image of a PLLA fibers random mat (right) [70]

2.4. Applications

Electrospun nanofibers, as was discussed in the introduction, have obtained great attention during the past decades due to their advantageous properties. Thus, over the years, they have been tested in different fields and they have proven to be suitable for many applications. In this section, a brief description of these applications is illustrated, dividing them into areas of interest [59].

1. **Tissue engineering applications**:

Tissue engineering is a relevant field of research that combines several branches of knowledge, including material science. The role of biocompatible materials is crucial, and one of the main challenges is to obtain the best material to mimic the complex 3D structure of tissues that needs to be replaced [62].

Nanofibers are ideal candidates for this role because they can be obtained from biocompatible and biodegradable polymers, and they possess a three-dimensional porous structure which can be engineered to be used as scaffold matrices. These substrates can promote cell-matrix and cell-cell interaction, favouring cellular migration and proliferation (Figure 2.19) [59, 61].
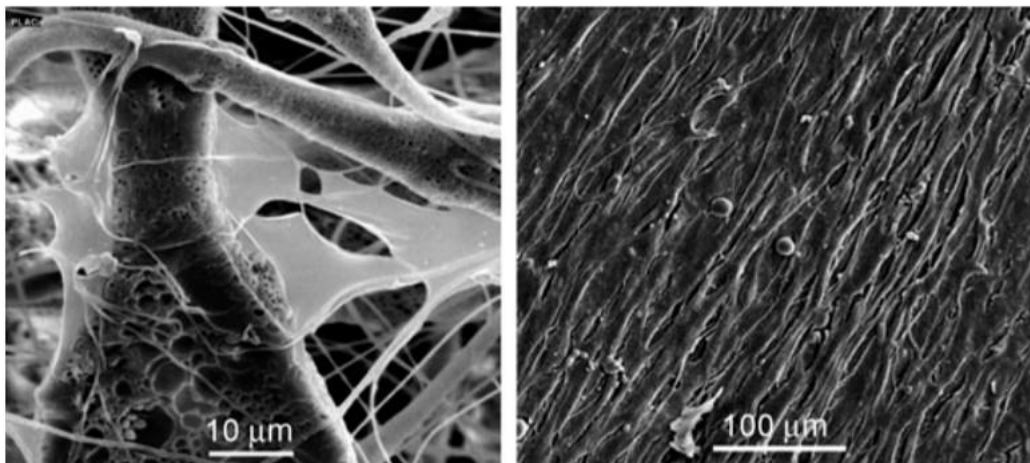
Figure 2.19. SEM images of stem cells seeded onto a PLA scaffold (left) and of oriented cell growth on a scaffold of alligned PLA fibers (right) [61].

Electrospun nanofibers, thanks to the high surface-to-volume ratio and their porosity, are promising also for wound dressing applications. A biodegradable polymer network, deposited onto a burn or an injury, helps the normal formation of skin. The porous structure is fundamental to maintain a balanced exchange of liquid and gases with the external environment while preventing the entering of bacteria. It has been observed that the risk of scarring, using electrospun dressing, is reduced with respect

to more conventional practices [61]. Moreover, one of the main advantages is that the polymer can be directly spun onto the wounded skin (Figure 2.20) [58].

Finally, one last application related to tissue engineering is drug delivery. Also in this case, the large surface area is the relevant property which makes electrospun nanofibers a serious candidate for this application [59]. Drugs can be loaded in the nanofibers (acting as a carrier) in different ways: in a particle form, attached onto the nanofibers or incapsulated inside a tubular structure; with a configuration in which both drug and carrier can be nanostructured, that could lead to an interlaced configuration of fibers or to a blend of the two components [61].

Figure 2.20. Application of nanofibers for
wound dressing directly on the skin [58]

2. **Filtration and protection:**

Nanofibers possess a remarkable filtration efficiency due to their architecture. They can trap with no difficulties particles with dimension lower than 0.5 mm; by charging them, it is possible to improve filtration efficiency by working on electrostatic attraction [59]. Moreover, the use of organic or inorganic fillers during the electrospinning is common nowadays to improve the functionality of the nanofibers, making them able to collect various substances [60].

In the field of individual protection, the ability to filtrate chemical substances makes nanofibers ideal candidates for protection clothing. An engineered nanofiber mat could be able to neutralize dangerous substances and, at the same time, it can be permeable to air and water vapour, which makes the material breathable [58, 62].

3. **Sensors:**

The filtration ability of nanofibers could be used to make them very efficient sensors; coating them with a specific medium allow to obtain molecular detectors [58]. The large surface area available helps to absorb more analyte's molecules, enhancing the sensing ability. The large variety of spinnable polymers and the different architectures obtainable could lead to a use of fibers as electrochemical or biochemical sensors [59]. Some examples are nanofibers functionalized with nanocarbon composites, like carbon nanotubes, graphene and graphene quantum dots: their general working principle is related to the modification of the nanofibers electrical properties once the analyte is adsorbed [71]. Another common functionalization process regards the use of metallic nanoparticles, like silver or gold. By embedding them into nanofibers matrix or just depositing on the nanofibers surface, it is possible to exploit their plasmonic behaviour; SERS measurements enable the detection of various organic and inorganic substances even at very low concentration [60, 72, 73].

4. **Energy generation applications:**

It is possible to obtain conductive fibers mats by exploiting different routes. Nanofibers containing nanocarbons have demonstrated to possess some interesting electrical properties, especially when carbon nanotubes are embedded inside the fibers; however there are some concerns related to nonuniform dispersion of fillers, which limits the improvement [71]. Another filed of research is related to the electrospinning of conducting polymers. One of the most investigated is polyaniline (PANI); since it is poorly soluble in many common solvents, several attempts have been made to exploit combinations with spinnable polymers, like blends with PEO or poly(ε-caprolactone) [74]. However, one of the main drawbacks is the decrement of conductivity, thus there is still ongoing research to find the most suitable blend and configuration (for example, some experiments were done on core-shell architectures). In general, the potential applications for conductive nanofibers are broad, covering many fields like optoelectronics (nanowires, LEDs), photovoltaic devices, micromachines (sensors, actuators), photo-responsive materials [59, 63].

5. **Composite and textiles applications:**

Traditional fibers, like carbon and glass ones (which usually possess a micrometric dimension order), due to their superior properties in terms of mechanical strength or modulus, are used as reinforcement in composite materials. In theory, nanofibers possess even better mechanical properties that traditional fibers; thus, their implementation in a new category of composites materials could open new perspectives for composites materials with enhanced properties [58]. The magnitude of reinforcement in a composite depends on the aspect ratio of the fibers (length versus

diameter); the very low radial dimension of nanofibers allows to have higher aspect ratios, therefore a stronger effect. Moreover, nanofibers have low impact on light refraction due to their dimension; thus, the mismatch of refractive index between matrix and reinforcement is less pronounced, and this allows to obtain materials that can still be transparent after the reinforcement. However, there are some concerning related to fibers dispersion techniques which could be a strong limitation for future applications [61]. Furthermore, a similar application field regards the implementation of nanofibers in conventional textile patterns; main advantages are related to improvement in permeability, thermal insulation, and wind resistance [61].

In Figure 2.21 a recap of the several application fields is proposed.
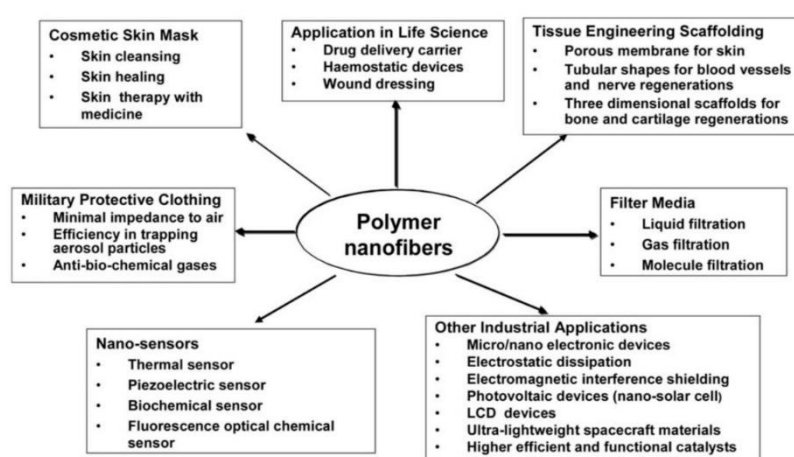
Figure 2.21. Potential applications of electrospun polymer nanofibers [61].

2.5. Aim of the thesis work

The purpose of this thesis is the investigation of two types of polyynes inside polymeric electrospun nanofibers. These carbon chains differ in their termination. The first part of the work is focused on the detection of a halogenated polyyne. The second part regards the analysis of hydrogenated polyynes; both a mixture of multiple chains and a single size-selected molecule are studied. The detection of carbon chains in nanofibers is supported by other measurements in liquid and in polymeric films, in order to highlight similarities and differences between those environments. All these characterizations are performed employing low concentrated polyynes solution, since some production methods cannot provide a higher amount of carbon chains. This means that the detection cannot be performed by simple Raman spectroscopy, due to its intrinsic sensibility threshold. Silver nanoparticles have been implemented in every sample preparation to exploit their plasmonic effect; thus, the investigation is carried on by Surface Enhanced Raman Spectroscopy (SERS) measurements.

3   Materials and experimental methods

In this chapter a description of the synthesis procedures and experimental characterization methods is provided. The chapter is divided into two main sections. The first one contains a presentation of the main materials; it involves the description of the synthesis and the main properties of polyynes, silver nanoparticles and polymers exploited in this thesis. In the second part the experimental methods are described; samples have been analysed using an UV-Vis spectrometer, a Raman spectrometer, and a Scanning Electron Microscope. For each of them the experimental setup is discussed.

3.1. Materials

The aim of this work is to detect and characterize polyynes embedded in electrospun nanofibers. Raman spectroscopy is the simplest technique that allows to detect the presence of polyynes when they are stabilized in a solid matrix, like polymeric nanofibers. Therefore, to accomplish the observation of carbon chains, it is fundamental to detect the characteristic Raman signal of polyynes. However, due to their low concentration, it is required to also use metallic nanoparticles and exploit their enhancement effect, thus performing a SERS measurement. This concise description introduces the three main components used in this project: polyynes (which act as analytes), metallic nanoparticles (in the role of enhancers) and a polymer (the matrix). For each one of these components, specific materials were chosen, and the reason behind each selection is discussed in the next paragraphs.

3.1.1. Polyynes

For this work, it was established to characterize two different types of polyyne molecules: halogenated and hydrogenated ones. This choice was made considering that, even if they belong to the same family of carbon allotropes, there are several features which make interesting to study both inside polymeric nanocomposites. The following description is useful to appreciate these features and to make clear this decision.

Halogenated polyynes: C_4Cl

The investigation of halogenated polyynes concerns *de facto* the study of a single molecule, whose structure is shown in Figure 3.1. These polyynes consist of a chain

made of four sp-hybridized carbon atoms and of two heterogeneous terminations: on one side a chlorine atom, and on the other side a group composed by a phenyl ring para-substituted with a nitrile group. From now on, this molecule will be referred as C_4Cl for simplicity, highlighting the halogenated terminal group.
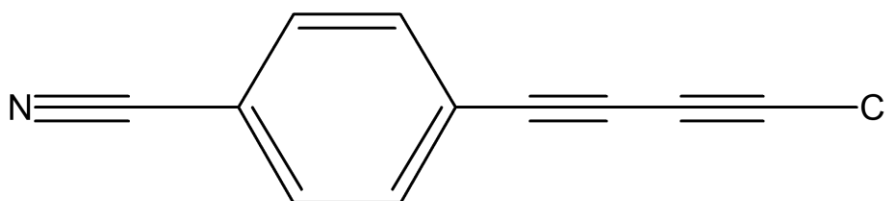
Figure 3.1. C_4Cl molecular structure

The synthesis of C_4Cl polyynes follows a multiple-steps chemical route which is not described in this work, because it was not performed or assisted by the author. The relevant features possessed by these molecules are different: first, C_4Cl polyynes are available in a very stable powder form, which permits to precisely control the concentration in solution and offers the possibility to have highly concentrated solutions. Second, these polyynes are stable in many organic solvents: it is a valid advantage, because knowing that the molecules does not degrade helps the sample's preparation phase and allows to perform multiple characterizations starting from the same solution, which would be difficult to do if the synthesized molecules were highly instable. Moreover, as it was explained in chapter 2, solvent plays an important role in electrospinning and not all the solvents are suitable for this technique, thus the possibility to have molecules stable in different solvents allows the optimization of spinning conditions. C_4Cl have been diluted in several solvents, in relation with the specific experiment to be performed: acetonitrile (ACN), dimethyl sulfoxide (DMSO), dichloromethane (DCM) and dimethylformamide (DMF).

Hydrogenated polyynes

The molecular structure of investigated hydrogenated polyynes is rather simple. It consists in a central sp carbon chain with various length, terminated on both sides by a hydrogen atom. These kind of polyynes are synthesized via physical methods (described in chapter 1.2.2**Errore. L'origine riferimento non è stata trovata.**): chains with different lengths and, in general, longer than the C_4Cl are obtained (therefore interesting because closer to the carbyne model). Moreover, these production processes make their synthetization easier, faster and allow the use of less environmental dangerous solvents (hydrogenated polyynes can be synthesized even in water). The main disadvantages concerning these compounds are their limited stability, compared with the C_4Cl, and the fact that they can be obtained only in low concentrated solutions (in the order of 10^{-6} mol/L).

In this work, hydrogenated polyynes were produced by Pulsed Laser Ablation in Liquid (PLAL), whose experimental setup is now briefly descripted (Figure 3.2).

It consists in a Nd:YAG pulsed laser (Quantel Q-Smart 850) which works at a repetition rate of 10Hz and 6ns of pulse duration. This solid-state laser has the fundamental harmonic at 1064 nm but can also work at 532 nm and 355 nm by implementing specific non-linear optical modules. Anyway, in this work, only the fundamental frequency was used to produce polyynes. The working principle of this apparatus is the following: the laser beam leaves the head of the solid-state device and reaches a 45° inclined mirror, which deviates it toward a glass vial containing the solution and, at the bottom, the graphite target. The vial is kept in a spiral horizontal motion by a motorized three-dimensional support controlled *via* computer to avoid the local consumption of the target during the ablation. The vertical distance of the vial from the ground is set taking into consideration the effect of the solution refractive index on laser propagation, thus achieving the desired laser spot size on the target (for all the ablations, this size was set to 0.766 mm of radius). Other relevant parameters are the energy per unit pulse (controlled by a power meter) and the fluency (i.e., the energy per unit surface).
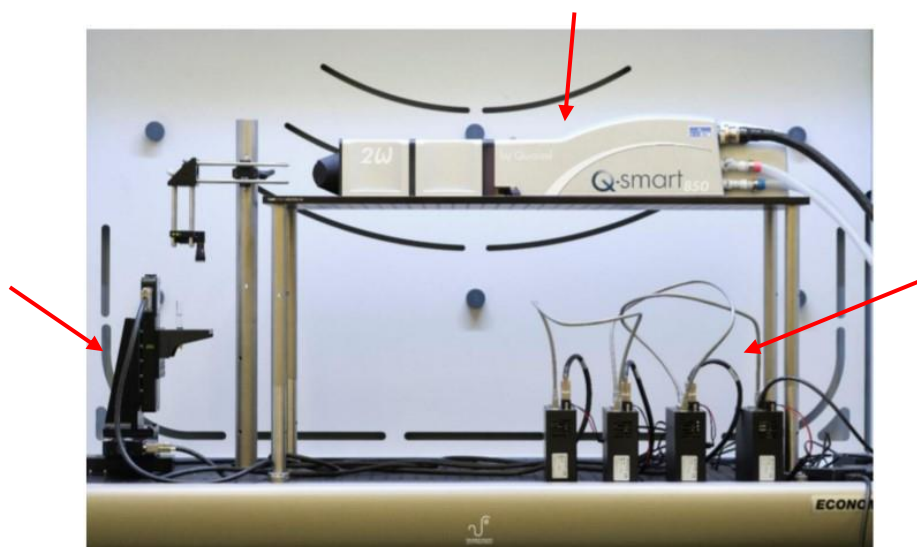
Figure 3.2 PLAL apparatus, where there are visible the vial support (left), the solid-state laser (upper center) and the motors that actuate the vial movement (bottom right)

Hydrogenated polyynes obtained by PLAL are defined as a mixture, which means that multiple chains with different length are present in the ablated solution. Polyynes mixtures are the simplest systems exploited in this part of the work, since no other synthetization step was required before the integration with the polymeric solutions. These mixtures were obtained with two different parameters setup: the first one was a 30 minute ablation of 1 mL of water with an energy pulse of 50 mJ/pulse; the second

one was a 15 minute ablation of 2 mL of acetonitrile with an energy pulse of 50 mJ/pulse. The choice of this parameters was made on a consolidated history of tests performed over the years by other researchers in the lab. In both cases, the result consists in a solution with a dispersion of hydrogenated polyynes with different lengths. The decision of performing the PLAL with two different solvents came from some considerations: water was first selected because it is the same solvent used for dissolving PVA and for silver nanoparticles synthesis (as explained in the next two subchapters), therefore it allowed a secure miscibility. However, the stability of polyynes in water is poor, thus the subsequent choice was acetonitrile (ACN). Since it is an organic solvent, ACN ensures a higher polyyne production and stability [28]. This is because, with an organic solvent, carbon is also present in the liquid and not only in the graphite target, therefore the laser ablation is more efficient; in addition, hydrogenated polyynes are apolar molecules, thus they are more stable in ACN than in more polar solvents like alcohols or water. The higher concentration of polyynes in ACN mixtures allows to separate and embed a size-selected hydrogenated polyyne inside nanocomposites.

The size-selected polyyne that we chose is a chain with eight sp carbon atoms (HC$_8$H). It was collected starting from a 4 mL mixture of polyynes in ACN (obtained from two ablation with the setup parameters previously presented). This solution was concentrated using a Rotavapor, then filtered through a syringe; the collection was performed exploiting a Reverse-Phase High Performance Liquid Chromatography (RP-HPLC). The instrument is a Shimadzu Prominence UFLC; it is equipped with a photodiode array detector UV-Vis spectrometer, and it employs different separation columns. The one selected in this case was a C18 column (Phenomenex Luna® C18). The method was chosen, as for the ablation parameters, considering previous separations performed with the same solvent: specifically, a gradient method exploiting a mixture of acetonitrile and water, starting from 65% of ACN and ending at 95%, with a duration of 45 minutes. The collection was performed by looking at the instantaneous absorption spectra and knowing the position of the absorption peaks for each size-selected polyyne, which are tabulated values [28]. The choice of HC$_8$H molecule derives from the fact that it showed the most intense UV-Vis absorption signal; thus, it was the most concentrated chain in the mixture.

3.1.2. Silver nanoparticles colloidal solutions

The role of metallic nanoparticles in this work is to enhance the laser effect during SERS measurements, allowing the investigation of low concentrated polyynes, as was explained in chapter 1**Errore. L'origine riferimento non è stata trovata.**. The choice of using silver nanoparticles (AgNP) as SERS enhancers was made principally because there are several examples in literature regarding the detection of polyynes, in solution or in polymeric nanocomposites, with the aid of AgNP; in this way, there is the

possibility to compare the experimental result of this work with the previous ones [56, 57].

Silver nanoparticles were synthesized mainly following the so-called *Lee-Meisel approach* [75]: this method consists in the reduction of silver nitrate ($AgNO_3$) and subsequent stabilization of silver-clusters in a water solution: both reduction and stabilization are performed by adding sodium citrate, while the temperature is kept slightly below 100°C and the solution is vigorously stirred.

To produce specific SERS active substrates (discussed in chapter 4), silver nanoparticles were also synthesized following another process, which is quite similar to the above method: $AgNO_3$ is reduced by sodium borohydride ($NaBH_4$), while the nanoparticle stabilization is still made by sodium citrate [76]. The main difference is that $NaBH_4$ is a stronger reducing agent, therefore the nanoparticle average dimension is lower than with the Lee-Meisel approach.

The calculation of the average nanoparticles' diameter can be made by exploiting the regression performed by [76]. It correlates the diameter with the wavelength of the absorption peak (λ_{LSPR}), according to the equation ($NP_{size}(nm) = 0.78 \times (\lambda_{LSPR}) - 266$ (3.1):

$$NP_{size}(nm) = 0.78 \times (\lambda_{LSPR}) - 266$$

$$(3.1)$$

In general, silver nanoparticles prepared with the Lee-Meisel method possess an absorption peak in the region of 400-450 nm, while for the ones prepared with $NaBH_4$ it is slightly below 400 nm. Figure 3.3 shows some of the preparations exploited in this work to highlight the difference between the two methods, but also the intrinsic variability of the absorption peak even when AgNP are synthesized with the same
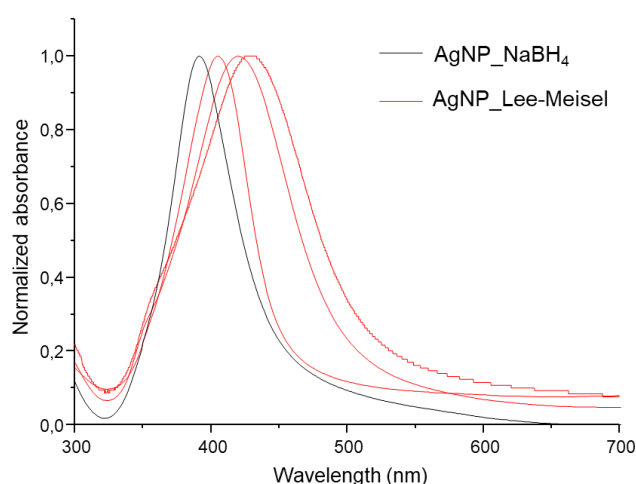
Figure 3.3. UV-Vis absorption spectra of some AgNP colloids
synthesized during this work

approach. This phenomenon is due to the effect of environment and, of course, the systematic errors related to a manual preparation.

Using the two chemical methods here reported, the concentration of nanoparticles in the final water colloid is certainly lower than 10^{-3} mol/L ($AgNO_3$ starting concentration). To boost the SERS effect of AgNP embedded inside nanocomposites, some applications required that colloids concentration was increased by using a laboratory centrifuge. For the AgNP obtained by sodium citrate reduction, the concentration was performed at 8000/9000 rpm (depending on the nanoparticles dimension) for 20 minutes, while for the AgNP obtained by $NaBH_4$ the parameters were 14000 rpm for 20 minutes. The final concentration factor has been kept around 40 times of volume-reduction for each preparation.

3.1.3. Polymers

Polymers are the building constituent for nanocomposites production, therefore the choice of the specific kind of polymer was crucial. Most of the samples were prepared by exploiting poly(vinyl alcohol) (PVA). PVA is a water-soluble polymer obtained industrially by hydrolysis of poly(vinyl acetate) [77]. It is non-toxic, biocompatible, with good thermal and chemical stability, and with a density of 1.19 g/cm^3. Thanks to its properties, it is a widely used polymer in several application fields, like medical, cosmetics, pharmaceutical, and food industry [78]. Most importantly, in literature there are many papers dealing with production of electrospun nanofibers starting from PVA solutions, with studies on fibers morphology and parameters effects [77-79]. Figure 3.4 shows its molecular structure.
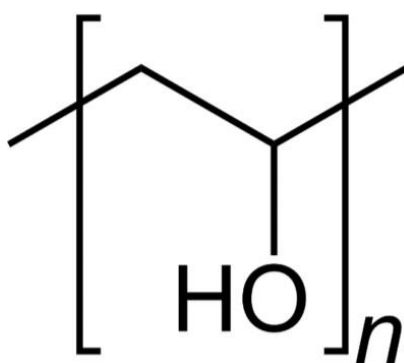
Figure 3.4. PVA repetitive unit

PVA solubility was a fundamental issue in the choice of the polymer. The synthesis of nanocomposites required the preparation of a precursor solution containing polyynes, AgNP and PVA. Therefore, the solubility of these three items in a common solvent was not negligible. Starting from PVA and AgNP, previous works [57, 80] have described how PVA can be dissolved insides water colloids containing nanoparticles obtained

with the Lee-Meisel approach. Other studies present different procedures in which nanoparticles are synthesized directly inside a PVA solutions, sometimes even during or after the electrospinning process [72, 73, 81-83], but it was decided to produce AgNP first, and then dissolve PVA inside, because it is the simplest method and offers a comparison with other works related to polyynes investigations.

For what concerns the addition of polyynes at the PVA/AgNP solutions, different approaches have been considered depending on the type of polyynes. As previously reported, in this work we use both halogenated polyynes (not soluble in water) and hydrogenated polyynes (synthetized in water and ACN). The general adopted approach was to dissolve PVA in water or water-AgNP mixtures; then, polyynes solutions were prepared and blended with the polymeric mixtures by magnetic stirring. PVA was always dissolved in the right amount to have a 10% in weight (%wt) concentration in the final blend. It is important to underline that polyyne addition was always made after the dissolution of PVA, since the latter is performed at a temperature between 80-95°C and that would have caused a high risk of polyyne degradation. Polyynes obtained with ablation in water were easily mixed with PVA and AgNP. In the cases of C_4Cl and of polyynes ablated in ACN, since they are not available in water environments, a more complicated process is needed; a great advantage came from the fact that PVA can be dissolved also in some water-organic solvents mixtures, even if the second addendum is not a true solvent of the polymer [79, 84, 85]. By looking at the work of Gupta *et al* [85], it was found that PVA can be electrospun with success in water-DMSO mixtures up to 30%vol of DMSO with no evident defects; since DMSO is a solvent in which C_4Cl is stable, it was decided to use water-DMSO mixture for polyynes integration. For the polyynes ablated in ACN, some solubility tests were performed, starting from the considerations made by Sacchi [86]; in her thesis work, she found that PVA is soluble in water-ACN mixtures up to a 42% volume addition of ACN. However, in the literature there were not found examples of PVA fibers electrospun from those solutions. Therefore, some electrospinning test were performed using PVA water solutions with 10%, 20%, 30%, 40%vol of ACN (results are shown in chapter 4) to find the best configuration for polyynes addition.

The second polymer implemented in this work is poly(methyl methacrylate) (PMMA). It is a thermoplastic polymer, obtained by free radical chain-growth polymerization of methyl methacrylate (MMA). It shows good mechanical properties and an excellent value of 92% of transmittance for visible light; its density is around 1.18 g/cm^3. Other relevant properties are scratch resistance, environmental stability, UV stability (it absorbs radiations below 300 nm), and biocompatibility. Figure 3.5 shows its molecular structure. The choice of PMMA was necessary because PVA water solubility hindered the possibility of covering a nanofiber sample with the AgNP water-colloids

and leave it dry. Therefore, PMMA was exploited for that single experiment (involving C_4Cl polyynes and described in detail in the next chapter) thanks to its hydrophobicity. Moreover, PMMA nanofibers embedding polyynes have been already investigated in Vidale's [87] and Terranova's [88] works; these two sources were considered for the choice of electrospinning parameters and for polyyne integration, which was done exploiting dimethylformamide (DMF) as a common solvent.
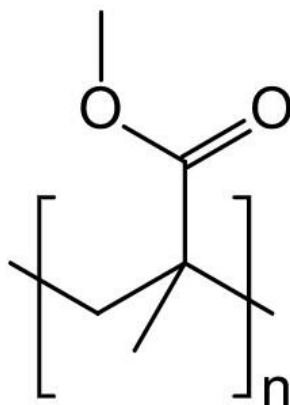
Figure 3.5. PMMA repetitive unit

Polymeric nanocomposites produced in this work are essentially nanofibers and films. Films were made only from PVA solutions and were obtained with two methods: drop casting and spin coating. Drop casting is the simplest film deposition technique and it consists in the deposition of the liquid polymeric solution onto a substrate, then the sample is put under a chemical hood and left to dry. Spin coating, instead, is used to provide more uniformity and consists in depositing the solution on a substrate placed over a rotating support, which spins during the solidification process. Two different experimental setups were used for spin coating. The first is a Laurell spin-coater (model ws-400B-6npp/lite). The second is a simpler, hand-made apparatus, showed in Figure 3.6: it consists in a rotating computer vent (onto which the substrate is placed) actuated by an analogic controller.
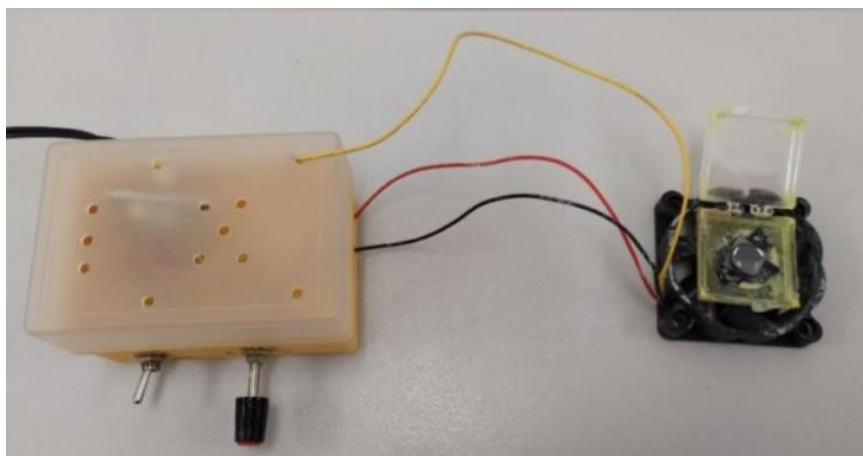
Figure 3.6. Hand-made spin coater used in this work

Nanofibers were obtained by electrospinning, both from PVA (the majority) and PMMA solutions. The experimental setup (horizontal) is shown in the Figure 3.7 and contains all the principal elements described in chapter 2. Polymeric solutions were placed in Hamilton Gastight syringes with volume of 2.5 or 5 mL; the feed rate is provided by an infusion pump KDS Scientific (model series 200), while voltage is applied to the needle by a High Voltage Power Supply (Spellman SL30P300). Flow rate, voltage and needle-collector distance were chosen each time by considering the type of solution and the polymer concentration; the exact values are reported in the next chapter, case by case.

Figure 3.7. Electrospinning setup used in this work

In general, the applied potential was kept between 12 and 17 kV, the flow rate between 0.3 and 0.5 mL/h for PVA solution and around 0.05 mL/h for PMMA solutions, and the distance between 20-25 cm. Several preliminary tests were performed by spinning nanofibers on a glass substrate, and immediately observing them at the optical microscope to have a rough morphological evaluation. During all the experiments temperature and relative humidity were marked, but the instrument works in an open environment therefore no real control on these two parameters could have been done.

3.2. Characterization techniques

3.2.1. UV-Vis absorption

UV-Vis spectroscopy was implemented for the analysis of polyynes in solution and for the silver nanoparticles colloid characterization. As explained in chapter 1.3.1, polyynes exhibit a strong absorption in the ultraviolet frequency range, with specific absorption peaks related to the chain length and to the terminal groups. This experimental technique was used for the investigation of both the C$_4$Cl and the hydrogenated polyynes, checking their stability over time and the number of peaks present in the mixtures obtained from laser ablations. For what concerns silver nanoparticles, the absorption spectrum was inspected after each preparation to have a qualitative estimation of the average nanoparticle dimension and their size distribution.

UV-Vis analysis were performed with a Shimadzu UV-1800 spectrophotometer. The instrument general setup is described in Figure 3.8. It possesses two light sources, a deuterium and a halogen lamp, the first covering the region from about 190 nm to 340 nm and the latter from 340 nm to 1100 nm. The light beam goes through a filter and a monochromator, then it is split into two components: one beam encounters a cuvette containing the reference solution (the pure solvent), the other one passes through the sample solution. The output data is a spectrum in which the effect of the solvent is subtracted from the absorption behaviour of the analytes in solution, allowing the investigation of the molecules dissolved in the solution. In this work, all the measurements were performed in absorbance (the system can also work in transmittance); for the investigation of polyynes, a range from 190 to 400 nm was set, while for AgNP the range of analysis was between 300 and 700 nm. AgNP were always diluted in water to avoid saturation (since the relevant information was the position of the absorption peak, not its intensity)
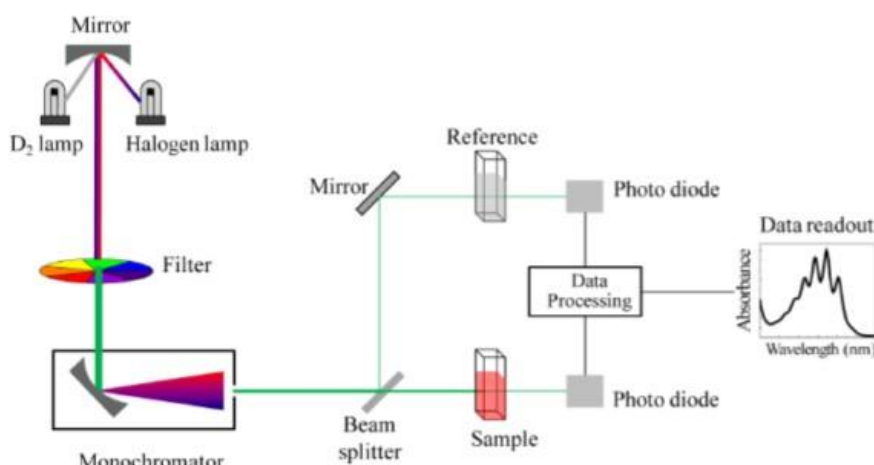
Figure 3.8. UV-Vis spectrophotometer schematic setup

3.2.2. Raman spectroscopy and SERS

Raman spectroscopy was the main technique exploited in this work. Since we investigated the presence of low concentrated polyynes in nanofibers, each Raman measurement was, indeed, a Surface Enhanced Raman Spectroscopy analysis, performed with the aid of the silver nanoparticles previously described.

The instrument used is a Renishaw inVia Raman microscope, whose generic setup is shown is Figure 3.9. It is equipped with a diode-pumped solid-state laser with two wavelengths available, one at 532 nm (green) and the other at 660 nm (red). The produced light beam is sent to the sample through the microscope objective; then, the reflected radiation is filtered (elastic and Anti-Stokes signals are excluded) and reaches the grating system, which separates the beam into the different constitutive frequencies. At the end the light is collected by the charge coupled device (CCD) detector and the inelastic signals (Stokes photons) are analysed. A spectrum acquisition can be executed in two modes: static and extended. The first is faster but its measure interval (in cm^{-1}) is fixed and depends on the grating used (1800 lines/mm), while the second allows the choice of the interval since it detects the whole spectral dispersion.

In this work, experimental measurements were performed with the green light (532 nm), because it is closer than the red one to the plasmonic peak of silver nanoparticles, thus allowing a higher enhancement of the SERS effect. All the samples were observed with a 50x microscope objective. For the majority of samples, the extended acquisition mode was chosen, because it was the only one able to detect signals from AgNP, polyynes and polymer at the same time.
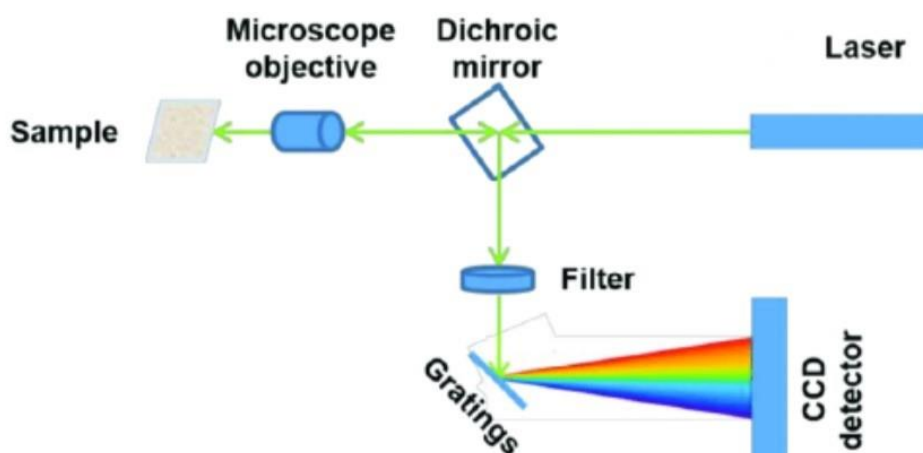
Figure 3.9. Raman spectrometer schematic setup

3.2.3. Scanning Electron Microscopy

Figure 3.10. SEM instrument

SEM observations were made on samples containing electrospun nanofibers with the aim of checking their morphology. The instrument used was a Zeiss Supra 40 Field Emission Scanning Electron Microscope (Figure 3.10). The schematic internal configuration of a SEM is depicted in Figure 3.11. Briefly, an electron gun emits a highly energetic electron beam though thermionic effect of an inside tungsten filament. The beam is then focused on the sample by magnetic lenses. Multiple detectors are present around the sample, with the scope of collecting different returning signals: as example, secondary electrons provide information on the surface morphology, while backscattered electrons or X-rays help to estimate sample's composition.
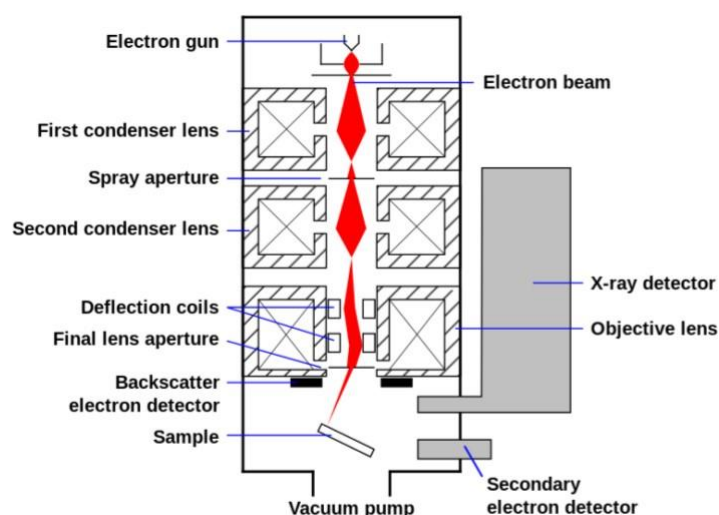
Figure 3.11. SEM schematic working principle

In this work, SEM measurements were performed on electrospun nanofibers collected on silicon substrates; to favour conductivity, samples were attached to their holders by using a conducting carbon tape, but in some cases a small effect of charge accumulation on the dielectric polymeric nanofibers was still present. Two different secondary electron detectors were exploited, InLens and SE2: using the former, images with higher colour contrast were obtained, useful to appreciate diameter dimension; with the latter, images possess a more defined depth and therefore the nanofibers architecture was observed more clearly (Figure 3.12). Distribution and average fiber diameter were calculated for specific samples (described in the next chapter); this analysis was performed by collecting a high number of diameters, then calculating their average value and their standard deviation with the help of ImageJ® software.
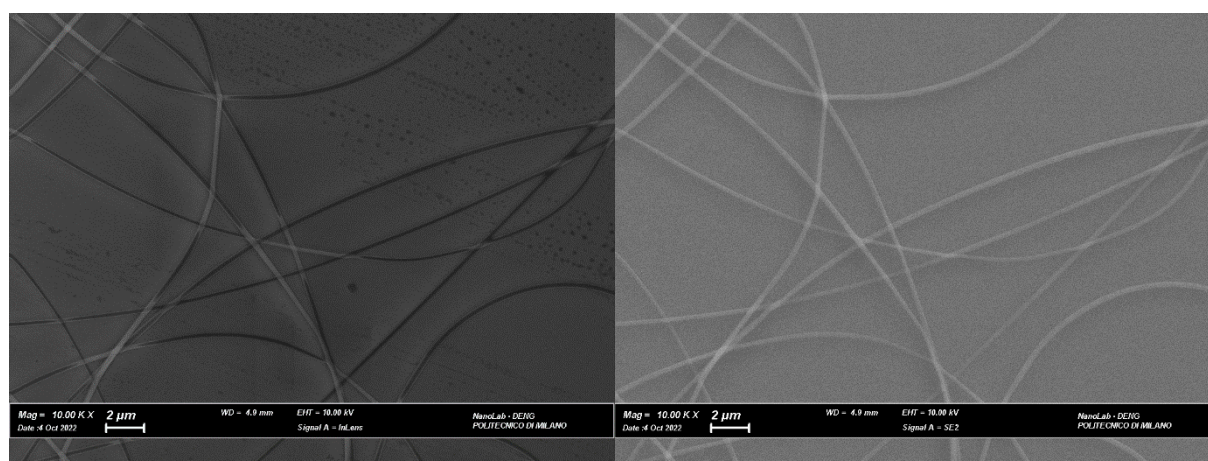
Figure 3.12 Example of a SEM image taken with both detectors: InLens (left), SE2 (right)

4 Experimental results

In this chapter the main experimental results are discussed. The first part is dedicated to the investigation of C_4Cl polyynes inside polymeric nanocomposites (films and nanofibers), while the second section contains the detection of hydrogenated polyynes.

It is important to remind that, in principle, C_4Cl polyynes are available in a solid form and they could be easily detected by Raman spectroscopy if a sufficiently high concentration is dispersed in a medium. However, hydrogenated polyynes obtained by laser ablation are poorly concentrated (approximately 10^{-6} mol/L in solution); therefore, they can only be detected by exploiting SERS effect. Since the aim of this work is to find a suitable method to investigate both type of polyynes and to obtain comparable results, in all the experiments C_4Cl polyynes were diluted up to a quantity non detectable with simple Raman measurements, ranging from 10^{-4} to 10^{-6} mol/L.

4.1. Investigation of the C_4Cl polyyne

The investigation of the halogenated polyynes inside electrospun nanofibers followed several steps. First, it was decided to study the molecules SERS response in liquid, since it is the simplest way to obtain a clear knowledge about the position and intensity of C_4Cl specific signals. Then, SERS measurements were done in PVA films, to see if the same response observed in liquid was present when molecules are embedded in a solid matrix together with a dispersion of silver nanoparticles. This kind of experiments has been already performed successfully for hydrogenated polyynes in previous works [57, 80, 86, 89], therefore it is interesting to see if the same conclusion holds for polyynes with different chemical structures. Moreover, SERS in films was useful because a polymeric film is a system more similar to an electrospun nanofiber than a liquid solution. Eventually, the investigation of C_4Cl inside nanofibers was performed by exploiting several different samples architectures, which will be exhaustively described in the appropriate sections. The last part of this subchapter deals with an interesting method of superficial SERS investigation of polyynes, performed with the aid of nanofibers.

4.1.1. SERS of C_4Cl in solution

SERS in liquid was done by preparing a strong diluted solution of C_4Cl in ACN, reaching a concentration of 10^{-5} mol/L, in order to be comparable with the concentration of polyynes from PLAL. At this level, molecules are too diluted to give

a Raman response, therefore only with the addition of silver nanoparticles the characterisation can be performed (thus doing a SERS measurement). The subsequent step was to mix the solution of C_4Cl with the colloid of silver nanoparticles obtained with the Lee-Meisel approach. Since it was not known which relative concentration of the two was the optimal, four different volume ratios were investigated, as shown in Figure 4.1.

Starting from the bottom of the graph, it is evident that by increasing the volume ratio of AgNP, multiple signals emerge and become more defined. The peak in the right part of the spectra (2254 cm^{-1}) was recognized as the C≡N stretch of acetonitrile; it is not constant because the volume of ACN varies in the different samples, therefore it could not be used as a reference, and it was simply neglected. The other main signals are highlighted. Starting from the left, at 1600 cm^{-1} it can be found the Raman characteristic peak of the phenyl group of the C_4Cl molecules, which is a typical footprint for aromatic compounds. It can be appreciated that this signal becomes stronger with the increase of AgNP in solution (apart from the blue and green spectra, which are similar), indicating a higher response from the molecules due to enhancement effect. For what concerns the other signals in region 1900-2200 cm^{-1}, they are likely to be related to SERS response of the polyynes, since they were found in the expected ECC region and follow the same incremental behaviour of the phenyl signal. The investigation in PVA films was crucial to help their characterization.
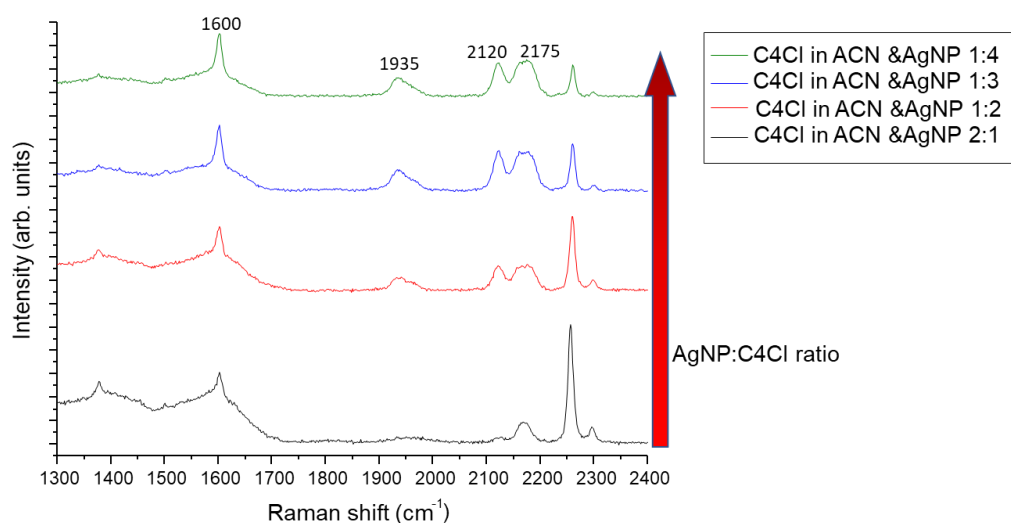
Figure 4.1 SERS spectra in liquid of different volume ratios of C_4Cl in ACN and AgNP colloid

4.1.2. SERS of C$_4$Cl in PVA films

To have a stronger confirmation that the observed SERS signals in the 1900-2200 cm^{-1} region were an indication of the C$_4$Cl presence, it was decided to perform the same investigation embedding the molecules and the nanoparticles in solid PVA films. Multiple SERS measurements were accomplished. For each test the changing parameter was the percentage in volume of the added AgNP colloid, to simulate in solid the same principle exploited for the SERS in liquid. Solutions were prepared firstly by diluting C$_4$Cl molecules up to 10^{-4} mol/L in DMSO; then, a solution of PVA dissolved in a mixture of water and AgNP colloid was prepared. The last step was blending the two solutions: DMSO was added in 10% of the total volume. PVA dissolved mass was calculated to reach 10%wt after the blending with DMSO. In the end, each solution possesses the same concentration of C$_4$Cl (10^{-5} mol/L in the total volume) and the same concentration of PVA; the only varying factor was the water-AgNP relative fractions. It was decided to prepare solutions with AgNP volume fractions of 33, 50, 66, 90%vol in the final blend. Films were deposited by drop casting on silicon substrates. For each fraction, a corresponding solution (and film deposition) without polyynes was made. The idea was to have a reference which helped understanding the role of silver nanoparticles in signal composition.

Results are shown in Figure 4.2. In each graph, the black line represents the reference (a PVA film with only AgNP inside) while the red line represents the sample with polyynes. The main peak at 2930 cm^{-1} is the characteristic C-H stretching of PVA. As can be clearly observed, in the films with polyynes inside, there is the appearance of a sharp signal peaked at 2175 cm^{-1} (except in the last case, where it is broader), and sometimes also a signal around 1975-80 cm^{-1}, which was not present in SERS in liquid. Thus, the first one seems to be a more reliable indication of C$_4$Cl presence, since it was observed both in liquid and solid-state experiments. Moreover, in all the samples, it can be noticed the phenyl signal at 1600 cm^{-1}, rising from the wide region under 1700 cm^{-1} that characterize the presence of AgNP. On the contrary, in the reference samples, a broad peak in the region from 2115 to 2180 cm^{-1} was found: depending on the sample, this signal consisted in a large peak or in a sum of two smaller contributions. This seemed to be an indication of the fact that even with silver nanoparticles only, a small signal can always be present in the ECC region. A simple, but solid, explanation is related to the presence of some carbon impurities infiltrated in the nanocomposite during the preparation or the drying phase; even a small quantity of this impurities could give a visible response due to the enhancement effect by AgNP. However, in all the test performed, it is possible to observe how the intensities of signals in the 1900-2200 cm^{-1} region increase when polyynes are present, indicating that they are detectable and distinguishable. Despite this, the SERS response did not grow monotonically with the rise of AgNP concentration, as the SERS in liquid experiment seemed to suggest. The best result was achieved with 50%vol concentration of AgNP

colloid, while with the 90%vol the peak at 2175 cm^{-1} is barely distinguishable from the broad signal band. This could represent the evidence that there is also an upper limit for AgNP amount to have a good enhancement effect.
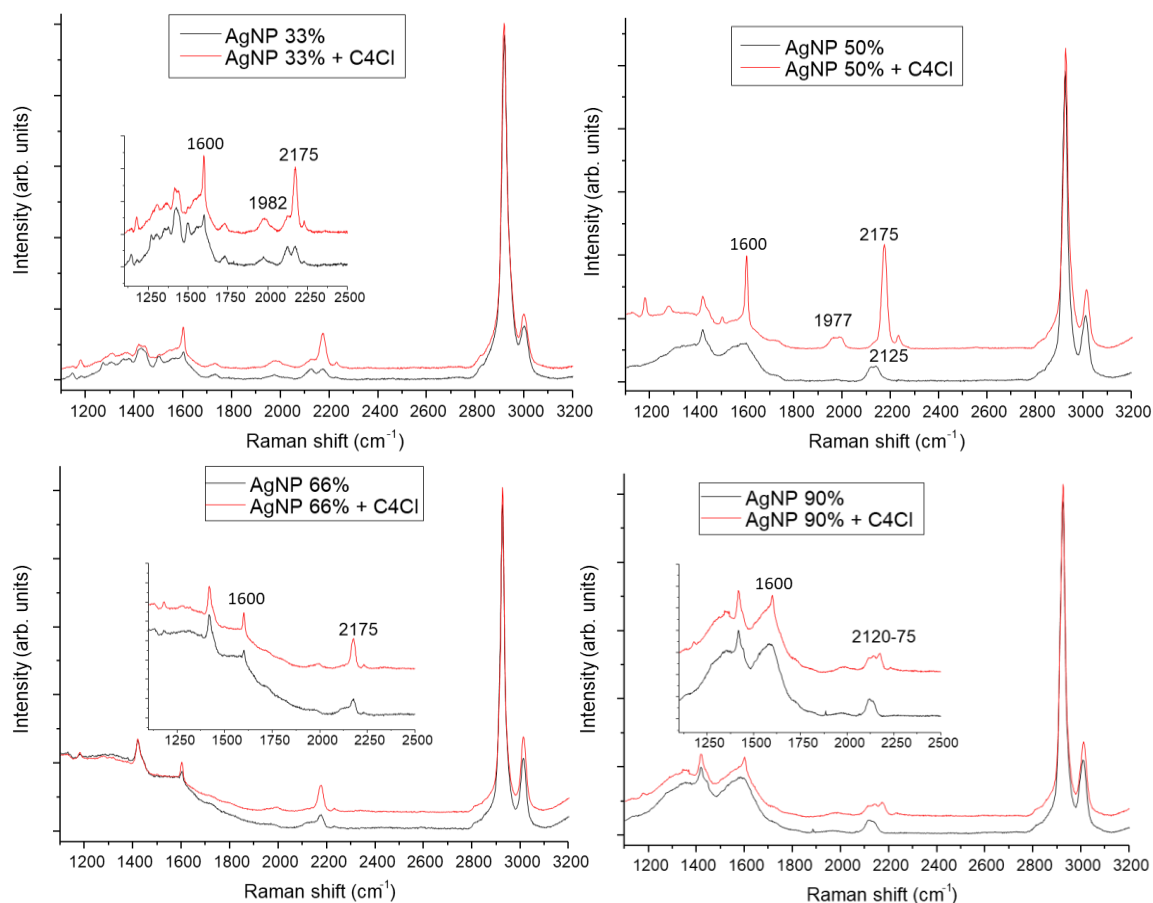
Figure 4.2 SERS spectra of PVA films containing C$_4$Cl (10^{-5} mol/L) with different AgNP loading. Each spectrum is normalized on PVA signal and shifted to make comparison with its reference. The inset, when present, helps to highlight the peaks in the polyynic region.

4.1.3. Nanofibers with AgNP under, above and inside

Alongside with the investigation of polyynes inside polymeric films, the aim of the thesis is still to perform the detection with C$_4$Cl molecule embedded in electrospun nanofibers. In a previous work [89], it was demonstrated that a SERS signal could also be observed by dropping the AgNP colloid on a silicon substrate and left it to dry, then subsequently placing a polymeric solution containing polyynes and wait until it solidifies. Based also on these results, we investigated three different configurations to detect C$_4$Cl signals. In the first one, similarly to the work just described, nanoparticles were deposited on a silicon substrate and then the nanofibers containing C$_4$Cl have been electrospun above them (*AgNP under the fibers*). In the second approach, nanofibers have been electrospun on a silicon substrate and then AgNP have been

deposited on their top (*AgNP above the fibers*). Lastly, a solution containing both polyynes and AgNP has been electrospun on a silicon substrate (*AgNP inside the fibers*); different ratios of nanoparticles have been investigated (the same used for SERS experiments in film).

The main objective of this tests was to search the method that better combines the need of a simple configuration (suitable for different polymers/solvents/polyynes) while maintaining a good SERS enhancement. The next three subchapters will show the morphology and the results obtained with these configurations.

4.1.3.1. AgNP above the fibers

The sample was prepared starting from a solution of PMMA instead of PVA. This choice was done since PVA is a water-soluble polymer, then it is impossible to drop the AgNP water colloid upon the nanofibers without a complete dissolution of them. Therefore, PMMA, which is insoluble in water, was adopted for this configuration. Sample preparation followed multiple steps. First, a solution of PMMA in DMF was prepared; meanwhile, C_4Cl molecules were also diluted in DMF, since it is an organic solvent in which the polyyne has shown to be stable. Furthermore, the two components were blended; dissolution of PMMA and dilution of C_4Cl were performed to reach a concentration of 6%wt for PMMA and 10^{-5} mol/L for the polyyne in the total volume. This solution was then electrospun with the following parameters on three silicon substrates:

- Feed rate: 0.05 mL/h

- Applied voltage: 12 kV

- Distance: about 24 cm

- Time of spinning: about 1 minute

- Temperature (T): 21.3 °C

- Relative humidity (RH): 52%

After the spinning procedure, some drops of AgNP colloid, with varying concentrations, were deposited on each sample. The AgNP colloid was placed at its normal concentration (the one obtained from the Lee-Meisel preparation), then diluted in water 10 times and 100 times; eventually, the three specimens were left to dry.

Figure 4.3 and Figure 4.4 show SEM images of the samples. In the one made from non-diluted colloid, nanofibers are completely covered by silver nanoparticles, while already with a 10-time dilution the coverage is strongly reduced. In the last case (100-time dilution) nanoparticles are barely visible.
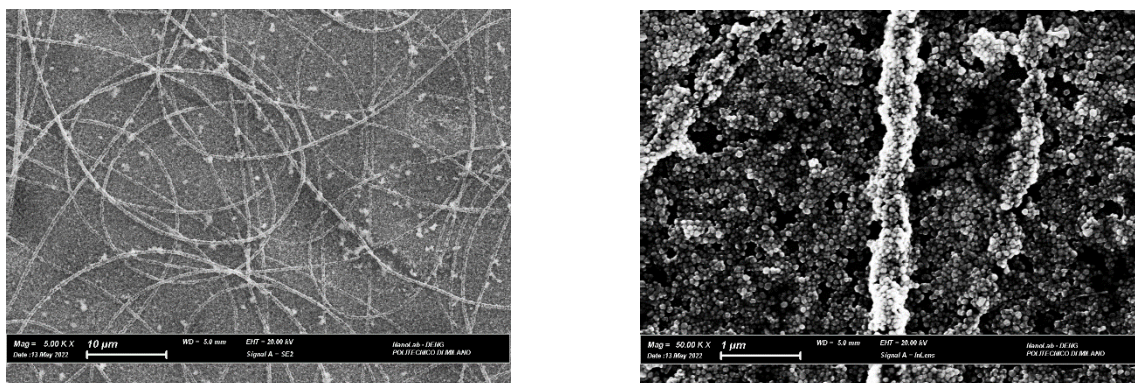
Figure 4.3 SEM images of PMMA nanofibers with undiluted AgNP dispersed above, made at different magnifications (5000x on the left, 50000x on the right).
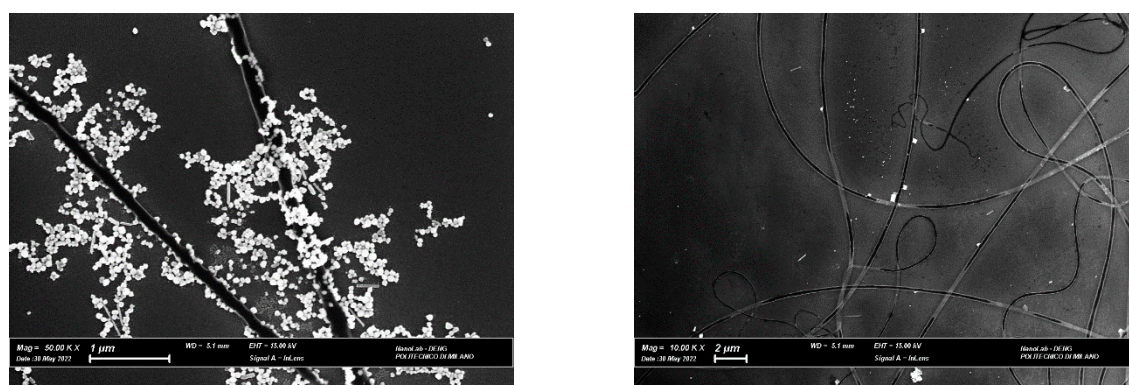
Figure 4.4 SEM images of PMMA with diluted AgNP dispersed above: 10-time dilution (left) and 100-time dilution (right)

Raman spectra were measured for all the three cases, and the results are shown in Figure 4.5 In the picture, also a spectrum of nanofibers obtained from a solution of PMMA 6%wt in DMF with the same electrospinning parameters (except for T and RH which were slightly different, and a time of 5 minutes) is proposed as a reference.

The reference spectrum of PMMA is helpful to describe some features of nanofibers Raman spectra. The three peaks in the region 2800-3100 cm^{-1} are the characteristic polymer C-H stretch, while the peak at 1730 cm^{-1} is the C=O stretching. Moreover, there are other peaks in the spectrum that are not related to PMMA but represent the footprint of some molecules in the atmosphere; at 2332 cm^{-1} there is a strong signal of nitrogen, while at 1557 cm^{-1} there is an oxygen signal. It is more likely to see these very

sharp peaks when few nanofibers are analysed, because a lower amount of material is excited; therefore, the polymer relative signal is weak enough to see also the Raman responses of molecules in the surrounding environment. Some of these signals will be present also in other spectra; of course, with thicker samples is more difficult to observe nitrogen or oxygen peaks, since their intensity is very low compared to the analysed material.
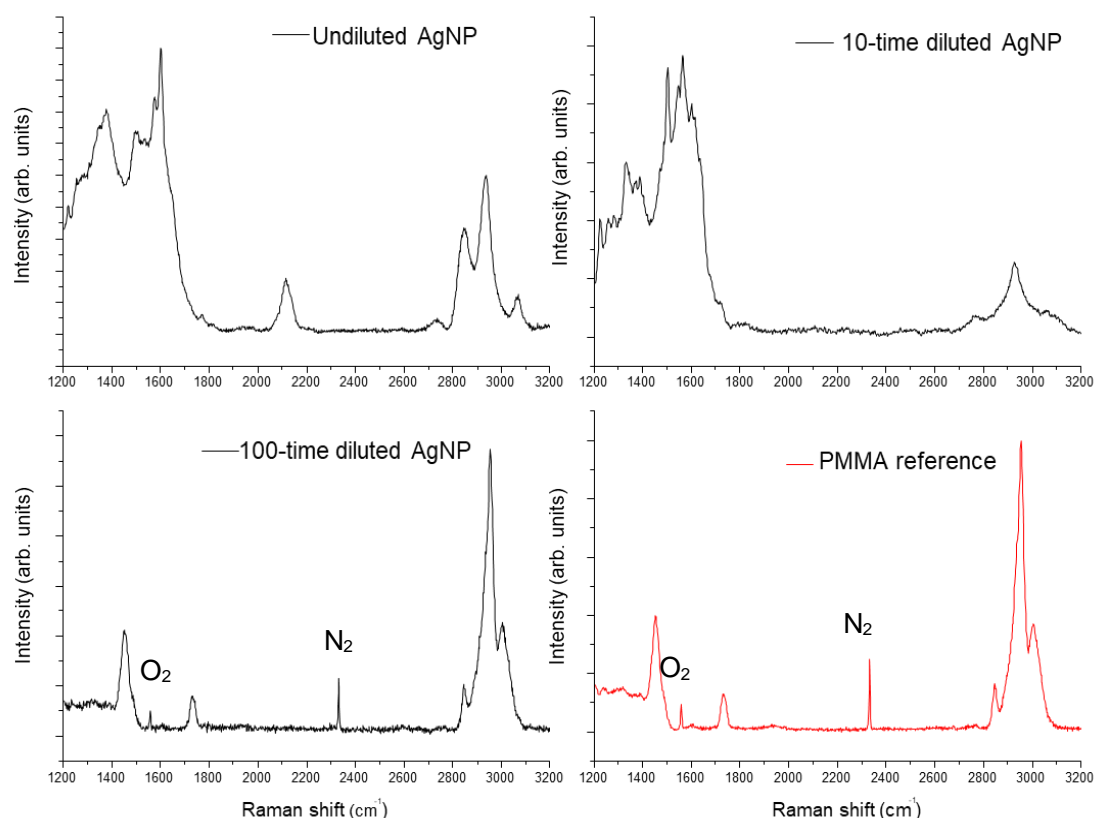
Figure 4.5 In black, the Raman spectra of the three PMMA nanofibers with AgNP (at different dilutions) deposited above them. In red, the reference spectrum of PMMA nanofibers.

Considering the samples containing polyynes and with AgNP above, for the undiluted sample and for the 10-times diluted sample (which have a non-negligible presence of nanoparticles, as the SEM images have shown) the characteristic intense and wide nanoparticles peak region under 1700 cm^{-1} is visible. This is not valid for the 100-times diluted sample, whose spectrum is almost identical to the reference one, since practically only PMMA nanofibers are present (as observed in SEM images). The only sample showing a signal in the polyynic region is the specimen with undiluted nanoparticles deposited. However, the peak is situated around 2115 cm^{-1}, which is not the position found during SERS measurements in liquid and films; the position of this peak is the same of the contamination signals found in the reference PVA films

described in the previous section. Therefore, also in this case, it was supposed that the enhancement effect of silver nanoparticles is strong enough to highlight impurities deposited on the surface during sample's preparation or handling. To confirm this hypothesis, the same solution of PMMA used for the reference was electrospun on a silicon substrate, and then a drop of undiluted AgNP colloid was deposited. Results are shown in Figure 4.6; it is evident that, even when polyynes are not present, a signal appears around 2115-20 cm^{-1}, confirming that it is due to the nanoparticles effect on impurities and has nothing to do with polyynes detection.

In addition to these considerations, the absence of the phenyl signal confirms that, unfortunately, with this configuration no characteristic signals of C_4Cl were observed. This result could depend on the fact that fibers are already dried when the colloid is deposited; thus, the interaction between polyynes and nanoparticles in principle could only happen if a C_4Cl molecule is close enough to the nanofiber surface and a nanoparticle is in proximity. In addition, PMMA insolubility in water does not allow even a small superficial permeation of the colloid in the matrix, incrementing the separation between polyynes and nanoparticles.
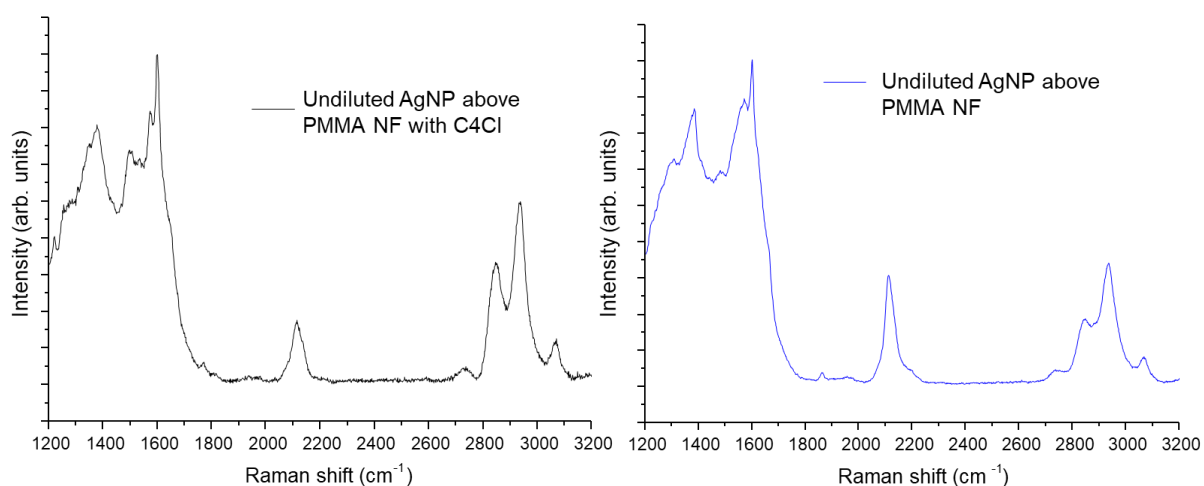
Figure 4.6. Comparison between PMMA nanofibers (NF) with undiluted AgNP dispersed above: NF with polyynes (left) and NF without polyynes (right)

4.1.3.2. AgNP under the fibers

The production of these samples was very similar to the one previously described. In this case, the first step was to cover the silicon substrates with few drops of AgNP colloid, in the same three concentrations as before (undiluted, 10-times dilutes, 100-times diluted). After water evaporation, these silicon-AgNP substrates were used to collect electrospun nanofibers. As the water was already evaporated from the surface, PVA nanofibers could have been spinned without being ruined. Here, six samples

were prepared, three with PVA nanofibers and three with PMMA nanofibers; the production method for the latter is the same described in the above section.

PVA nanofibers were obtained from mixing a 90%vol of a water solution containing the dissolved polymer with 10%vol of a DMSO solution inside which C_4Cl was diluted up to 10^{-4} mol/L. The final polyynes concentration was then 10^{-5} mol/L and calculation were made to obtain a PVA concentration of 10%wt. Fibers were electrospun at 0.5 mL/h, 13 kV and distance of 24 cm for about 1 minute. Temperature was around 21°C and relative humidity was 53%.

Figure 4.7 and Figure 4.8 show SEM images of the first two samples with PVA fibers. On the silicon with the undiluted colloid, nanofibers can be clearly seen lying on a ground full of silver nanoparticles; the other sample shows a clear reduction of nanoparticles coverage, as was equally observed for the reverse configuration (Figure 4.3 and Figure 4.4). Images of the specimen with AgNP diluted 100 times were not reported because, as happened with PMMA nanofibers, nanoparticles are barely seen.
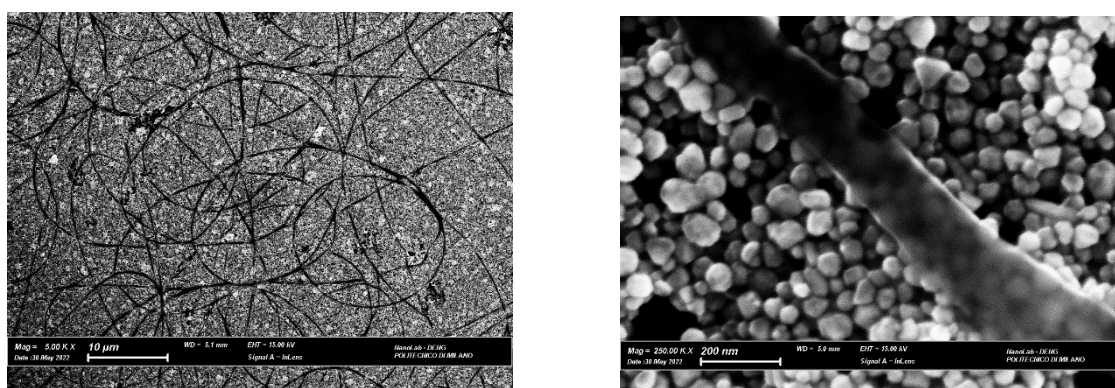
Figure 4.7 SEM images of PVA nanofibers on undiluted AgNP ground, taken at different magnitudes (5000x on the left, 250000x on the right)
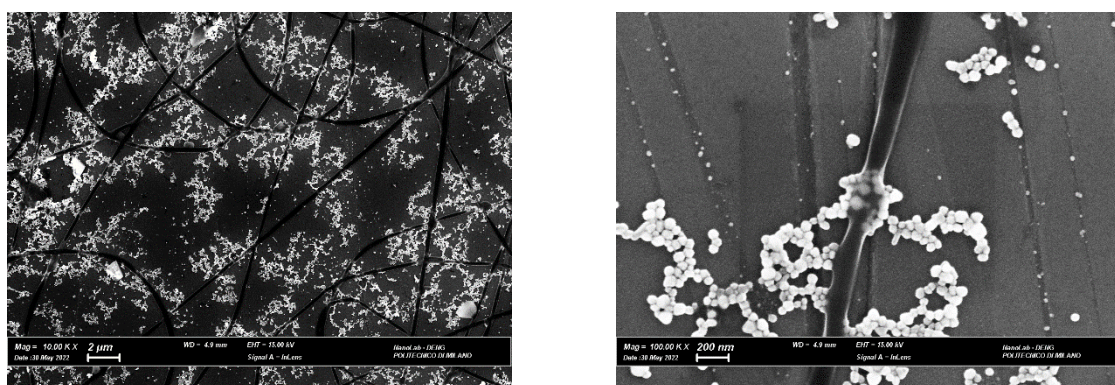
Figure 4.8 SEM images of PVA nanofibers on AgNP 10-times diluted ground, taken at different magnitudes (10000x on the left, 100000x on the right)

Figure 4.9 displays the Raman spectra of the three PVA samples with AgNP at different concentrations. The red spectrum refers to PVA nanofibers obtained from an identical solution (90%vol water, 10%vol DMSO, without polyynes) and electrospun with similar parameters; it was used as a reference for spectra evaluation. The results are similar to the ones from PMMA fibers with AgNP above: a strong response from nanoparticles is visible for the undiluted and 10-times diluted samples, while in the third one AgNP are practically absent, and the spectrum is equal to the reference one. The peak at 2115 cm^{-1} related to contaminations is still present. The absence of any signals around 2175 cm^{-1} seems to confirm that the C_4Cl are still not detectable.

As in the case of AgNP above nanofibers, the interactions between polyynes and AgNP are probably hindered. In these two configurations, polyynes are not directly in contact with AgNP, and this has probably precluded the polyynes to benefit from the enhancement effect. The same Raman experiments were performed for the PMMA fibers, but the results are similar to the one just discussed, showing the same behaviour of the AgNP and the absence of any C_4Cl signal.
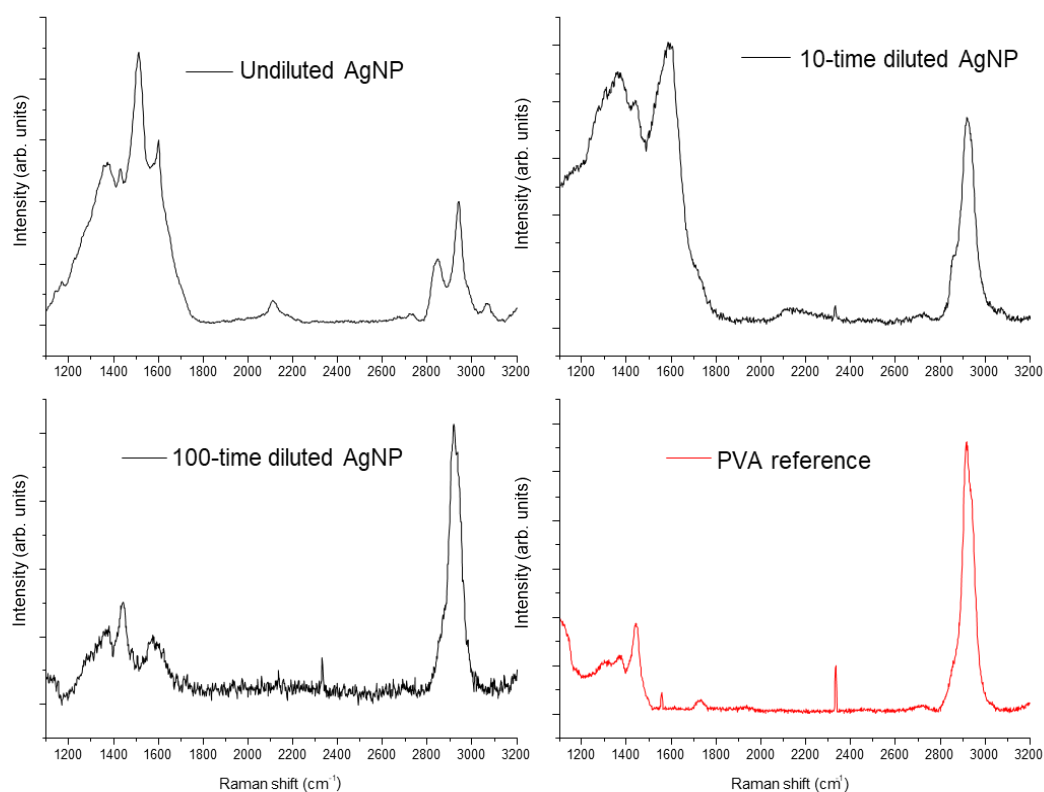
Figure 4.9 In black, the Raman spectra of the three PVA nanofibers with AgNP (with different dilutions) deposited under them. In red, the reference spectrum of PVA nanofibers.

4.1.3.3. AgNP inside the fibers

The third configuration exploited the same solutions used for film deposition (section 4.1.2). The aim, in this case, was to obtain nanofibers with both AgNP and C_4Cl inside the polymeric matrix. Six different nanofibers samples were collected on silicon substrates: AgNP colloids at 33%, 50% and 66% in volume, each in the formulation with and without polyynes (see 4.1.2 for the solution preparation). Electrospinning was performed at 0.5 mL/h, 13kV and about 23 cm of distance: time was kept between 20 and 60 seconds. Since the samples were produced in different days, temperature and humidity were not constant: this could affect fibers morphology, but a check of the quality was made with an optical microscope before each deposition, to assure that nanofibers were beadless.

Figure 4.10 contains SEM images of the PVA nanofibers with AgNP at 50% and 66% vol with C_4Cl inside, and of PVA-only nanofibers electrospun with the same parameters. From a qualitative point of view, the addition of polyynes and nanoparticles did not change nanofibers appearance.
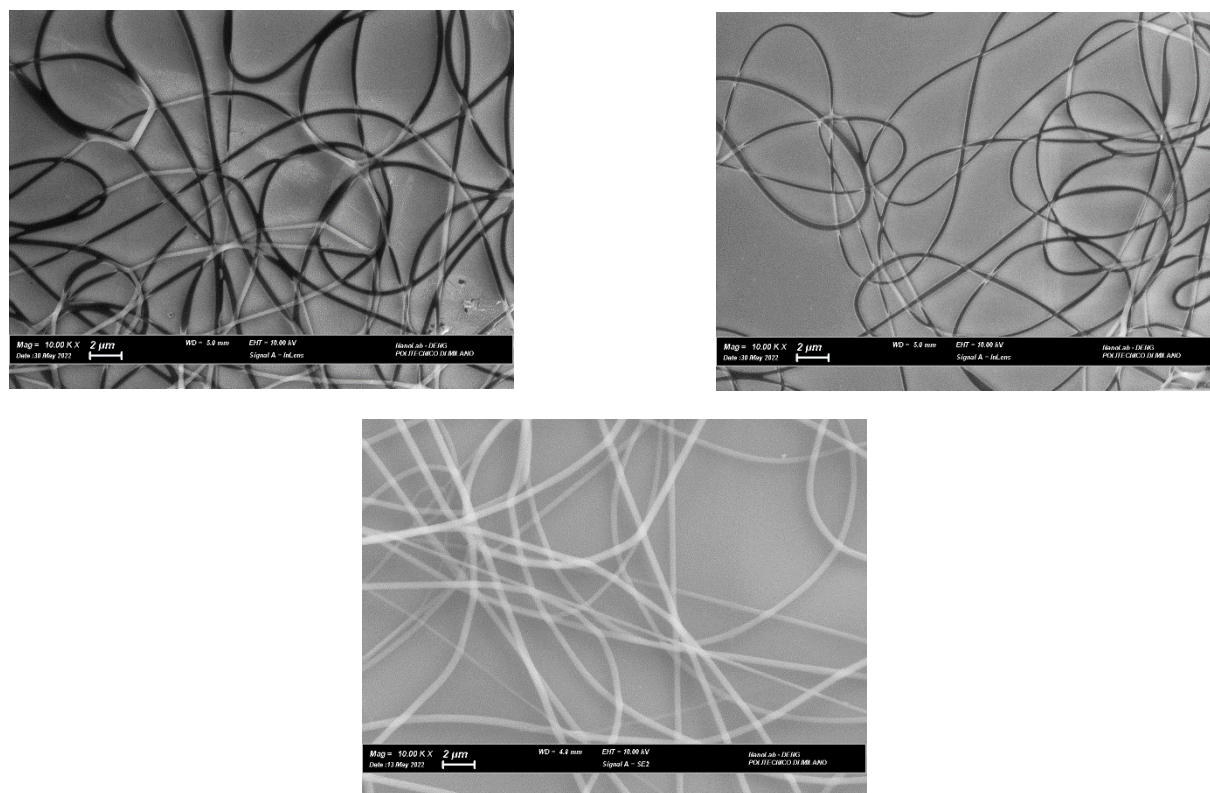
Figure 4.10 SEM images of: PVA nanofibers with C_4Cl and AgNP 50% (upper left) or 66% (upper right); PVA nanofibers (bottom center)

SERS spectra were measured for all the samples. However, none of them shows a signal in the polyyne region. In addition, their analysis brought up some issues related to signals homogeneity: nanoparticles effect on the SERS spectrum proved to be strongly dependent on the point of the specimen onto which the laser was focused. This effect was observed both for nanofibers embedding polyynes and nanofibers without them. Figure 4.11 shows an example of two SERS spectra of the sample prepared from a solution with 50%vol of AgNP colloid and no polyynes: near each graph is shown a picture of the measured spot, taken with the optical microscope of the spectrometer (50x). By focusing the laser on a denser region, the shape of the spectra changes completely due to the strong response of the nanoparticles, which is way more intense than the PVA characteristic signal at 2930 cm^{-1}. Figure 4.12 displays a similar behaviour for nanofibers obtained from the solution with 50%vol of AgNP and C_4Cl. In this second example it is evident that neither of these two spectra has some signal related to C_4Cl molecules. Similarly, the other samples (33% and 66%vol of AgNP and polyynes in DMSO) did not show any results toward polyynes detection.
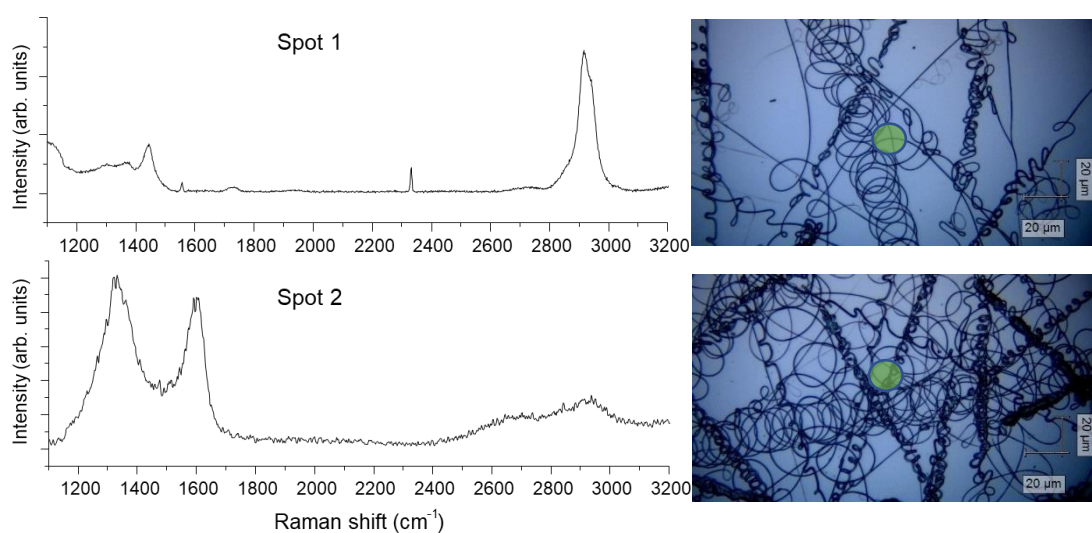
Figure 4.11 SERS spectra (left) and microscope images (right) of two different measured spots for a nanofibers sample with 50%vol of AgNP. The green dot gives the idea of laser spot dimension.
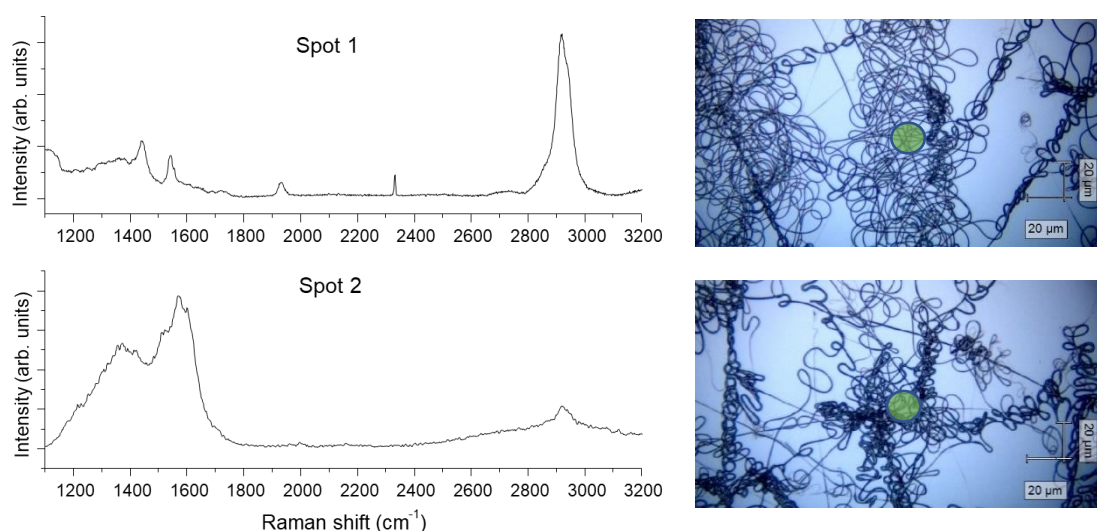
Figure 4.12 SERS spectra (left) and microscope images (right) of two different measured spots for a nanofibers sample with 50%vol of AgNP and C$_4$Cl. The green dot gives the idea of laser spot dimension.

4.1.4. Detection of C$_4$Cl by SERS active substrates

The above section described several experiments performed with the aim of investigating halogenated polyynes inside electrospun nanofibers. However, none of the three sample's configurations exhibited some considerable results. Therefore, it was decided to try another approach to detect C$_4$Cl molecules, still exploiting electrospun nanofibers. This time, nanofibers were used as an active SERS substrate instead of as an embedding matrix. As was explained in chapter 2, electrospun fibers can be used as sensors to detect numerous analytes: one of the methods is to incorporate plasmonic metallic nanoparticles inside fibers matrix or on their surface. In this way, even a poor concentrated substance interacting with the nanofibers can be detected by SERS effect at the fibers surface.

Thus, it was decided to perform the investigation of halogenated polyynes after they were deposited on the surface of two SERS active substrates made from nanofibers. The production of these kind of samples was done following a method perfectionated over the years by the research group of Functional and Nanostructured Materials of the department of Chemistry and Materials at Politecnico di Milano.

Two samples were synthesized, one with silver nanoparticles from the Lee-Meisel approach, and the other with silver nanoparticles from NaBH$_4$ reduction method. In both cases, AgNP were concentrated by using a centrifuge: 20 minutes at 8000 rpm for the first AgNP, 20 minutes at 14000 rpm for the latter ones. The different centrifuge intensity was due to the average dimension of nanoparticles. The absorption peak of AgNP from Lee-Meisel approach was found at 420 nm, the peak of the AgNP from

NaBH₄ reduction was found at 390 nm; by exploiting eq. $NP_{size}(nm) = 0.78 \times (\lambda_{LSPR}) - 266$
(3.1, average nanoparticles size was calculated to be approximately 60 nm and 38 nm. Thus, smaller AgNP required stronger centrifugation to be separated from the supernatant. Figure 4.13 shows the two absorption spectra.
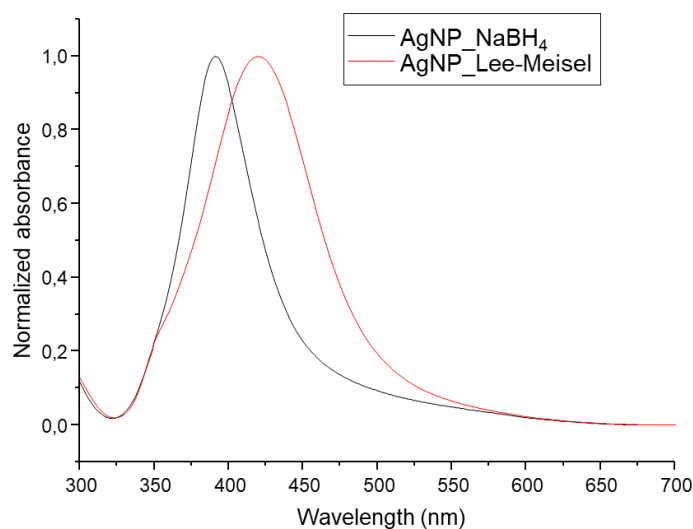
Figure 4.13 Normalized absorption spectra of the two synthesized AgNP colloids

Volume was reduced from 50 mL to 1.26 mL (a factor of about 40 times). Then, PVA was dissolved in both AgNP solutions to reach a concentration of 10%wt. Each solution was spinned on a substrate made of an alumina foil stuck on a glass substrate. Electrospinning parameters were chosen after multiple preliminary tests. For the Lee-Meisel AgNP they were set to 0.1 ml/h, 17 kV, 20 cm. For the NaBH₄ reduced AgNP they were set to 0.5 ml/h, 17 kV, 20 cm. In both cases the temperature was around 23 °C and RH was 48%. The difference in the feed rate was related to short-circuit phenomena risen during the second spinning operation. This is an issue that could happen when very conducting solutions are used, and it is related to the discharging of the needle through the infusion pump; it causes the appearance of a small instantaneous current and the drop of the applied potential. It was found that by increasing the feed rate, this behaviour became less frequent and thus the applied potential remained constant.

Electrospinning was performed for about an hour until the solution was consumed. Deposition was done for a longer time with respect to the samples previous described, because in this situation the aim was to have a nanofiber mat sufficiently dense and thick to be used as an active substrate for SERS detection of polyynes.

The solution with concentrated Lee-Meisel AgNP was also spinned for some tents of seconds on silicon pieces to observe the fibers at SEM. Figure 4.14 shows their morphology. The main difference from the previous fibers containing silver

nanoparticles (Figure 4.10) is evident: after the concentration, it is possible to appreciate the nanoparticles distribution on the fibers surface and therefore have a clue of their presence inside the nanofibers. Moreover, observing so clearly AgNP on nanofibers surface indicates that there can be a closer interaction between analyte and nanoparticles, thus promising a more efficient SERS.
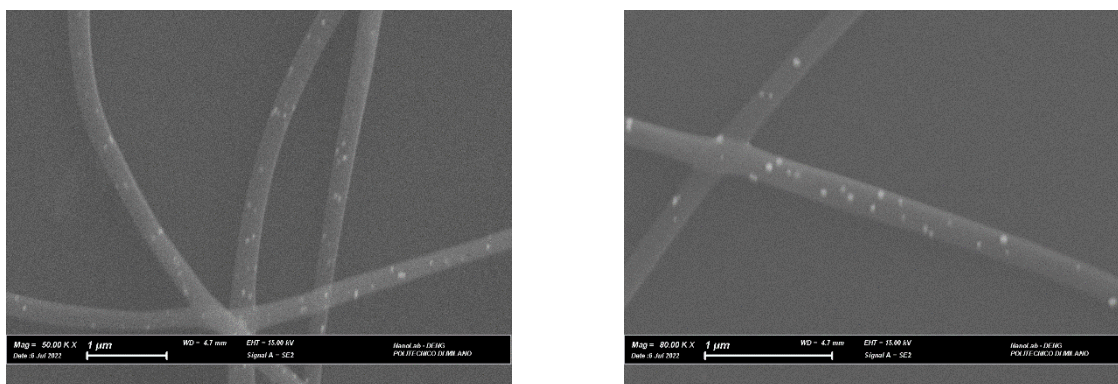
Figure 4.14 SEM images of PVA nanofibers with concentrated AgNP (Lee-Meisel) at different magnifications (50000x on the left, 100000x on the right)

After substrates production, the analytes solutions were prepared: C_4Cl molecules were diluted up to 10^{-4}, 10^{-5}, 10^{-6} mol/L in dichloromethane (DCM). From each solution, few drops were put on the two samples and, after solvent evaporation, a SERS spectrum was acquired on each spot. Results are shown in Figure 4.15.
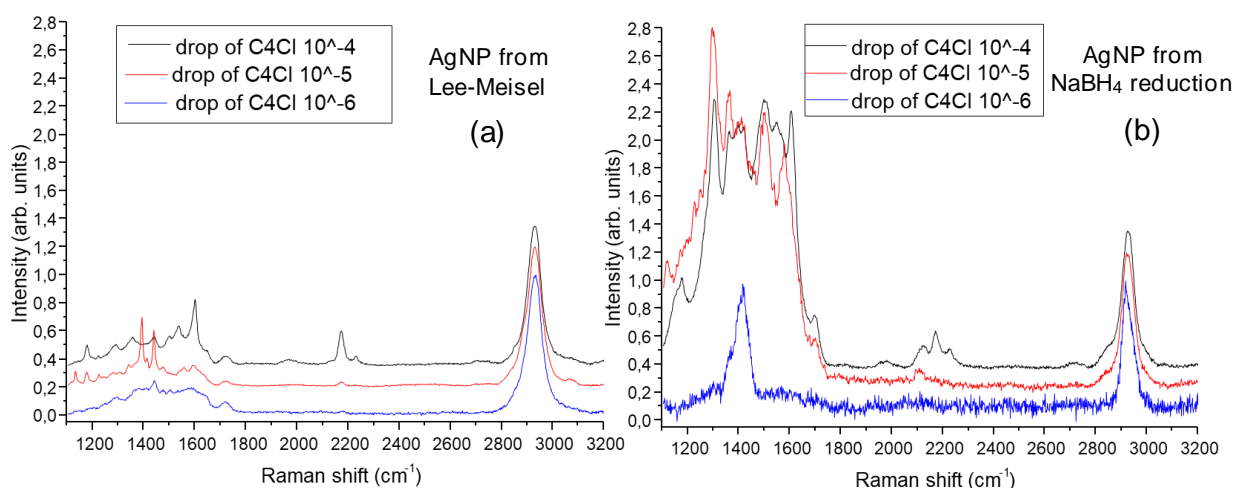
Figure 4.15. SERS spectra of the superficial polyynes investigation. All the spectra are normalized on PVA peak and vertically shifted to make comparisons.

In both samples, the drop from the solution with $C_4Cl\,10^{-4}$ mol/L (black line) shows a distinguishable signal centred around 2175 cm^{-1}. In the spectrum from the Lee-Meisel AgNP substrate (Figure 4.15a), even a sharp signal at 1600 cm^{-1} is visible (the phenyl ring), higher than the nanoparticles response. Also in the other substrate there is a similar peak, but it has the same intensity of the wide AgNP region, so it is not a strong evidence. It is important to notice that, in both spectra of the 10^{-4} mol/L solution drops, the signal at 2175 cm^{-1} possesses a little shoulder at higher wavenumbers, but only in Figure 4.15b (AgNP from NaBH$_4$ reduction) there is a lower signal on the left of the peak; this second shoulder is centred around 2115-20 cm^{-1}, highlighting that also here a carbon contamination could be present. In fact, by looking at the spectra referring to the $C_4Cl\,10^{-5}$ mol/L solution drops, it is evident that only in Figure 4.15a there is a (weak) signal at 2175 cm^{-1}, while in Figure 4.15b the observed peak corresponds to the same contamination contribution present in the above spectrum (the black line). Therefore, the substrate made from Lee-Meisel AgNP seems to be slightly better in the enhancement of polyynes response, even if the intensity of the signal is still very low. This behaviour is probably due to the different position of nanoparticles absorption peak. Since the laser excitation is at 532 nm (see chapter 3), the plasmonic effect of Lee-Meisel AgNP can be much more exploited, because their absorption peak is closer (420 nm) than the other AgNP (390 nm) to the laser frequency. Therefore, a higher enhancement is favourable; the experimental confirmation shown here convinced us to use only Lee-Meisel AgNP for other detection experiments that will be presented in the second section of this chapter. However, it is evident from the very less intense signal of the $C_4Cl\,10^{-5}$ mol/L solution, and from the fact that in both samples the drop of $C_4Cl\,10^{-6}$ mol/L solution did not give any results, that the enhancement effect is still moderate, and the problem of detection is not solved.

One last experiment was performed to investigate polyynes presence, since the test just presented, exploiting AgNP concentrated, has given some results. Therefore, it was decided to try once again to embed the polyynes in PVA nanofibers, this time with concentrated nanoparticles inside. The solution was prepared with a similar procedure of the ones described before: PVA was dissolved in a solution of concentrated AgNP (from Lee-Meisel method), then a 10%vol of DMSO containing C_4Cl was added. Calculations were made to have in the final solution PVA at 10%wt, C_4Cl at 10^{-5} mol/L and AgNP concentrated in volume by a factor of 40 times with respect of the as prepared colloid.

This solution was then electrospun at 0.3 mL/h, 15 kV, 20 cm for about 1 hour and half. Deposition time was kept high to obtain a dense nanofibers mat, thus more material under the laser focus and, therefore, a stronger signal; moreover, a dense sample should possess better homogeneity when measured in different spots. Figure 4.16 shows on the left a picture of the sample as prepared, with fibers deposited on an aluminium foil attached over a glass; on the right it displays a SEM image of some nanofibers deposited on a silicon, as was done for the above SERS substrate to observe

its morphology. Nanofibers show a similar morphology (uniform and beadless) than the ones prepared with non-concentrated nanoparticles (Figure 4.10). A quantitative comparison was done between the fibers with concentrated AgNP and the ones with concentrated AgNP plus C_4Cl in DMSO. ImageJ software was used to collect a number of diameter measurements between 80 and 100 and from these data average diameter and standard deviation were obtained.

Figure 4.16 PVA nanofibers with C_4Cl and concentrated AgNP, electrospun for: 1:30 h (left, photograph) and less than one minute (right, from SEM)

Nanofibers from dissolution of PVA only in concentrated AgNP showed an average diameter of 248 ± 54 nm, while the nanofibers from a solution with the addition of C_4Cl in DMSO displayed an average diameter of 318 ± 48 nm. The second sample has a higher mean size, but both results are included in the respective standard deviations; therefore, it can be said that the addition of DMSO could cause a slight increase in the fibers dimension, but more tests are required, and that is out of the scope of this work.

The thick sample containing C_4Cl molecules was analysed under Raman spectroscopy, and the resulting SERS spectra is shown in Figure 4.17. There is no presence of a strong peak indicating the polyyne. A small broad region is present around 2160-90 cm^{-1}, which could be a response from polyynes, but it cannot be affirm with confidence, since there is no way to exclude that is originated from a small source of contamination or even a background noise; also, there is no evidence of the phenyl signal arising at 1600 cm^{-1}.

This experiment concludes the investigation of halogenated polyynes in electrospun nanofibers. Polyynes detection was achieved with no doubt in liquid solutions, onto the surface of SERS substrates and in polymeric films; however, the integration inside nanofibers did not lead to the same results. Excluding SERS in liquid and detection on SERS active substrates, which are not comparable and were performed to offer an overview on multiple ways to detect low concentrated polyynes, it is quite singular to find an unequal response inside films and nanofibers, since in principle they are both polymer matrices. It can be assumed that the electrospinning process plays a role in

the final dispersion of AgNP and polyynes, up to a point that it does not allow an easy interaction between them. Moreover, some hypothesis can be made regarding the ability of the molecule itself to be enhanced by SERS effect, but these considerations will be presented after having shown a comparison with the investigation of hydrogenated polyynes, which is the topic of the next subchapter.
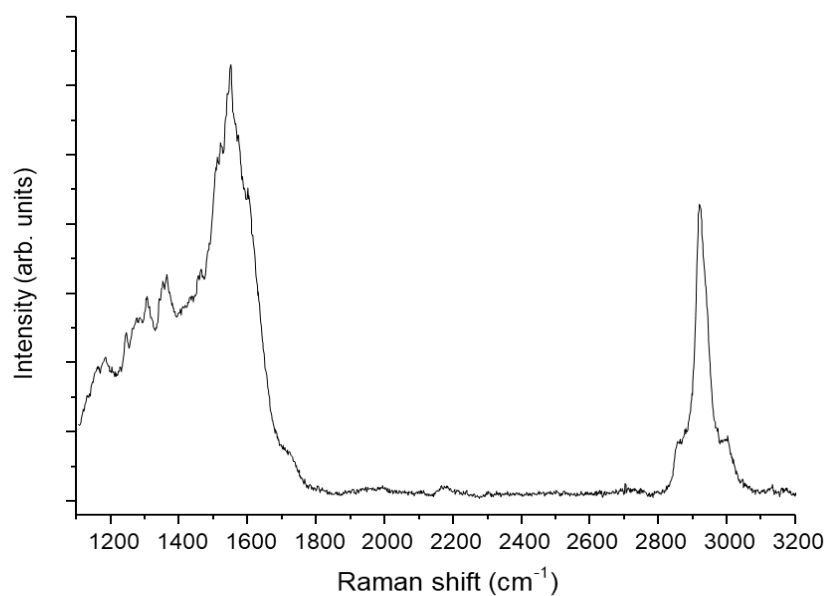
Figure 4.17. SERS spectrum of PVA nanofibers embedding C_4Cl and concentrated AgNP

4.2. Investigation of hydrogenated polyynes produced by laser ablation

The detection of hydrogenated polyynes was performed following similar procedures exploited for halogenated molecules. First, a SERS in liquid experiment was done to verify the kind of signals produced by a mixture of polyynes. It was decided to start with the characterization of polyynes produced by PLAL in water, since it was easier to integrate them in PVA-AgNP solutions. Then, polyynes mixtures were investigated in PVA nanofibers and in polymeric films from the same solutions. The second part of this subchapter is focused on the detection of the same molecules, but this time synthesized by ablations in ACN, since they are more concentrated. PVA is insoluble in acetonitrile, thus the first aim has been to perform different tests and obtain a solution integrating PVA, AgNP colloid and polyyne in ACN, which does not present phase separations and can be electrospun in continuous fibers. The last evaluation with polyynes mixtures was performed with the SERS active substrate made of nanofibers that was presented in section 4.1.4. This experimental work is concluded by investigating the presence of size-selected polyynes (HC_8H) inside PVA film and nanofibers.

4.2.1. Stability and SERS in solution

Hydrogenated polyynes produced by pulsed laser ablation in liquid are known to be unstable in solution; moreover, a strong polar solvent like water increases the hostility of the environment. Therefore, at the beginning of this part of the work, it was necessary to perform a stability test to understand how long polyynes can survive before degradation, since their integration inside polymeric solutions must be done in that time window. Figure 4.18 displays the UV-Vis spectra of a water solution just after the ablation and the following day (the solution was kept in a refrigerator); as can be clearly seen, there is an overall decrease of spectrum intensity. Only the main peak at 198 nm is still present with relevance, but this general rapid decline means that a lot of chains are degraded. Since the initial polyynes concentration is already low, it was decided to prepare a new polyynes solution for each test, to avoid that degradation could affect the results.
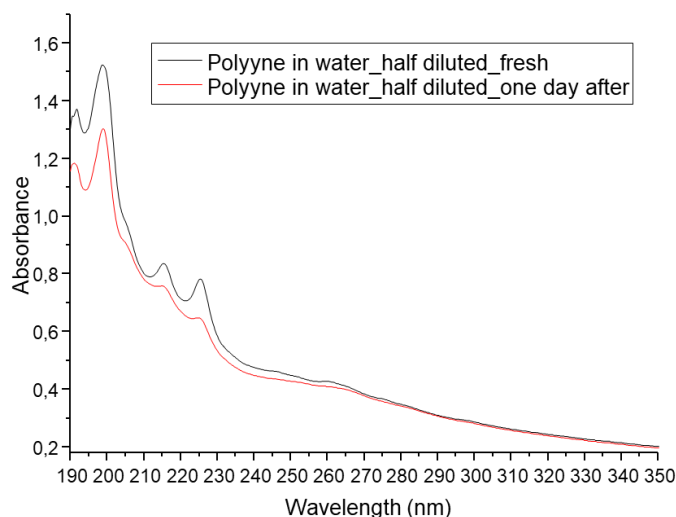
Figure 4.18. UV-Vis spectra of polyynes from ablation in water,
fresh and after one day of storage

SERS measurements were performed with a procedure similar to the one adopted for
C_4Cl detection. Since the concentration of polyynes obtained with PLAL is already
lower (about 10^{-6} mol/L) than the Raman sensitivity, no dilution was necessary. The
polyynes solution was easily mixed with the aqueous AgNP colloid at different
volume ratios (in the work presented in this subchapter, only nanoparticles from the
Lee-Meisel method were used). Figure 4.19 shows the results: each volume ratio is
indicated in the label. The broad response covering from 3100 to 3700 cm^{-1} is the O-H
stretching signal of water and it is very strong since water is the only solvent present.
The other main signals are in the 1500-1600 cm^{-1} and in the 1800-2200 cm^{-1} regions; the
first one is related to AgNP presence, as was highlighted in many other samples. The
second region contains the polyynic signals; in this case they are not sharp and peaked
responses since the analyte is a mixture of chains with different concentration and size.
These results agree with many previous SERS experiments performed on
hydrogenated polyynes [39, 49, 52]. In this case, differently from the halogenated
polyynes described before, the strongest SERS response in the ECC region comes from
an equal volume ratio between polyynes mixture and AgNP colloid.
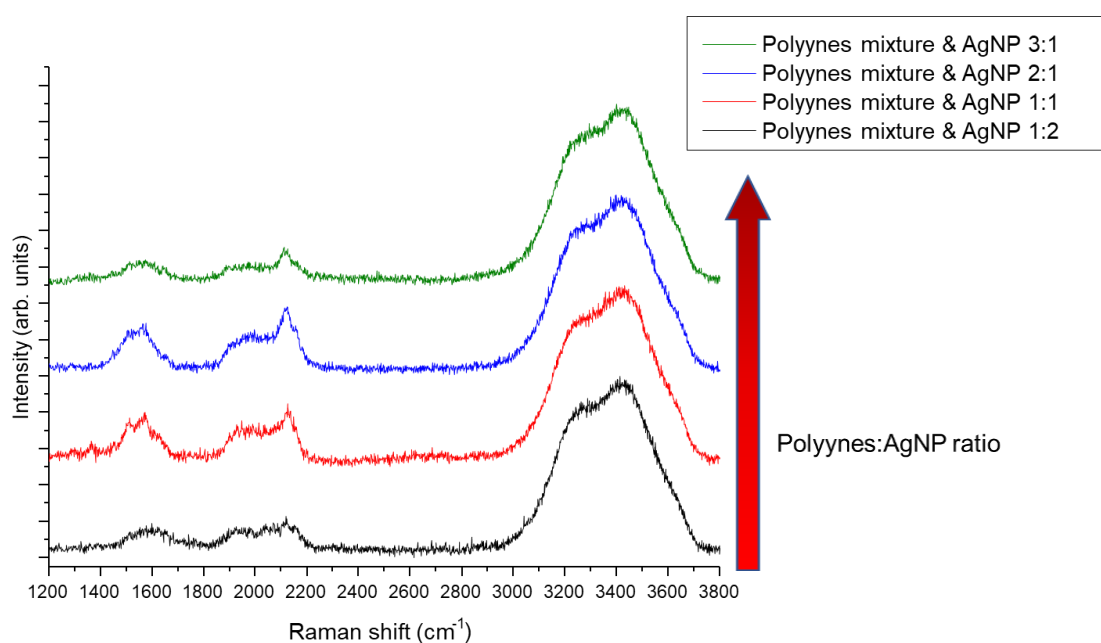
Figure 4.19 SERS in liquid of polyynes mixtures produced with PLAL in water mixed with AgNP colloid at different ratios.

4.2.2. Detection of polyynes from ablation in water

The investigation of hydrogenated polyynes was first performed implementing some of the configurations adopted for the halogenated polyynes. Even if no appreciable results were found with C_4Cl, it was decided to perform similar experiments to understand if the problem of detection was related to a bad SERS-response of the polyyne or if it is a more general problem of the detection method. These experiments involved the dispersion of the AgNP under the fibers and inside them. The first trial was performed as follows: the undiluted AgNP colloid was deposited onto an aluminium (Al) foil and left to dry. This Al-AgNP substrate was then used to collect electrospun fibers from a solution of PVA and polyynes mixture in water: the solution was made by mixing 50%vol of water containing polyynes with 50%vol of a water solution with PVA. As always, the overall polymer concentration resulted to be 10%wt. Electrospinning was performed at 0.5 mL/h, 13 kV, 20 cm for 45 minutes, to collect a dense mat of nanofibers. Temperature and HR were respectively 25.4°C and 29%. The second sample was prepared by using the same electrospinning parameters and collecting the fibers on an Al foil. In this case, the solution was made by mixing equal parts of PVA dissolved in the AgNP colloid and polyyne mixture in water, therefore exploiting the configuration with nanoparticles inside the fibers. Both samples were analysed by Raman spectroscopy: as it happened with C_4Cl, only some contaminations signals from the AgNP were found. The configuration with AgNP

above the fibers was not tried since PMMA cannot be blended with polyynes in water or in acetonitrile (the first is a non-solvent, the second a poor solvent).

The third attempt consists in embedding polyynes inside nanofibers with the presence of concentrated AgNP. Nanoparticles were concentrated up to a 40 times volume reduction and PVA was dissolved in them; this solution was then blended in an equal volume with a polyynes mixture in water. Electrospinning was performed on an Al substrate with the following parameters: 0.3 mL/h, 17 kV, 20 cm for 1:40 hours. Temperature and RH were 25.6°C and 46%. A drop from the remaining solution was taken to deposit a film on a silicon substrate by spin coating (Laurell instrument).

Figure 4.20 shows the SERS spectra of both samples, the thick nanofibers mat (also called "membrane") and the polymeric film. The two spectra are very similar, with an intense two peaked signal in the polyynic region; the left region (under 1600 cm^{-1}) is, as in all other cases, expression of AgNP presence. The PVA characteristic peak around 2930 cm^{-1} displays a singular shape, as if it is composed by a combination of two responses; this is the only sample displaying that behaviour, therefore it is still quite challenging to determine what is the main cause that originates it, since silver nanoparticles and hydrogenated polyynes are present also in other compounds. However, the main goal of this work is to detect polyynes presence in nanofibers: this method, exploiting concentrated nanoparticles and a mixture of hydrogenated polyynes, demonstrated to be highly effective.
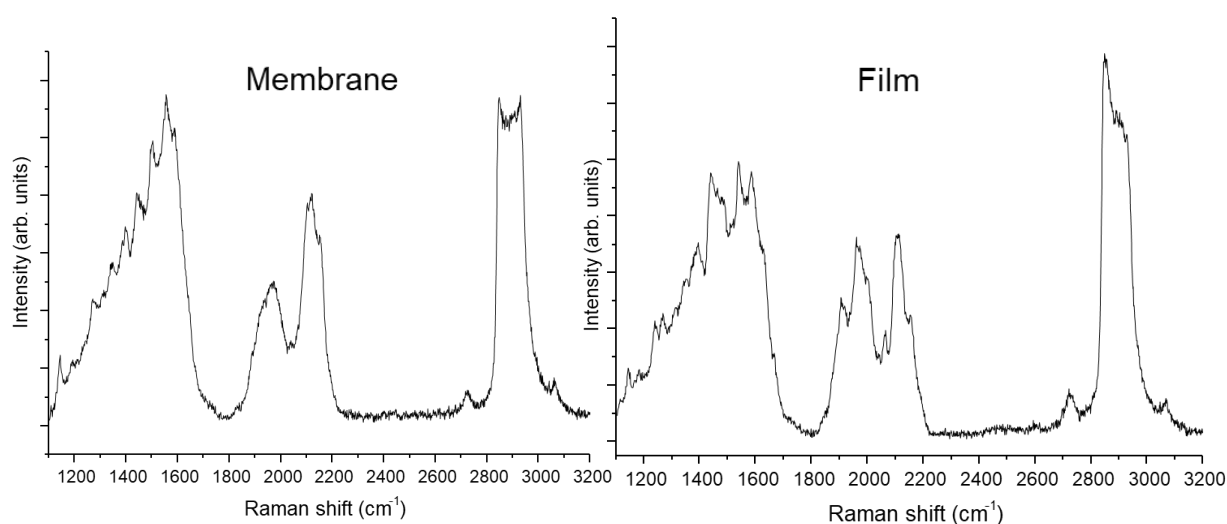
Figure 4.20 SERS spectra of PVA electrospun membrane (left) and spin-coated film (right) embedding polyynes from PLAL in water

The result is even more impressive considering that polyynes concentration from PLAL is around 10^{-6} mol/L, while the C$_4$Cl molecules have been always diluted up to 10^{-5} mol/L in all solutions. This factor opens a discussion on the different ability of a polyyne to interact with silver nanoparticles. It is possible that results so different from

each other could be the consequence of a more intense interaction of hydrogenated polyynes with silver nanoparticles. As was previously said, a mixture is composed by chains with different lengths, mainly HC_6H and HC_8H in a water mixture but also longer chains (with lower concentrations). On the contrary, the halogenated polyyne (C_4Cl) is the shortest chain analysed (only four carbon atoms in the sp region) and presents bulky terminal groups compared with the small hydrogens. All these factors could have played a role in defying the intensity of enhancement. Anyway, these experiments have proved that SERS of polyynes is achievable also in nanofibers with a significant response, exploiting a system that could be adjusted with no extreme difficulties to be used for the detection of other polyynes. Moreover, the huge difference between hydrogenated and halogenated polyynes could help to analyse if a preferential interaction (or on the contrary, a hostile one) between AgNP and specific polyynes is present.

One particular result obtained in the section 4.1.3.3 was the huge difference between the signals acquired in two spots of the same sample (Figure 4.11 and Figure 4.12). A possible explanation could be that a higher fiber density under the laser spot was directly linked to a more intense nanoparticles signal, which could overwhelm the PVA response and change the spectra appearance. Another interpretation could be that the nanoparticles are not always distributed in a very homogeneous way, therefore it is possible to find points with very high concentration of AgNP and points where PVA is the only acquired signal. However, by spinning for a much longer time (as was done in this case) the system should result as isotropic as possible, because under the laser spot there is a huge number of nanofibers. Therefore, it was decided to perform a SERS measurement in 20 points of the nanofibers sample (the membrane), along the path shown in Figure 4.21, trying to obtain a qualitative representation of signals variability. The graph displays the acquired spectra; in all of them the response is still composed of two main broad peaks, even if the profile and the relative intensity of these two regions is variable along the sample. Anyway, compared with the completely different spectra found for the nanofibers in Figure 4.11 and Figure 4.12, this sample shows a remarkable homogeneity, confirming that a dense substrate is preferential to avoid inhomogeneous responses.
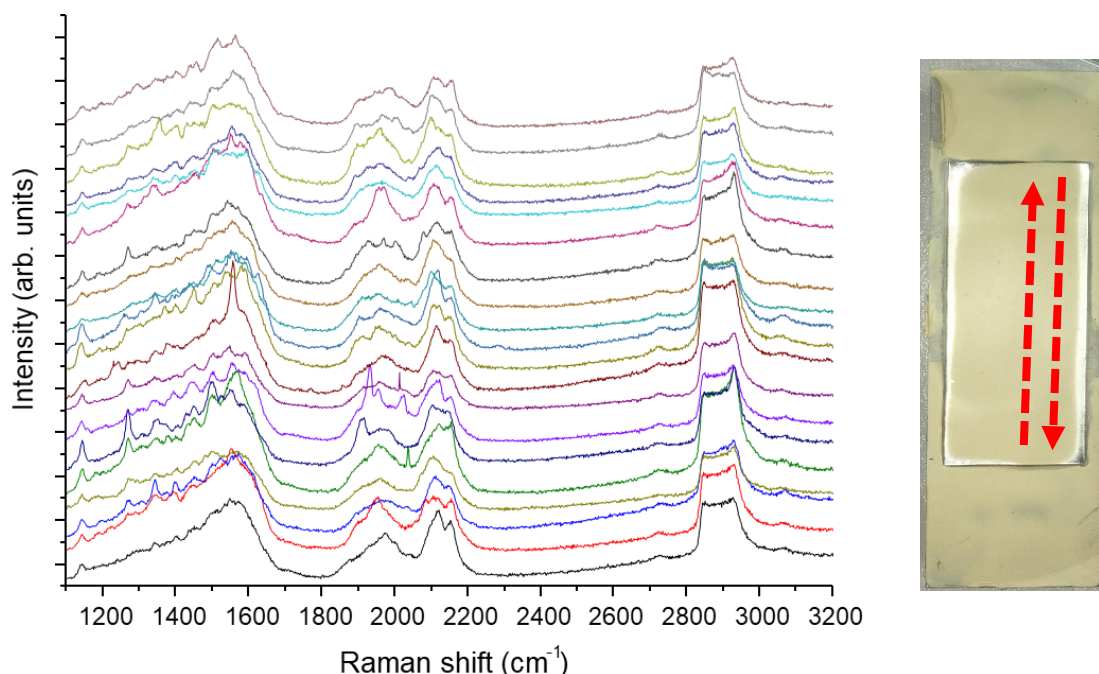
Figure 4.21 SERS spectra from the homogeneity test (left) and picture of the sample showing the collection path for the 20-points (right)

Another important issue related to hydrogenated polyynes is their stability. As was said in chapter 1, polymeric matrices help to stabilize polyynes and delay their degradation. To check if this is still valid in electrospun nanofibers, the sample was analysed multiple times over a time span of two months; Figure 4.22 sums up the spectra evolution. Measurements were performed each time on a random point, since the goal was to observe the general trend; considering what was said about the non-constant signal profile, the analyses show that polyynes are still present in the nanofibers even after more than 60 days, with an intensity comparable with the fresh measurement.
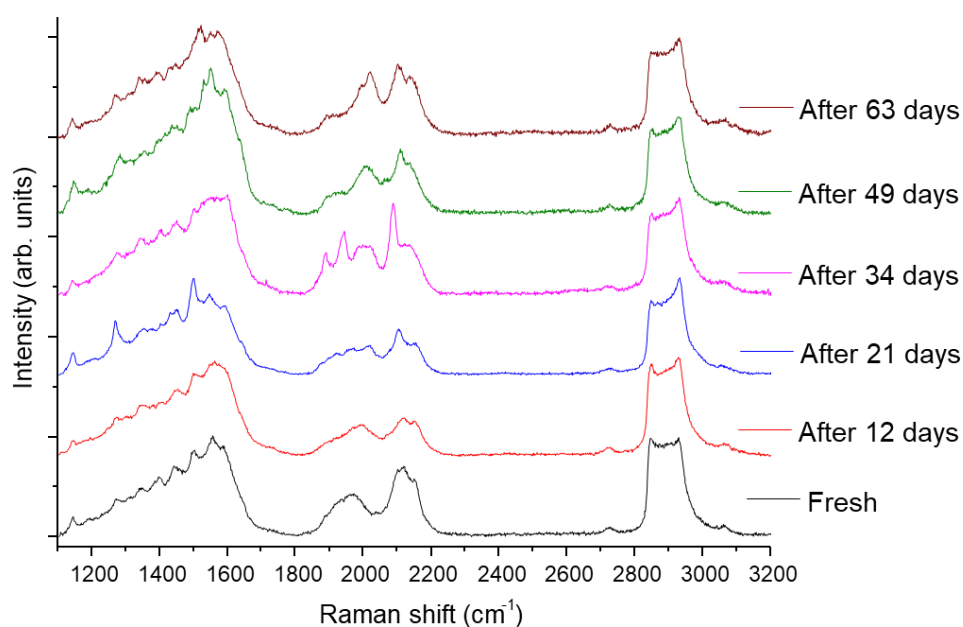
Figure 4.22 SERS spectra of electrospun membrane containing polyynes in water measured at different time intervals (spectra are normalized on PVA peak and shifted to make comparisons).

4.2.3. Detection of polyynes from ablation in acetonitrile

The second system deals with hydrogenated polyynes synthesized by PLAL in ACN. As was explained, ACN has demonstrated to be a good solvent for polyynes production since it allows higher stability and concentrations; the latter is a crucial feature and was exploited to obtain size separated polyynes by HPCL collection. Figure 4.23 shows the UV-Vis spectrum of polyynes from ablation in ACN compared with the spectrum previously shown (Figure 4.18) of water ablated solution. It should be taken into consideration that the black line refers to a solution diluted 10 times (to avoid saturation of the measurement) while the red one is only half diluted. The green vertical lines correlate each absorption peak with the corresponding polyyne: longer chains are visible only in the ACN solution. This graph helps to appreciate the higher polyynes production of acetonitrile and why it was chosen. Anyway, before starting with the characterization of the mixture and size selected polyynes, an optimization of electrospinning parameters was done, to allow the production of continuous and beadless nanofibers from water-ACN blends.
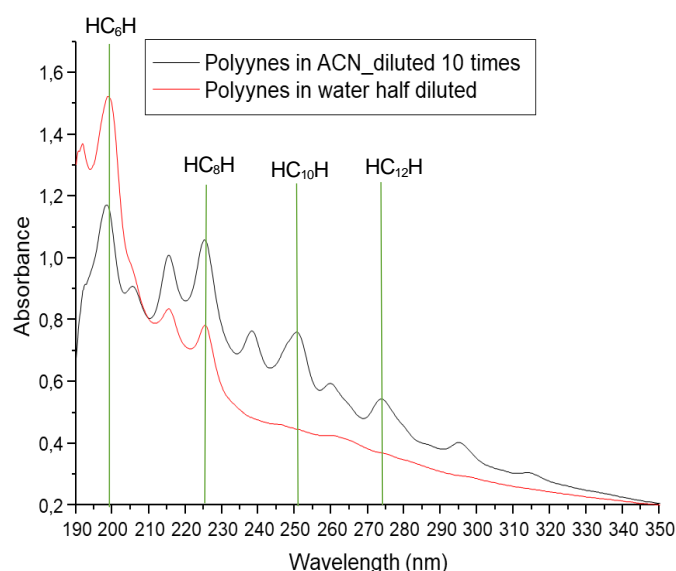
Figure 4.23 Comparison of the absorption spectra for polyynes synthesized in water and ACN. Green line highlight absorption peaks of individual carbon chains

4.2.3.1. Optimization of electrospinning for PVA in water-ACN solutions

In her work [86], Sacchi found out that PVA could be dissolved in water-ACN solutions up to 42%vol fraction of acetonitrile. She performed her tests with a 5%wt concentration of PVA, but in this work all the solutions are made with a double polymer concentration. Therefore, to make sure that this result still holds in our case, PVA was dissolved at 10%wt in 5 different water-ACN blends. First, the polymer was dissolved in water, then ACN was slowly added, while keeping the solution on stirring: acetonitrile volume fractions were set at 10, 20, 30, 40, 45 %. Figure 4.24 shows the obtained solutions: as can be seen, up to 40%vol of ACN the blends are transparent and limpid, while at 45%vol solution becomes opaque, meaning that PVA is aggregating, and it is not soluble anymore. That confirms Sacchi's results.

Then, the first four solutions were electrospun on glass substrates and their morphology was checked with optical microscope at 20x, 50x and 100x. The electrospinning parameter optimization was performed as follows: distance needle-collector was kept around 20 cm, while applied potential and flow rate were permutated to exploit all the combinations. Voltage was maintained between 13 and 17 kV while the flow rate between 0.3 and 0.5 mL/h. Among all the tested combinations, for each solution the three best results were chosen, considering which nanofibers have shown an absence or a small quantity of defects. With these parameters, nanofibers were collected on silicon substrates to be analysed at SEM.

Therefore, a total of 12 samples (three for each of the four blended solutions) were observed at SEM. For each sample, 100 diameter measurements were performed with

the aid of ImageJ software. Then, the mean size and the standard deviation (SD) were obtained. Table 1 offers a recap of the results. Nanofibers are divided first by solution composition, then by exploited electrospinning parameters.
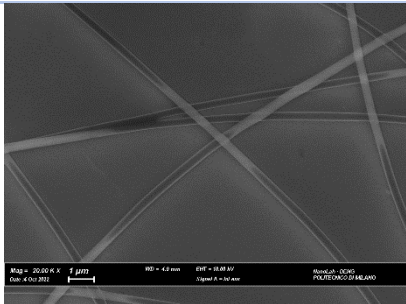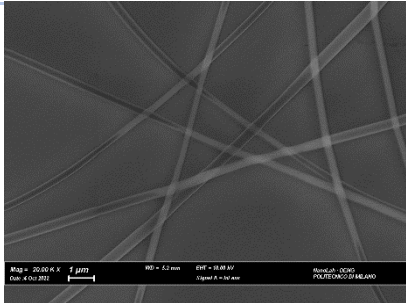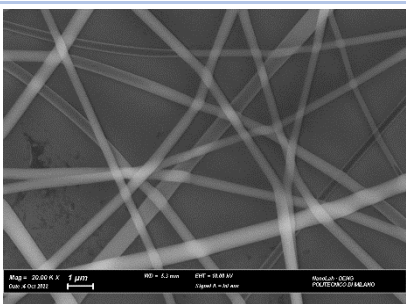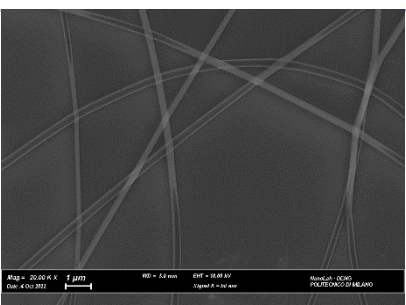
Figure 4.24 PVA in water-ACN blends, with ACN volume fraction of (from the left to the right): 10, 20, 30, 40, 45 %
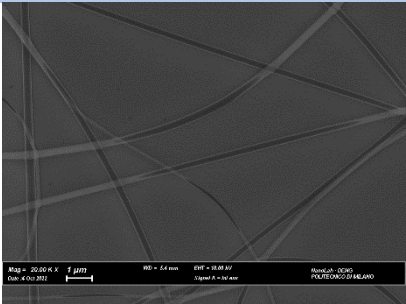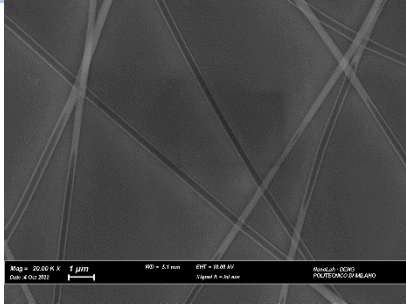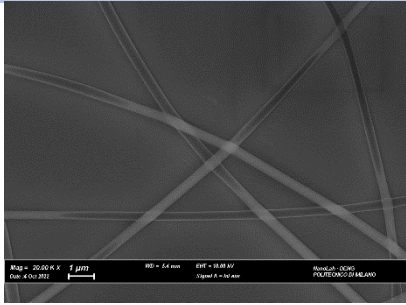
Table 1. Effect of different electrospinning parameters and of solution composition on the diameter and on the morphology of PVA nanofibers.

Volume fractions water:ACN	Electrospinning parameters	Average diameter ± SD	SEM image
0.9:0.1	0.3 mL/h, 15 kV	263 ± 32 nm	

	0.5 mL/h, 13 kV	272 ± 50 nm	
	0.5 mL/h, 17 kV	238 ± 42 nm	
0.8:0.2	0.3 mL/h, 13 kV	321 ± 40 nm	
	0.3 mL/h, 15 kV	314 ± 39 nm	

	0.5 mL/h, 15 kV	313 ± 39 nm	
	0.3 mL/h, 13 kV	342 ± 72 nm	
0.7:0.3	0.3 mL/h, 15 kV	443 ± 118 nm	
	0.5 mL/h, 13 kV	266 ± 59 nm	

0.6:0.4	0.3 mL/h, 13 kV	273 ± 71 nm	
	0.5 mL/h, 15 kV	361 ± 48 nm	
	0.5 mL/h, 17 kV	390 ± 56 nm	

Nanofibers morphology is, of course, affected by the presence of acetonitrile: the observed general trend is an increment in diameter size and distribution, even if some parameter combinations succeed in the mitigation of this phenomenon. However, these tests have shown that uniform and homogeneous fibers with dimension lower than 0.5 micron can be obtained even with considerable amount of ACN in solution. That is an important result, since it allows to integrate a higher quantity of polyynes mixture inside the fibers without losing uniformity.
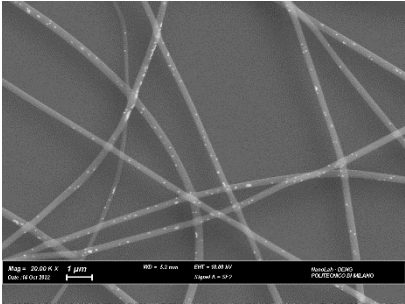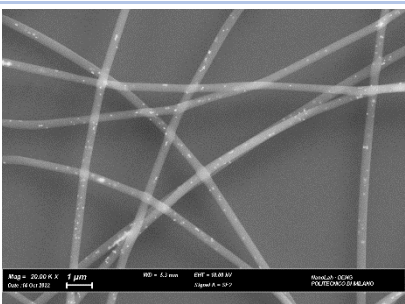
4.2.3.2. Nanocomposites embedding polyynes mixtures
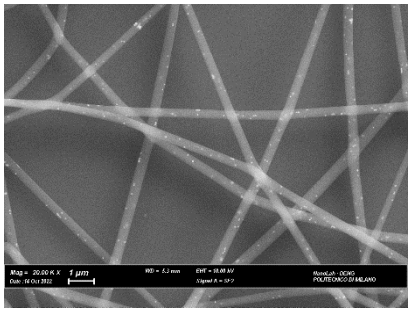
The analysis of polyynes mixtures from ablation in ACN was conducted with the same procedure than the previous one in water. It was decided to exploit the maximum amount of polyynes that could be integrated, therefore the PVA 10%wt solution was prepared with 60%vol of concentrated AgNP and 40%vol of polyyne mixture in ACN. The solution was then electrospun for few seconds on three silicon substrates, using

the same parameters of Table 1 for a 0.6:0.4 water:ACN mixture, to make comparison with the optimization tests. This time the polymer was dissolved not in simple water, but in the concentrated AgNP colloid, therefore the effect of nanoparticles on the morphology should be indagated.

Table 2 summarizes the new average diameter calculations performed with the three silicon samples. Size acquisition and analysis were done in the same way described before. The average diameters are similar than the ones in Table 1, with a dispersion slightly lower: thus, it can be affirmed that the addition of nanoparticles did not have a strong impact on nanofibers dimensions. The best parameters to obtain thinner nanofibers remain 0.3 mL/h, 13 kV, as was for the optimization tests, but all the fibers show a uniform morphology. Moreover, SEM images show also in this case a good dispersion of AgNP on the samples surface.

Table 2. Diameter analysis for the nanofibers with concentrated AgNP and polyynes in ACN

Volume fractions AgNP concentrated: polyyne mixture in ACN	Electrospinning parameters	Average diameter ± SD	SEM image
0.6:0.4	0.3 mL/h, 13 kV	282 ± 51 nm	
	0.5 mL/h, 15 kV	352 ± 42 nm	

	0.5 mL/h, 17 kV	363 ± 38 nm	

Going back to polyynes detection, the solution was electrospun for longer time (1:00 h) on the Al substrate to obtain the membrane. Temperature and HR were 24.8°C and 44%. A drop from the remaining solution was deposited on a silicon substrate and spin-coated to obtain a thin film. The nanofibers membrane on Al, the nanofibers on silicon and the film were analysed by Raman spectroscopy. Figure 4.25 shows the results. Also in this case, the polyynic signal is strong and visible, with a shape like the one seen before in water. There is no surprise in that, since the molecules are almost the same: as it was already explained, the main difference between water and ACN is that the second solvent allows the production of more polyynes during laser ablation, (therefore longer chains can be detected in the UV-Vis spectrum, see Figure 4.23). The main result here is to have achieved a clear polyynes detection even starting from a synthetization in a solvent not favourable for our PVA nanofibers, which has set some limits for polyynes integration. Another interesting fact is that the signal on the right spectrum was obtained by focusing few nanofibers under the laser spot: this means that, for polyynes detection, with this configuration there is no need to create a very dense sample with the aim of having more "material" excited by the laser. However, here and for the next experiment presented, it was decided to produce again the membrane to perform the homogeneity test and have comparable results.
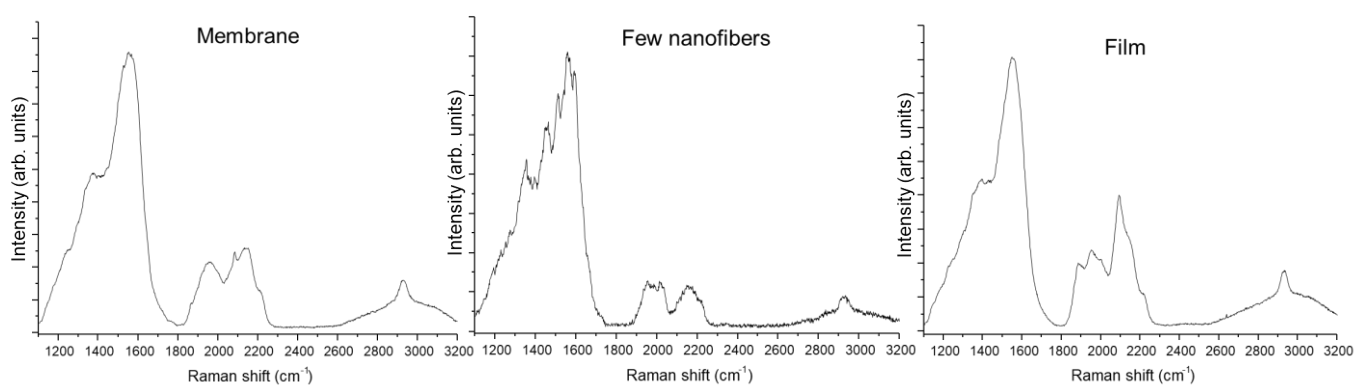
Figure 4.25 SERS spectra of PVA samples embedding polyynes from PLAL in ACN. Measurements are performed on different samples: an electrospun membrane (left), few nanofibers (center), a spin-coated film (right)

As was done for the previous sample, homogeneity and stability tests were performed. Figure 4.26 Figure 4.27 show the results, respectively. A compatible signal response was found along 16 points of the sample. Polyynes are still detectable after 40 days, even if the signal intensity starts to decrease after two weeks and then seems to stabilize; probably the most unstable chains are already degraded, but the presence of carbon chains is still observable. The analysed window time is reduced, compared to Figure 4.22, only because this specimen was produced weeks later than the other one.
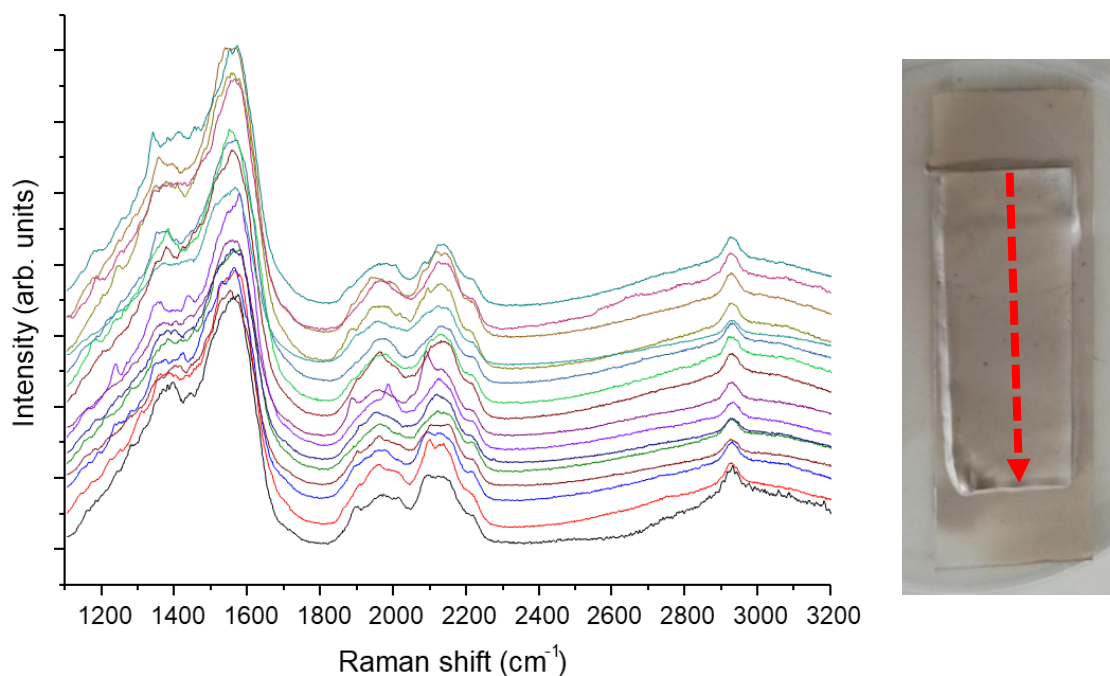
Figure 4.26 SERS spectra from the homogeneity test (left) and picture of the sample showing the collection path for the 16-points (right)
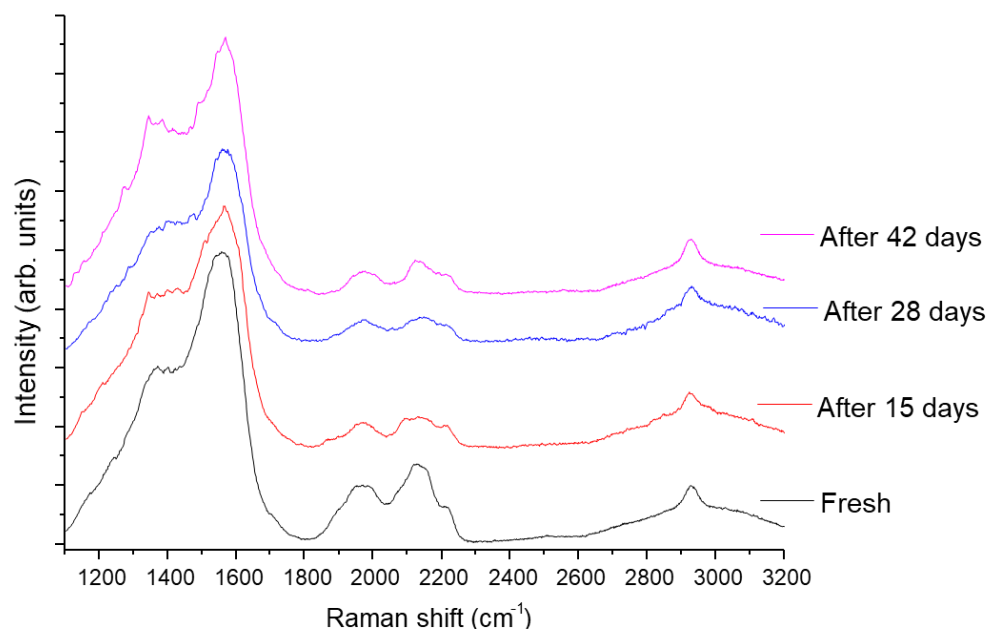
Figure 4.27 SERS spectra of electrospun membrane containing polyynes in ACN measured at different time intervals (spectra are normalized on PVA peak and shifted to make comparisons)

4.2.3.3. Detection of polyynes by SERS active substrates

Before moving to the investigation of the size-selected polyynes, one last characterization is presented for completeness. It involved the production of a SERS active substrate by exploiting the same procedure described in section 4.1.4 for C_4Cl superficial investigation. Polyynes were produced in ACN, and few drops were put on the substrate; after solvent evaporation, SERS was performed focusing the laser inside the drop region. Figure 4.28 offers a comparison between this result and the most intense signal acquired with the halogenated molecule. It should be notice that mixture concentration is in the order of 10^{-6} mol/L, while C_4Cl concentration in the drop is 100 times higher. Nevertheless, hydrogenated polyynes signal is more intense (PVA peak is used as reference), confirming the hypothesis that the interactions of polyynes with AgNP are better for the investigated hydrogenated polyynes than for the halogenated compound analysed in this work. The mixture response is peculiar; it presents a comb-like profile. A proposed explanation is that the system is so sensitive in the enhancement that allows to see the characteristic signals of size-selected polyynes, which are known to be shifted in relation to the sp chain length.
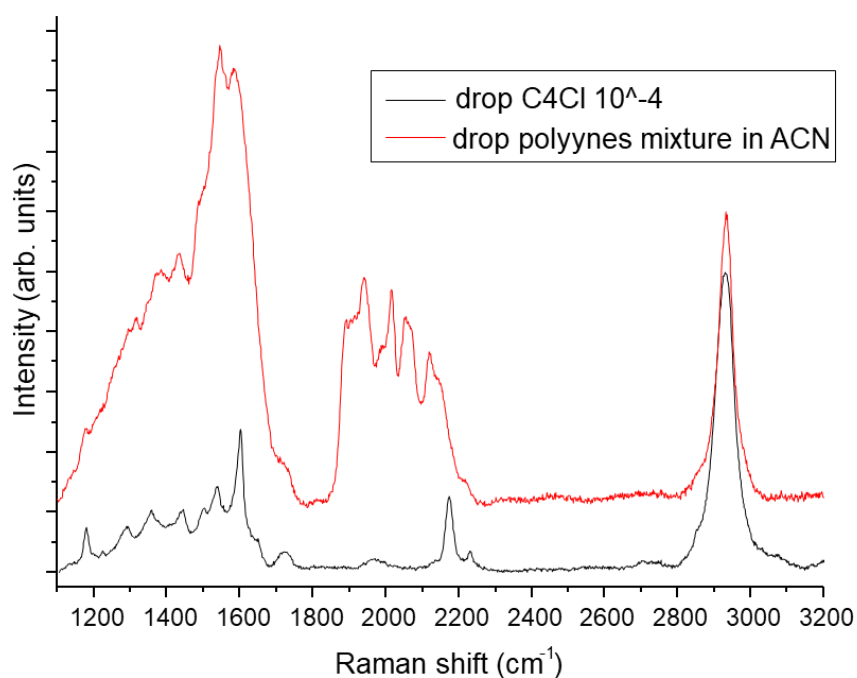
Figure 4.28 Comparison of the superficial SERS investigation performed for hydrogenated and halogenated polyynes

4.2.3.4. Nanocomposites embedding a size-separated polyyne

The last investigation was done on size-selected polyynes, HC_8H molecules. As explained in chapter 3, a solution containing these specific polyynes was obtained by HPLC separation of a concentrated and filtered mixture in ACN. HC_8H resulted to be the most abundant polyynes in the mixture, thus chosen to be embedded in nanocomposites. Samples were prepared like in the previous presented case. A 40%vol of the water-ACN solution containing HC_8H (coming from HPCL) was blended with a 60%vol of PVA dissolved in concentrated AgNP. This solution was electrospun for few seconds on a silicon piece and for 1:05 h on the Al substrate. A drop of the same solution was spin coated on silicon.

Figure 4.29 sums up the SERS spectra acquired. A very strong signal arises in the polyynic region, with a sharp profile; peaks are found at 1898, 1947 and 2082 cm^{-1}. Those peaks are in agreement with the SERS measurements of HC_8H performed by Tabata *et al* [47], thus confirming that these are the ECC signals of our size-selected chain. Moreover, it is evident that the signal intensity is so high that annihilates PVA peak at 2930 cm^{-1}. However, it is better to avoid a quantitative comparison with the previous spectra of polyynes mixtures, because the ablated solution was first concentrated with Rotavapor and then diluted by HPLC, therefore it is difficult to make precise assumptions on HC_8H concentration. Nevertheless, the very high intensities of these signals are a solid confirmation that even size-selected molecules

have been detected in the fibers and films. Also in this case the detection is achievable even when few nanofibers are analysed.
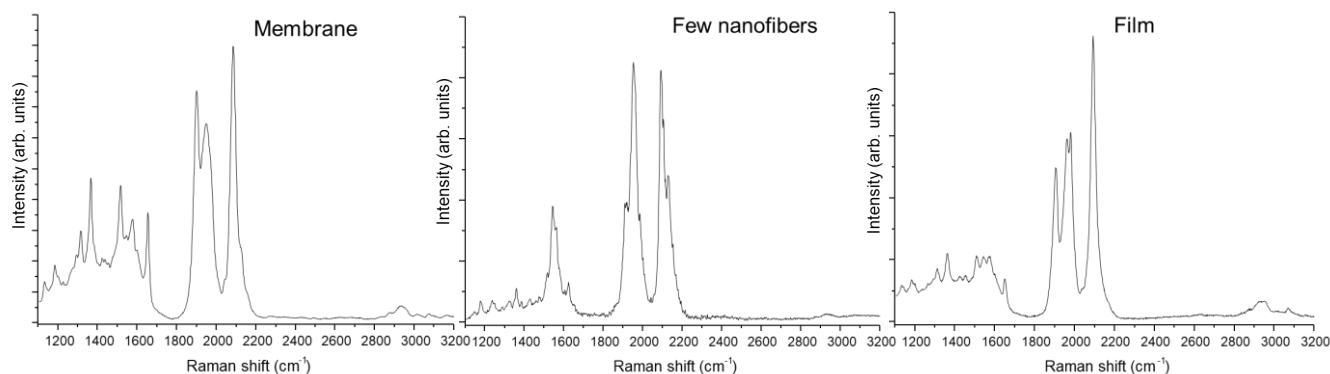
Figure 4.29 SERS spectra of PVA samples embedding size-selected polyynes (HC$_8$H) from PLAL in ACN. Measurements are performed on different samples: an electrospun membrane (left), few nanofibers (center), a spin-coated film (right)

The analysis is concluded by presenting the results of a 16-point homogeneity test and the stability test up to 30 days, shown in Figure 4.30 and Figure 4.31. A uniform and durable response is present also for this sample. As was observed for the previous sample, also here the polyyne signals are lowered after two weeks, then they seem to stabilize (still remaining very intense, compared with PVA peak).

In conclusion, this experimental section has shown that this sample configuration (AgNP concentrated inside polymeric nanofibers) has demonstrated to allow the detection of both low concentrated hydrogenated polyynes mixtures and specific size-selected chains. The investigation of HC$_8$H, compared with the results obtained for C$_4$Cl polyynes, confirms another time the dependence of the SERS response to the investigated polyyne; moreover, it shows that the most probable factor determining this behaviour is probably the different polyynes endgroup, since here single-length chains (as C$_4$Cl polyynes) were detected.
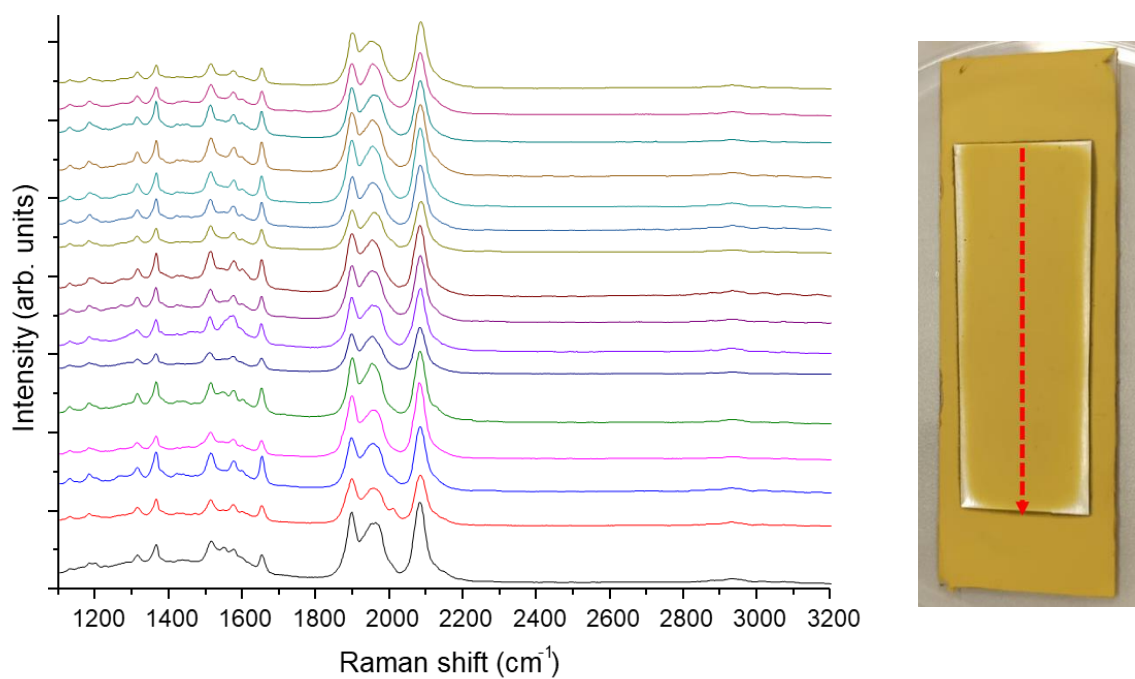
Figure 4.30 SERS spectra from the homogeneity test (left) and picture of the sample showing the collection path for the 16-points (right)
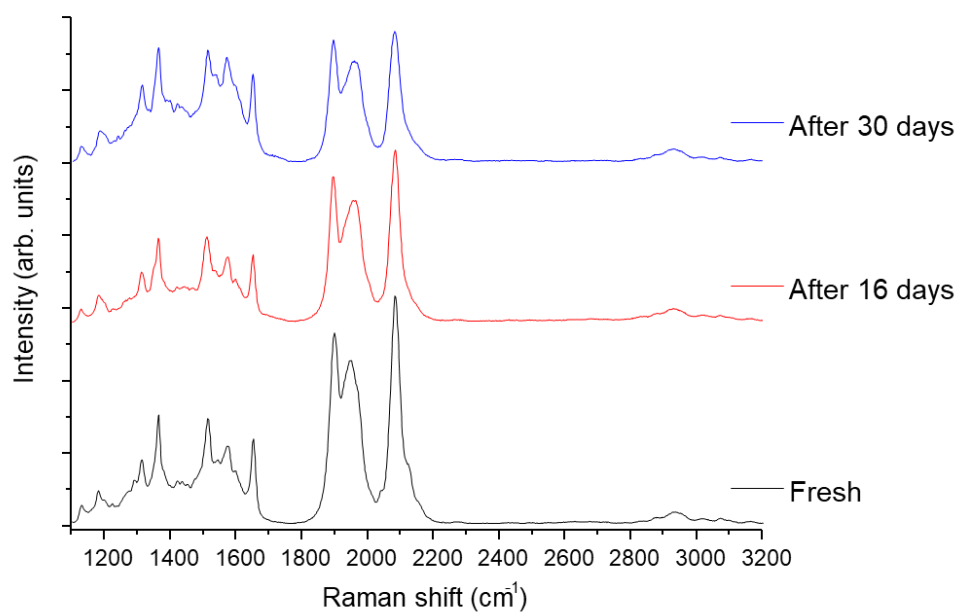
Figure 4.31 SERS spectra of electrospun membrane containing HC_8H polyynes in ACN measured at different time intervals (spectra are normalized on PVA peak and shifted to make comparisons)

5   Conclusion and future developments

The aim of this thesis work was the investigation of two different endcapped polyynes, halogenated and hydrogenated, embedded in electrospun nanofibers. Hydrogenated polyynes were produced by Pulsed Laser Ablation in Liquid (PLAL), which is a technique limiting the obtainable concentration at approximatively 10^{-6} mol/L. Since Raman spectroscopy is not sensitive enough to detect such low concentrated analytes, Surface Enhanced Raman Scattering (SERS) measurements were performed to allow the analysis. It was decided to investigate also the halogenated polyynes at low concentrations (10^{-5} mol/L in the electrospun polymer solution) in order to compare results and obtain a detection method feasible for different carbon chains.

The experimental work consisted in testing various samples configurations with the purpose of finding the most efficient way to observe polyynes SERS signals in nanofibers. For both the investigated carbon chains, SERS tests in liquid and polymeric films were done; that has provided a more complete knowledge of polyynes SERS responses in different medium. SERS signals of halogenated polyynes (C_4Cl chains) were detected both in solutions and PVA films, highlighting the characteristic SERS responses of this molecule: the phenyl signal at 1600 cm^{-1} and the ECC mode at 2175 cm^{-1}. However, the tests performed with polyynes embedded in nanofibers did not bring any important results: configurations with silver nanoparticles (AgNP) placed above, under or inside the fibers only showed peaks related to some contaminations. Experiments performed with hydrogenated polyynes led to similar results, except for one sample configuration, which instead proved to be extremely successful for the detection of this kind of polyynes. SERS signals were clearly observed in PVA nanofibers embedding polyynes and concentrated AgNP; polyynes from PLAL in water or ACN, and even size-separated chains (HC_8H) were detected. Signals in nanofibers were comparable with the ones in film, as a confirm on the efficiency of this configuration. In addition, polyynes have been detected up to several weeks after samples production, proving that the stabilization observed in polymeric films is also valid for nanofibers. That result is of extreme importance, since it is the first time that low concentrated carbon chains produced with physical methods have been observed in electrospun nanofibers.

One important consideration that could be done after this experimental work is related to the huge difference in halogenated and hydrogenated polyynes SERS responses. Results indicate that hydrogenated polyynes exhibit a stronger interaction with silver nanoparticles and, therefore, their observed SERS enhancement is extremely high. To

explain this phenomenon, we excluded the polydispersity of chain lengths in hydrogenated mixtures as a relevant factor, since the experiment with HC_8H demonstrated that also size-separated chains could be easily detected. Therefore, it is probable that the huge difference in terminal groups has played a crucial role; C_4Cl carbon chains possess a chlorine termination on one side and a substituted phenyl ring on the other, which are both bulkier endgroups than the hydrogen atoms characterizing the other polyynes.

Another critical issue is the fact that SERS signals of halogenated polyynes were observed in PVA films with the addition of the AgNP colloid, without exploiting concentration of nanoparticles. The same holds for hydrogenated polyynes, as was verified in previous works. However, polyynes detection in nanofibers required the use of concentrated AgNP as SERS enhancers. A possible explanation is that electrospinning causes an inhomogeneous dispersion of AgNP inside the nanofibers, when they are not concentrated; this could hinder the interaction between polyynes and nanoparticles, affecting the SERS response. That explains why a high variability of signals, depending on the analysed point, was observed in the fibers. AgNP concentration, instead, seems to attenuate the dispersion effect, probably because having more nanoparticles in solution allows a uniform distribution along the fibers. However, even in this case, if nanoparticles interaction with polyynes is weak, SERS effect is probably not as efficient as it is in polymeric films; this could be the reason for the absence of halogenated polyynes signals in nanofibers, while the strong AgNP-polyynes interaction in hydrogenated ones made the detection possible.

Those hypotheses open to the possibility of exploiting this detection configuration for other polyynic systems, to evaluate more specifically the differences in their responses and to be able to better understand the mechanisms behind selective SERS enhancement of polyynes. Thus, future works could deal with the adaptation of this detection system, with the purpose of integrating various polyynic species and creating a wider collection of SERS measurements in nanofibers. Other polyynes from laser ablation (like cyano or chlorine terminated chains) or polyynes with bulkier endgroups (similar to the C_4Cl ones) could be embedded in nanofibers; their investigation would allow to understand more deeply the role of terminal groups and the effect of electrospinning in SERS detection of low concentrated polyynes.

Bibliography

[1] A. Hirsch, "The era of carbon allotropes," Nature Materials, vol. 9, pp. 868-871, Nov. 2010.

[2] S. Nasir, M. Hussein, Z. Zainal and N.A. Yusof, "Carbon-Based Nanomaterials/Allotropes: A Glimpse of Their Synthesis, Properties and Some Applications," Materials, vol. 11, -02-13. 2018.

[3] R. Zhang and J. Jiang, "The art of designing carbon allotropes," Front. Phys, vol. 14, pp. 13401-17, 2019.

[4] H.W. Kroto, J.R. Heath, S.C. O'Brien, R.F. Curl and R.E. Smalley, "C60: Buckminsterfullerene," Nature, vol. 318, pp. 162-163, 1985.

[5] S. Iijima, "Helical microtubules of graphitic carbon," Nature, vol. 354, pp. 56-58, 1991.

[6] K.S. Novoselov, A.K. Geim, S.V. Morozov, D. Jiang, Y. Zhang, S.V. Dubonos, I.V. Grigorieva and A.A. Firsov, "Electric field effect in atomically thin carbon films," Science, vol. 306, pp. 666-669, 2004.

[7] M.C. McCarthy and P. Thaddeus, "Microwave and laser spectroscopy of carbon chains and rings," Chemical Society Reviews, vol. 3, pp. 177-185, 2001.

[8] A.G. Whittaker, E.J. Watts, R.S. Lewis and E. Anders, "Carbynes: carriers of primordial noble gases in meteorites," Science, vol. 209, pp. 1512-1514, 1980.

[9] C.S. Casari, "CARBON ATOMIC WIRES: FROM STARS TO NANOTECHNOLOGY," Istituto Lombardo-Accademia Di Scienze E Lettere-Rendiconti Di Scienze, 2012.

[10] C. Glaser, "Beiträge zur kenntniss des acetenylbenzols," Berichte Der Deutschen Chemischen Gesellschaft, vol. 2, pp. 422-424, 1869.

[11] C.S. Casari, M. Tommasini, R.R. Tykwinski and A. Milani, "Carbon-atom wires: 1-D systems with tunable properties," Nanoscale, vol. 8, pp. 4414, 2016.

[12] M.R. Bryce, "A review of functional linear carbon chains (oligoynes, polyynes, cumulenes) and their applications as molecular wires in molecular electronics and optoelectronics," Journal of Materials Chemistry. C, Materials for Optical and Electronic Devices, vol. 9, pp. 1524-1546, Aug 26,. 2021.

[13] P. Atkins and L. Jones, "LJ Chemical Principles The Quest for Insight," 2009.

[14] A.H. Castro Neto, "The carbon new age," Materials Today, vol. 13, pp. 12, 2010.

[15] P.S. Karthik, A.L. Himaja and S.P. Singh, "Carbon-allotropes: synthesis methods, applications and future perspectives," Carbon Letters, vol. 15, pp. 219-237, Oct 31,. 2014.

[16] F.P. Bundy, W.A. Bassett, M.S. Weathers, R.J. Hemley, H.U. Mao and A.F. Goncharov, "The pressure-temperature phase and transformation diagram for carbon; updated through 1994," Carbon, vol. 34, pp. 141-153, 1996.

[17] B. Hausmann, I. Bulu, V. Venkataraman, P. Deotare and M. Lončar, "Diamond nonlinear photonics," Nature Photonics, vol. 8, pp. 369-374, 2014.

[18] C. Soldano, A. Mahmood and E. Dujardin, "Production, properties and potential of graphene," Carbon, vol. 48, pp. 2127-2150, 2010.

[19] A.C. Ferrari, F. Bonaccorso, Z. Sun and T. Hasan, "Graphene photonics and optoelectronics," Nature Photonics, vol. 4, pp. 611-622, Sep. 2010.

[20] F. Xia, H. Yan and P. Avouris, "The Interaction of Light and Graphene: Basics, Devices, and Applications," Jproc, vol. 101, pp. 1717-1731, Jul. 2013.

[21] S. Yamashita, "A Tutorial on Nonlinear Photonic Applications of Carbon Nanotube and Graphene," Jlt, vol. 30, pp. 427-447, Feb 15,. 2012.

[22] V. Georgakilas, J.A. Perman, J. Tucek and R. Zboril, "Broad family of carbon nanoallotropes: classification, chemistry, and applications of fullerenes, carbon dots, nanotubes, graphene, nanodiamonds, and combined superstructures," Chem.Rev., vol. 115, pp. 4744-4822, 2015.

[23] C.S. Casari and A. Milani, "Carbyne: from the elusive allotrope to stable carbon atom wires," MRS Communications, vol. 8, pp. 207, -04-05. 2018.

[24] K. Zhang, Y. Zhang and L. Shi, "A review of linear carbon chains," Chinese Chemical Letters, vol. 31, pp. 1746-1756, Jul. 2020.

[25] S. Szafert and J.A. Gladysz, "Carbon in one dimension: structural analysis of the higher conjugated polyynes," Chem.Rev., vol. 103, pp. 4175-4206, 2003.

[26] A. Milani, M. Tommasini, V. Barbieri, A. Lucotti, V. Russo, F. Cataldo and C.S. Casari, "Semiconductor-to-Metal Transition in Carbon-Atom Wires Driven by sp2 Conjugated End Groups," J. Phys. Chem. C, vol. 121, pp. 10562, -05-08. 2017.

[27] F. Banhart, "Chains of carbon atoms: a vision or a new nanomaterial?" Beilstein Journal of Nanotechnology, vol. 6, pp. 559-569, 2015.

[28] S. Peggiani, P. Marabotti, R.A. Lotti, A. Facibeni, P. Serafini, A. Milani, V. Russo, A. Li Bassi and C.S. Casari, "Solvent-dependent termination, size and stability in polyynes synthesized via laser ablation in liquids," Phys. Chem. Chem. Phys., vol. 22, pp. 26312, 2. 2631.

[29] L. Shi, P. Rohringer, K. Suenaga, Y. Niimi, J. Kotakoski, J.C. Meyer, H. Peterlik, M. Wanko, S. Cahangirov, A. Rubio, Z.J. Lapin, L. Novotny, P. Ayala and T. Pichler, "Confined linear carbon chains as a route to bulk carbyne," Nature Mater, vol. 15, pp. 634, -04-04. 2016.

[30] J.A. Januszewski and R.R. Tykwinski, "Synthesis and properties of long [n]cumulenes (n ≥ 5)," Chemical Society Reviews, vol. 43, pp. 3184-323, Apr 06,. 2014.

[31] W.A. Chalifoux and R.R. Tykwinski, "Synthesis of extended polyynes: Toward carbyne," Comptes Rendus. Chimie, vol. 12, pp. 341-358, 2009.

[32] W.A. Chalifoux and R.R. Tykwinski, "Synthesis of polyynes to model the sp-carbon allotrope carbyne," Nature Chemistry, vol. 2, pp. 967, 2010.

[33] F. Cataldo, Polyynes: synthesis, properties, and applications, CRC Press, 2005, .

[34] F. Cataldo, "Simple generation and detection of polyynes in an arc discharge between graphite electrodes submerged in various solvents," Carbon, vol. 41, pp. 2671, 2003.

[35] S. Peggiani, A. Senis, A. Facibeni, A. Milani, P. Serafini, G. Cerrato, A. Lucotti, M. Tommasini, D. Fazzi and C. Castiglioni, "Size-selected polyynes synthesised by submerged arc discharge in water," Chemical Physics Letters, vol. 740, pp. 137054, 2020.

[36] F. Cataldo, "Synthesis of polyynes in a submerged electric arc in organic solvents," Carbon, vol. 42, pp. 129-142, 2004.

[37] V. Amendola and M. Meneghetti, "What controls the composition and the structure of nanomaterials generated by laser ablation in liquid solution?" Physical Chemistry Chemical Physics, vol. 15, pp. 3027-3046, 2013.

[38] M. Tsuji, T. Tsuji, S. Kuboyama, S. Yoon, Y. Korai, T. Tsujimoto, K. Kubo, A. Mori and I. Mochida, "Formation of hydrogen-capped polyynes by laser ablation of graphite particles suspended in solution," Chemical Physics Letters, vol. 355, pp. 101, -03. 2002.

[39] G. Compagnini, V. Mita, L. D'Urso, R.S. Cataliotti and O. Puglisi, "Spectroscopic study of polyynes obtained by laser ablation in liquids," Journal of Raman Spectroscopy, vol. 39, pp. 177-181, Feb. 2008.

[40] H. Tabata, M. Fujii and S. Hayashi, "Laser ablation of diamond nanoparticles suspended in solvent: synthesis of polyynes," Chemical Physics Letters, vol. 395, pp. 138-142, 2004.

[41] R. Matsutani, K. Inoue, N. Wada and K. Kojima, "Wavelength dependence of polyyne preparation by liquid-phase laser ablation using pellet targets," Chemical Communications, vol. 47, pp. 5840-5842, 2011.

[42] A. Milani, M. Tommasini, V. Russo, A. Li Bassi, A. Lucotti, F. Cataldo and C.S. Casari, "Raman spectroscopy as a tool to investigate the structure and electronic properties of carbon-atom wires," Beilstein J. Nanotechnol., vol. 6, pp. 480, 2015.

[43] A. Milani, M. Tommasini, M. Del Zoppo, C. Castiglioni and G. Zerbi, "Carbon nanowires: Phonon and π-electron confinement," Physical Review. B, Condensed Matter and Materials Physics, vol. 74, Oct. 2006.

[44] A. Milani, M. Tommasini and G. Zerbi, "Connection among Raman wavenumbers, bond length alternation and energy gap in polyynes," Journal of Raman Spectroscopy, vol. 40, pp. 1931-1934, Dec. 2009.

[45] F. Innocenti, A. Milani and C. Castiglioni, "Can Raman spectroscopy detect cumulenic structures of linear carbon chains?" Journal of Raman Spectroscopy, vol. 41, pp. 226-236, Feb. 2010.

[46] Pilot, Signorini, Durante, Orian, Bhamidipati and Fabris, "A Review on Surface-Enhanced Raman Scattering," Biosensors, vol. 9, -04-17. 2019.

[47] H. Tabata, M. Fujii, S. Hayashi, T. Doi and T. Wakabayashi, "Raman and surface-enhanced Raman scattering of a series of size-separated polyynes," Carbon (New York), vol. 44, pp. 3168-3176, 2006.

[48] A. Lucotti, M. Tommasini, M.D. Zoppo, C. Castiglioni, G. Zerbi, F. Cataldo, C.S. Casari, A.L. Bassi, V. Russo, M. Bogana and C.E. Bottani, "Raman and SERS investigation of isolated sp carbon chains," Chemical Physics Letters, vol. 417, pp. 78-82, 2006.

[49] C.S. Casari, V. Russo, A. Li Bassi, C.E. Bottani, F. Cataldo, A. Lucotti, M. Tommasini, M. Del Zoppo, C. Castiglioni and G. Zerbi, "Stabilization of linear carbon structures in a solid Ag nanoparticle assembly," Appl. Phys. Lett., vol. 90, 2007.

[50] G. Grasso, L. D'Urso, E. Messina, F. Cataldo, O. Puglisi, G. Spoto and G. Compagnini, "A mass spectrometry and surface enhanced Raman spectroscopy study of the interaction between linear carbon chains and noble metals," Carbon, vol. 47, pp. 2611-2619, 2009.

[51] K. An, G. Wei, G. Qi, L. Sheng, L. Yu, W. Ren and X. Zhao, "Stability improvement of C8H2 and C10H2 embedded in poly(vinyl alcohol) films with adsorption on gold nanoparticles," Chemical Physics Letters, vol. 637, pp. 71-76, Sep 16,. 2015.

[52] A. Lucotti, C.S. Casari, M. Tommasini, A. Li Bassi, D. Fazzi, V. Russo, M. Del Zoppo, C. Castiglioni, F. Cataldo, C.E. Bottani and G. Zerbi, "sp Carbon chain interaction with silver nanoparticles probed by Surface Enhanced Raman Scattering," Chemical Physics Letters, vol. 478, pp. 45, -06-11. 2009.

[53] A. Milani, A. Lucotti, V. Russo, M. Tommasini, F. Cataldo, A. Li Bassi and C.S. Casari, "Charge Transfer and Vibrational Structure of sp-Hybridized Carbon Atomic

Wires Probed by Surface Enhanced Raman Spectroscopy," Journal of Physical Chemistry. C, vol. 115, pp. 12836-12843, Jul 07,. 2011.

[54] S.Z. Al Sheheri, Z.M. Al-Amshany, Q.A. Al Sulami, N.Y. Tashkandi, M.A. Hussein and R.M. El-Shishtawy, "The preparation of carbon nanofillers and their role on the performance of variable polymer nanocomposites," Designed Monomers and Polymers, 2019.

[55] J. Lim, S. Bee, L. Tin Sin, C.T. Ratnam and Z.A. Abdul Hamid, "A review on the synthesis, properties, and utilities of functionalized carbon nanoparticles for polymer nanocomposites," Polymers, vol. 13, pp. 3547, 2021.

[56] S. Okada, M. Fujii and S. Hayashi, "Immobilization of polyynes adsorbed on Ag nanoparticle aggregates into poly (vinyl alcohol) films," Carbon, vol. 49, pp. 4704-4709, 2011.

[57] S. Peggiani, A. Facibeni, A. Milani, C. Castiglioni, V. Russo, A. Li Bassi and C.S. Casari, "In situ synthesis of polyynes in a polymer matrix via pulsed laser ablation in a liquid," Mater. Adv., vol. 1, pp. 2729, 2020.

[58] Z. Huang, Y. Zhang, M. Kotaki and S. Ramakrishna, "A review on polymer nanofibers by electrospinning and their applications in nanocomposites," Composites Science and Technology, vol. 63, pp. 2223, -11. 2003.

[59] N. Bhardwaj and S.C. Kundu, "Electrospinning: A fascinating fiber fabrication technique," Biotechnology Advances, vol. 28, pp. 325-347, 2010.

[60] J. Xue, T. Wu, Y. Dai and Y. Xia, "Electrospinning and electrospun nanofibers: Methods, materials, and applications," Chem.Rev., vol. 119, pp. 5298-5415, 2019.

[61] A. Greiner and J. Wendorff, "Electrospinning: A Fascinating Method for the Preparation of Ultrathin Fibers," Angewandte Chemie (International Ed.), vol. 46, pp. 5670-5703, Jul 23,. 2007.

[62] D. Li and Y. Xia, "Electrospinning of Nanofibers: Reinventing the Wheel?" Advanced Materials (Weinheim), vol. 16, pp. 1151-1170, Jul 19,. 2004.

[63] A. Frenot and I.S. Chronakis, "Polymer nanofibers assembled by electrospinning," Current Opinion in Colloid and Interface Science, vol. 8, pp. 64, 2003.

[64] D.H. Reneker, A.L. Yarin, E. Zussman and H. Xu, "Electrospinning of Nanofibers from Polymer Solutions and Melts," .

[65] A. Haider, S. Haider and I. Kang, "A comprehensive review summarizing the effect of electrospinning parameters and potential applications of nanofibers in biomedical and biotechnology," Arabian Journal of Chemistry, vol. 11, pp. 1165, 2018.

[66] S. Tan, R. Inai, M. Kotaki and S. Ramakrishna, "Systematic parameter study for ultra-fine fiber fabrication via electrospinning process," Polymer (Guilford), vol. 46, pp. 6128-6134, 2005.

[67] S.L. Shenoy, W.D. Bates, H.L. Frisch and G.E. Wnek, "Role of chain entanglements on fiber formation during electrospinning of polymer solutions: good solvent, non-specific polymer–polymer interaction limit," Polymer (Guilford), vol. 46, pp. 3372-3384, 2005.

[68] H. Liu and Y. Hsieh, "Ultrafine fibrous cellulose membranes from electrospinning of cellulose acetate," Journal of Polymer Science. Part B, Polymer Physics, vol. 40, pp. 2119-2129, Sep 15,. 2002.

[69] J. Pelipenko, J. Kristl, B. Janković, S. Baumgartner and P. Kocbek, "The impact of relative humidity during electrospinning on the morphology and mechanical properties of nanofibers," International Journal of Pharmaceutics, vol. 456, pp. 125-134, Nov 01,. 2013.

[70] I. Jun, Y. Chung, Y. Heo, H. Han, J. Park, H. Jeong, H. Lee, Y.B. Lee, Y. Kim and H. Seok, "Creating hierarchical topographies on fibrous platforms using femtosecond laser ablation for directing myoblasts behavior," ACS Applied Materials & Interfaces, vol. 8, pp. 3407-3417, 2016.

[71] J.K.Y. Lee, N. Chen, S. Peng, L. Li, L. Tian, N. Thakor and S. Ramakrishna, "Polymer-based composites by electrospinning: Preparation & functionalization with nanocarbons," Progress in Polymer Science, vol. 86, pp. 40-84, Nov. 2018.

[72] C. Marega, J. Maculan, G. Andrea Rizzi, R. Saini, E. Cavaliere, L. Gavioli, M. Cattelan, G. Giallongo, A. Marigo and G. Granozzi, "Polyvinyl alcohol electrospun nanofibers containing Ag nanoparticles used as sensors for the detection of biogenic amines," Nano, vol. 26, pp. 075501, Jan 28,. 2015.

[73] Y. Chen, J. Cao, H. Wei, Z. Wu, X. Wang and Y. Pei, "Synthesis of polyvinyl alcohol/Ag electrospun nanofibers as highly efficient flexible SERS substrates," Vibrational Spectroscopy, vol. 114, pp. 103246, May. 2021.

[74] S.I. Abd Razak, I.F. Wahab, F. Fadil, F.N. Dahli, A.Z. Md Khudzari and H. Adeli, "A Review of Electrospun Conductive Polyaniline Based Nanofiber Composites and Blends: Processing Features, Applications, and Future Directions," Advances in Materials Science and Engineering, vol. 2015, pp. 1, 2015.

[75] P.C. Lee and D. Meisel, "Adsorption and surface-enhanced Raman of dyes on silver and gold sols," J. Phys. Chem.; (United States), vol. 86, pp. 3391-3395, Aug 01,. 1982.

[76] A. Amirjani, F. Firouzi and D.F. Haghshenas, "Predicting the Size of Silver Nanoparticles from Their Optical Properties," Plasmonics, vol. 15, pp. 1077-1082, 2020.

[77] C. Zhang, X. Yuan, L. Wu, Y. Han and J. Sheng, "Study on morphology of electrospun poly(vinyl alcohol) mats," European Polymer Journal, vol. 41, pp. 423-432, 2005.

[78] A. Koski, K. Yim and S. Shivkumar, "Effect of molecular weight on fibrous PVA produced by electrospinning," Materials Letters, vol. 58, pp. 493, -01. 2004.

[79] M.M. Mahmud, A. Perveen, M.A. Matin and M.T. Arafat, "Effects of binary solvent mixtures on the electrospinning behavior of poly (vinyl alcohol)," Mrx, vol. 5, pp. 115407, Sep 14,. 2018.

[80] M. Bottachiari, "Thermal Stability of Polyynes-PVA Nanocomposites Studied by Surface Enhanced Raman Spectroscopy," 2022. Master thesis at Politecnico di Miano

[81] W. Jin, H.J. Jeon, J.H. Kim and J.H. Youk, "A study on the preparation of poly(vinyl alcohol) nanofibers containing silver nanoparticles," Synthetic Metals, vol. 157, pp. 454-459, 2007.

[82] D. Kharaghani, H. Lee, T. Ishikawa, T. Nagaishi, S.H. Kim and I.S. Kim, "Comparison of fabrication methods for the effective loading of Ag onto PVA nanofibers," Textile Research Journal, vol. 89, pp. 625-634, Feb. 2019.

[83] L.J. Villarreal-Gómez, G.L. Pérez-González, N. Bogdanchikova, A. Pestryakov, V. Nimaev, A. Soloveva, J.M. Cornejo-Bravo and Y. Toledaño-Magaña, "Antimicrobial Effect of Electrospun Nanofibers Loaded with Silver Nanoparticles: Influence of Ag Incorporation Method," Journal of Nanomaterials, vol. 2021, pp. 1, -08-17. 2021.

[84] G.d.B. Cardoso, I.N. Souza, M.M. Pereira, L.P. Costa, M.G. Freire, C.M.F. Soares and ÁS. Lima, "Poly(vinyl alcohol) as a novel constituent to form aqueous two-phase systems with acetonitrile: Phase diagrams and partitioning experiments," Chemical Engineering Research & Design, vol. 94, pp. 317-323, Feb. 2015.

[85] D. Gupta, M. Jassal and A.K. Agrawal, "The electrospinning behavior of poly(vinyl alcohol) in DMSO-water binary solvent mixtures," RSC Advances, vol. 6, pp. 12947-12955, Oct 31,. 2016.

[86] A. Sacchi, "Carbon atomic wires-based nanocomposites Single step synthesis from polymeric solutions and in situ Raman characterization," 2019. . Master thesis at Politecnico di Miano

[87] A. Vidale, "Development of linear sp carbon chains in electrospun polymer nanofibers," 2018. Master thesis at Politecnico di Miano

[88] C. Terranova, "Synthesis and Brillouin Spectroscopy investigation of polymer electrospun fibers embedding Carbon Atom Wires," 2019. Master thesis at Politecnico di Miano

[89] S. Sala, "Linear sp carbon chains-polymer nanocomposites by Pulsed Laser Ablation in Liquid," 2020. . Master thesis at Politecnico di Miano.

List of Figures

List if Tables